

# **Ion channel TRPM4 activity and cardiac conduction disease**

**DISSERTATION**

zur Erlangung des Doktorgrades

- Dr. rer. nat -

des Fachbereiches Chemie

der Universität Hamburg

Von

**Yu Wu**

Anhui, P.R.China

**Hamburg, August 2012**

Diese Arbeit wurde am Institut für Neurale Signalverarbeitung des Zentrums für Molekulare Neurobiologie Hamburg und am Institut für Physiologie der Universität des Saarlandes angefertigt.

Gutachter: Prof. Dr. Olaf Pongs

Prof. Dr. Peter Heisig

Datum der Disputation: 19.10.2012

## **Erklärung über frühere Promotionsversuche**

Hiermit erkläre ich, dass vorher keine weiteren Promotionsversuche unternommen worden sind, oder an einer anderen Stelle vorgelegt wurden.

Hamburg, den .....

.....

(Unterschrift)

## **Eidesstattliche Versicherung**

Hiermit erkläre ich an Eides statt, dass die vorliegende Dissertationsschrift selbständig und allein von mir unter den angegebenen Hilfsmitteln angefertigt wurde.

Hamburg, den .....

.....

(Unterschrift)

# CONTENTS

<b>I</b>	<b>ABSTRACT .....</b>	<b>1</b>
<b>II</b>	<b>INTRODUCTION.....</b>	<b>3</b>
II.1	Cardiac arrhythmias and ion channel.....	3
II.2	TRPM4 channel and its involvement in cardiac conduction disease .....	7
II.3	SUMOylation and its regulation of ion channel.....	11
<b>III</b>	<b>AIMS OF STUDY .....</b>	<b>16</b>
<b>IV</b>	<b>MATERIAL .....</b>	<b>17</b>
IV.1	Buffers and solutions .....	17
IV.2	Primary antibodies .....	18
IV.3	Secondary antibodies .....	20
IV.4	DNA and protein standards.....	20
IV.5	Bacterial strains .....	20
IV.6	Bacterial media.....	21
IV.7	Plasmids.....	20

IV.8	Cell culture medium and materials.....	22
IV.9	Inhibitors.....	23
IV.10	Mouse strain.....	24
<b>V</b>	<b>METHODS .....</b>	<b>25</b>
V.1	Molecular biological methods.....	25
<b>V.1.1</b>	Molecular cloning.....	25
V.1.1.1	<i>Site directed mutagenesis.....</i>	25
V.1.1.2	<i>PCR program.....</i>	26
<b>V.1.2</b>	Transformation of bacteria.....	27
<b>V.1.3</b>	Purification of plasmid DNA.....	27
V.1.3.1	<i>Small scale plasmid DNA purification.....</i>	27
V.1.3.2	<i>Large scale plasmid DNA purification.....</i>	27
V.1.3.3	<i>Determination of DNA concentration.....</i>	27
V.1.3.4	<i>Sequencing of DNA.....</i>	28
<b>V.1.4</b>	Restriction digestion of DNA.....	28
<b>V.1.5</b>	Horizontal agarose gel electrophoresis of DNA.....	28
<b>V.1.6</b>	Gel purification and Ligation.....	29
V.2	Protein biochemical methods.....	29
<b>V.2.1</b>	SDS-PAGE electrophoresis.....	29
V.2.1.1	<i>Determination of protein concentration.....</i>	29
V.2.1.2	<i>SDS-PAGE.....</i>	29
<b>V.2.2</b>	Immunoblot analysis.....	30
V.2.2.1	<i>Electrophoretic transfer of proteins.....</i>	30
V.2.2.2	<i>Immunochemical detection of transferred proteins.....</i>	30
V.2.2.3	<i>Densitometric evaluation of band density.....</i>	31

V.2.2.4	<i>Stripping and re-probing of immunoblot</i> .....	31
V.2.2.5	<i>Co-immunoprecipitation</i> .....	31
<b>V.2.3</b>	<b>Lipid-raft fractionation</b> .....	<b>32</b>
V.2.3.1	<i>Non-detergent-based isolation of lipid rafts from total lysate of TRPM4 Flp In cells</i> .....	32
V.2.3.2	<i>Detergent-based isolation of lipid rafts from total lysate of TRPM4 Flp In cells</i> .....	32
V.2.3.3	<i>Non-detergent-based isolation of lipid rafts from membrane lysate of Myc-tagged TRPM4 knock-in mouse</i> .....	33
V.2.3.4	<i>Cholesterol assay</i> .....	33
<b>V.3</b>	<b>Cell biological methods</b> .....	<b>33</b>
<b>V.3.1</b>	<b>Cell culture</b> .....	<b>33</b>
V.3.1.1	<i>Maintenance of HEK 293 cells and Flp In cells</i> .....	33
V.3.1.2	<i>Transient transfection</i> .....	34
V.3.1.3	<i>Generating TRPM4 stably-expressing cell line</i> .....	34
<b>V.3.2</b>	<b>FACS analysis</b> .....	<b>35</b>
<b>V.3.3</b>	<b>Cell surface biotinylation</b> .....	<b>35</b>
<b>V.4</b>	<b>Electrophysiology</b> .....	<b>36</b>
<b>V.4.1</b>	<b>Experimental set up</b> .....	<b>36</b>
<b>V.4.2</b>	<b>Procedure for whole-cell recording</b> .....	<b>37</b>
V.4.2.1	<i>Whole-cell patch clamp configuration</i> .....	37
V.4.2.2	<i>Electrode</i> .....	37
V.4.2.3	<i>Measurement and data analysis</i> .....	37
<b>V.5</b>	<b>Calcium imaging</b> .....	<b>38</b>
<b>V.5.1</b>	<b>Principle of the method</b> .....	<b>38</b>
<b>V.5.2</b>	<b>Measurement of fura-2 AM fluorescence</b> .....	<b>39</b>
<b>V.5.3</b>	<b>Data analysis</b> .....	<b>39</b>

V.6	Studies on adult murine cardiomyocytes.....	40
<b>V.6.1</b>	Cardiomyocytes isolation .....	40
V.6.1.1	Setup procedure.....	40
V.6.1.2	Heart excision and aorta cannulation .....	40
V.6.1.3	Heart perfusion and mechanical isolation .....	41
<b>V.6.2</b>	Cell culture .....	41
<b>V.6.3</b>	Immunocytochemistry .....	42
<b>V.6.4</b>	Measurement of cardiomyocyte $[Ca^{2+}]_i$ transients .....	42
V.7	Statistical analysis .....	43
<b>VI</b>	<b>RESULTS.....</b>	<b>44</b>
VI.1	Expression of TRPM4 and TRM4 <sup>R164W</sup> channel.....	44
VI.2	SUMOylation regulates TRPM4 current via a non-covalently conjugating.....	46
VI.3	Caveolin-1 binding affects TRPM4 channel activity.....	51
VI.4	TRPM4 channels reside in cholesterol- and caveolin-rich membrane microdomains.....	56
VI.5	SUMOylation regulates TRPM4 channel via altered TRPM4 distribution in membrane microdomains.....	59
VI.6	Association of TRPM4 and caveolin-3 in murine heart	63
VI.7	Ouabain activates TRPM4 channel and alters its	

	distribution in membrane microdomains.....	65
VI.8	Ca <sup>2+</sup> response in TRPM4 deficient mice .....	67
<b>VII</b>	<b>DISCUSSION.....</b>	<b>72</b>
VII.1	SUMOylation stimulates TRPM4 current indirectly.....	72
VII.2	TRPM4 activity associated with high cholesterol microdomain .....	74
VII.3	TRPM4 promotes Ca <sup>2+</sup> influx via inhibition of Na <sup>+</sup> /K <sup>+</sup> -ATPase by Ouabain in cardiomyocytes .....	77
<b>VIII</b>	<b>REFERENCE .....</b>	<b>80</b>
<b>IX</b>	<b>APPENDIX.....</b>	<b>88</b>
IX.1	Abbreviations.....	88
IX.2	Hazardous substances list .....	90
<b>X</b>	<b>ACKNOWLEDGEMENTS.....</b>	<b>91</b>

# I ABSTRACT

Progressive familial heart block type I (PFHBI), and isolated cardiac conduction disease (ICCD) are associated with dominantly inherited mutations in the *trpm4* gene. It encodes a non-selective cation channel differentially expressed in cardiac tissues. In vitro expression studies indicated that all PFHBI/ICCD-related TRPM4 mutations markedly increased channel current density, without affecting single channel properties, open probability,  $\text{Ca}^{2+}$ -,  $\text{PIP}_2$ -, and ATP-sensitivity. Preliminary study suggested that TRPM4 current density is sensitive to post-translational SUMOylation, whereas the ones of the mutant channels are not. However, the mechanisms that link SUMOylation and increased current density are still unresolved.

Here, I identified caveolin-1 as a binding partner of TRPM4 that regulates its current in TRPM4 stably-expressing cells. TRPM4 channel preferably resided in membrane microdomains enriched in cholesterol and the cholesterol-binding protein, caveolin-1. SUMOylation-evoked stimulation of TRPM4 current was caveolin-1-dependent. Both activation of SUMOylation and cholesterol depletion affected TRPM4 localization within the plasma membrane by destabilizing caveolin-1 and its interaction with TRPM4, and increased TRPM4 current density. Moreover, I demonstrated that TRPM4<sup>R164W</sup>, corresponding to the ICCD mutation, associated with the highest percentage of complete atrioventricular block, lead to a four-fold higher current density and renders channel activity insensitive to SUMOylation and cholesterol. I propose that the mutation attenuates the interaction of caveolin-1 with TRPM4 and, thereby, enhances the residence of the TRPM4 channel in  $\text{PIP}_2$ -enriched microdomains more favorable for TRPM4 activity.

Moreover, I showed that the TRPM4 channel had a close functional association with the caveolae-related ion transporter,  $\text{Na}^+/\text{K}^+$ -ATPase, to regulate  $\text{Ca}^{2+}$  homeostasis and cardiac contraction *in vivo*.  $\text{Na}^+/\text{K}^+$ -ATPase and TRPM4 channel were functionally associated and could be co-immunoprecipitated. In mice, TRPM4 channel amplified pharmacologic effects mediated by  $\text{Na}^+/\text{K}^+$ -ATPase, and evoked more  $\text{Ca}^{2+}$  influx and stronger cardiac contraction, which was absent in TRPM4 deficient mice.

Taken together, these observations provide new insights into the physiological and pathological significance of TRPM4 channel in cardiac conduction.

## Zusammenfassung

Die Erkrankungen des Erregungsleitungssystems des Herzens *Progressive familial heart block type I* (PFHBI) und *Isolated cardiac conduction disease* (ICCD) sind beide assoziiert mit dominant vererbten Mutationen des TRPM4 Gens. Es kodiert für einen Kationen unselektiv leitenden Kanal mit differentieller Expression in verschiedenen kardialen Geweben. *In vitro* Expressionsstudien zeigten, dass alle PFHBI/ICCD Mutationen deutlich die Stromdichte von TRPM4 Kanälen erhöhten, ohne dabei Einzelkanaleigenschaften, Öffnungswahrscheinlichkeit,  $\text{Ca}^{2+}$ -,  $\text{PIP}_2$ - und ATP-Sensitivität zu beeinflussen. Vorabstudien wiesen darauf hin, dass die TRPM4 Stromdichte sensitiv für post-translationale SUMOylierung ist, die Stromdichte der mutierten Kanäle jedoch nicht. Die Mechanismen, welche SOMOylierung und erhöhte Stromdichte aneinander koppeln, sind allerdings bislang ungeklärt.

Nun konnte ich Caveolin-1 als einen Bindepartner von TRPM4 identifizieren, der seinen Stromfluss in TRPM4 stabil exprimierenden Zellen reguliert. Der TRPM4 Kanal hielt sich bevorzugt in Membran-Mikrodomänen auf, die reich an Cholesterin und dem cholesterinbindenden Protein Caveolin-1 sind. Die Stimulation von TRPM4 durch SUMOylierung war zudem abhängig von Caveolin-1. Sowohl die Aktivierung der SUMOylierung als auch eine Depletion von Cholesterin erhöhten die TRPM4 Stromdichte und beeinflussten zugleich die Lokalisation von TRPM4 in der Plasmamembran durch Destabilisierung von Caveolin-1 und seiner Interaktion mit TRPM4. TRPM4<sup>R164W</sup> entspricht jener ICCD Mutation, welche mit der höchsten Prozentrate von kompletten atrioventrikulären Block einher geht. Hier zeige ich, dass sie in einer vierfach erhöhten Stromdichte resultiert und die Kanalaktivität unempfindlich für SUMOylation and Cholesterin macht. Als mögliche Erklärung schlage ich vor, dass die Mutation die Interaktion von Caveolin-1 und TRPM4 abschwächt und dadurch den Anteil von TRPM4 Kanälen, die sich in für die Kanalaktivität günstigeren,  $\text{PIP}_2$ -reichen Mikrodomänen aufhalten, steigert.

Des Weiteren zeige ich, dass der TRPM4 Kanal und die  $\text{Na}^+/\text{K}^+$ -ATPase, ein mit Caveolae in Beziehung stehender Ionentransporter,  $\text{Ca}^{2+}$  Homöostase und kardiale Kontraktion *in vivo* in enger funktionaler Assoziation regulieren.  $\text{Na}^+/\text{K}^+$ -ATPase und TRPM4 Kanal waren funktionell assoziiert und konnten co-immunopräzipitiert werden. In Mäusen verstärkten TRPM4 Kanäle die pharmakologischen Effekte, die durch die  $\text{Na}^+/\text{K}^+$ -ATPase vermittelt werden, riefen dabei mehr  $\text{Ca}^{2+}$  Einstrom hervor und verursachen stärkere kardiale Kontraktionen. In TRPM4 defizienten Mäusen dagegen fehlten diese Effekte.

Zusammengenommen bieten diese Beobachtungen neue Einblicke in die physiologische und pathophysiologische Bedeutung des TRPM4 Kanals für die kardiale Erregungsleitung.

## II INTRODUCTION

### II.1 Cardiac arrhythmias and ion channel

Our heartbeat is essential for maintaining transport of nutrients, exchange of gases, removal of waste products, and circulation of hormones and antibodies to fulfill the requirements of the body. This process relies on proper generation and conduction of the cardiac electrical impulse, which is propagated through the heart by direct cell-cell coupling of cardiac muscle cells and through the cardiac conduction system (Fig II.1).

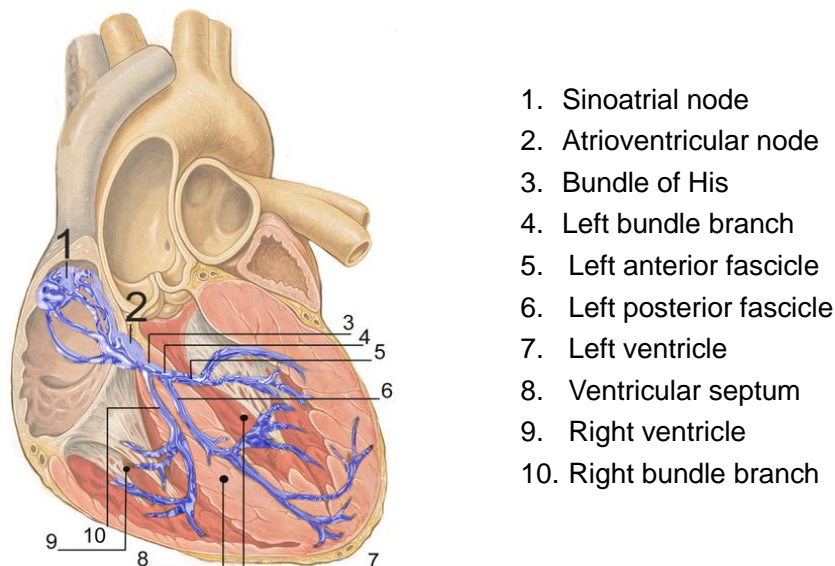


**Fig II.1 Heart conduction system.** From J. Heuser  
[http://en.wikipedia.org/wiki/File:RLS\\_12blauLeg.png](http://en.wikipedia.org/wiki/File:RLS_12blauLeg.png)

Cardiac conduction is initiated in sinus node (which is considered as a natural pacemaker), and then the impulse activates the atria and propagates to the atrioventricular (AV) node. Subsequently, the impulse is propagated through the rapidly conducting AV bundle, left and right bundle branches, and the Purkinje fiber network, from where it reaches the ventricular working myocardium (Boukens & Christoffels, 2012). The rhythmic contraction of our atria and ventricles requires the rapid activation of groups of cardiomyocytes, and individual cardiomyocytes are excited by the electrical current flowing from neighboring regions of

already excited cardiomyocytes. The propagating cardiac action potential fulfills these roles and it is accomplished by various ion channels localized on the membrane of cardiomyocytes (Fig II.2).

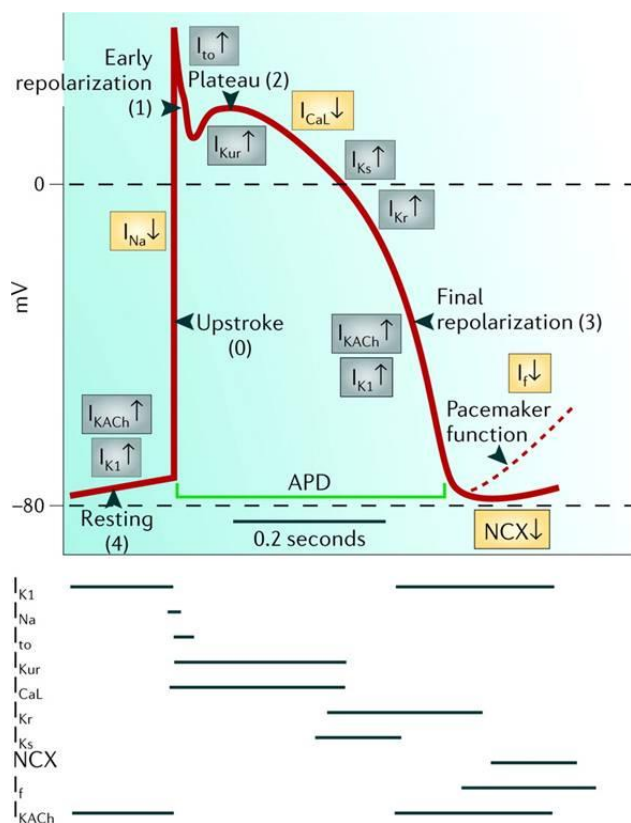


**Fig II.2 Membrane currents generate a normal action potential.**

Resting (4), upstroke (0), early repolarization (1), plateau (2), and repolarization (3) are the 5 phases of the action potential. A decline of potential at the end of phase 3 in pacemaker cells, such as the sinus node, is shown as a broken line. The inward currents,  $I_{Na}$ ,  $I_{Ca}$ , and  $I_f$ , are shown in yellow boxes; the sodium-calcium exchanger (NCX) is also shown in yellow. It is electrogenic and may generate inward or outward current.  $I_{KACh}$ ,  $I_{K1}$ ,  $I_{to}$ ,  $I_{Kur}$ ,  $I_{Kr}$ , and  $I_{Ks}$  are shown in grey boxes. The action potential duration (APD) is approximately 200ms (Grant, 2009).

In the adult heart, the underlying mechanism of cardiac disease is multifactorial and likely has a genetic component that predisposes for the development of these arrhythmias. In some cases, even a single mutation in a gene encoding an ion channel which is contributed to electrical patterning of action potential, has been identified to cause arrhythmia (Table 1)(Grant, 2009). For instance, the long QT syndrome (LQTS) is a rare inborn heart condition in which delayed repolarization of the heart following a heartbeat increases the risk of episodes of torsade de pointes (TDP, a form of irregular heartbeat that originates from the ventricles). More than 600 mutations have been identified in 13 LQTS genes, which respectively encode sodium ( $SCN_5A$ ), potassium ( $KCNQ_1$ ,  $KCNH_2$ ,  $KCNE_1$ ,  $KCNE_2$ ,  $KCNJ_2$ ), calcium channels ( $CACNA_1C$ ) and their associated proteins. Approximately 95% of LQTS patients are affected with either loss of function in  $I_{ks}$  (LQT1, 5) and  $I_{kr}$  (LQT2, 6) or gain of function in  $I_{Na}$  (LQT3)

(Zareba & Cygankiewicz, 2008). Nav1.5, the pore forming  $\alpha$ -subunit of the voltage-dependent cardiac  $\text{Na}^+$  channel, is an integral membrane protein involved in the initiation and conduction of action potentials. Mutations in the gene-encoding Nav1.5, SCN5A, have been associated with a variety of arrhythmic disorders, including Brugada syndrome, long QT, and sick sinus syndromes as well as progressive cardiac conduction defect and atrial standstill (Rook et al, 2012).

**Table 1 The Genetic Basis of Inherited Arrhythmias (Grant, 2009)**

Type	Gene	Protein	Functional Alteration
<b>LQTS</b>			
LQT1	KCNQ1	$I_{Ks}$ potassium channel $\alpha$ -subunit	Loss of function
LQT2	KCNH2	$I_{Kr}$ potassium channel $\alpha$ -subunit	Loss of function
LQT3	SCN5A	$I_{Na}$ cardiac sodium channel $\alpha$ -subunit	Gain of function
LQT4	ANK2	Ankyrin-B	Loss of function
LQT5	KCNE1	$I_{Ks}$ potassium channel $\beta$ -subunit	Loss of function
LQT6	KCNE2	$I_{Kr}$ potassium channel $\beta$ -subunit	Loss of function
LQT7	KCNJ2	$I_{K1}$ potassium channel subunit	Loss of function
LQT8	CACNA1C	Calcium channel $\alpha$ -subunit	Gain of function
<b>Short QT syndrome</b>			
S4T1	KCNH2	$I_{Kr}$ potassium channel $\alpha$ -subunit	Gain of function
S4T2	KCNQ1	$I_{Ks}$ potassium channel $\alpha$ -subunit	Gain of function
S4T3	KCNJ2	$I_{K1}$ potassium channel subunit	Gain of function
<b>Brugada syndrome</b>			
BrS1	SCN5A	$I_{Na}$ sodium channel $\alpha$ -subunit	Loss of function
BrS2	GPD1L	G-3PD 1-	Altered function
BrS3	CACNA1C	$I_{Ca}$ calcium channel $\alpha$ -subunit	Loss of function
BrS4	CACNB2b	$I_{Ca}$ calcium channel $\beta$ -subunit	Loss of function
BrS other	ANKRYN-B	Ankyrin-B	Altered function
<b>Catecholaminergic polymorphic VT</b>			
	RYR2	Cardiac ryanodine receptor	Gain of function
	CASQ2	Calsequestrin	Gain of function
<b>Idiopathic sick sinus syndrome</b>			
	HCN4	$I_f$ pacemaker channel subunit	Loss of function
	SCN5A	$I_{Na}$ cardiac sodium channel $\alpha$ -subunit	Loss of function
<b>Cardiac conduction disease</b>			
	SCN5A	$I_{Na}$ cardiac sodium channel $\alpha$ -subunit	Loss of function
<b>Familial atrial fibrillation</b>			
	KCNQ1	$I_{Ks}$ potassium channel $\alpha$ -subunit	Gain of function
	KCNE2	$I_{Kr}$ potassium channel $\beta$ -subunit	Gain of function
	KCNJ2	$I_{K1}$ potassium channel subunit	Gain of function
	KCNH2	$I_{Kr}$ potassium channel $\alpha$ -subunit	Gain of function

In this thesis, I focus on a cardiac arrhythmia related to cardiac conduction block. It is a condition where the depolarization wave initiated in the sinus node of the heart is slowed down or even blocked on the way to ventricular cardiomyocytes. The block site, its

completeness (partial or complete), and the number of blocks are largely variable from one individual to the other. Conduction block is not rare in the general population of young or old. Right bundle-branch block (RBBB) has a prevalence of about 0.1% in normal children, with a male predominance (Chiu et al, 2008). Complete RBBB with normal left ejection fraction and no diagnoses of cardiac disease was observed in 0.3% of individuals in a population of adult with a median age of 64 years (Miller et al, 2008). Furthermore, high-degree AV conduction block is life-threatening and is a major indication for pacemaker implantation (Ector et al, 2000).

In 1995, Progressive familial heart block type I (PFHBI; also known as PFHBIB), a progressive cardiac bundle branch disease in the His-purkinje system has been mapped to chromosome 19q13.3 (Brink et al, 1995). The patients were from 3 branches of a large South African Afrikaner pedigree with an autosomal-dominant form of PFHBI, firstly reported in 1977 (Brink & Torrington, 1977). Afterwards, a disease sharing phenotypic characteristics, described as isolated cardiac conduction disorder (ICCD) in a Lebanese kindred, has been mapped to the same chromosomal location (de Meeus et al, 1995). Since then, a series of candidate genes which encode either protein kinase or ion channel have been studied and finally excluded (Bardien-Kruger et al, 2002; Brink et al, 1995). In 1999, another progressive cardiac conduction disease sharing similar syndrome with PFHBI was identified to mutations in sodium channel SCN5A on chromosome 3 (Schott et al, 1999).

Until recent years, our group collaborated with cardiologists and human geneticists from Stellenbosch in South Africa, and Muenster in Germany, finally refined the genetic interval for the PFHBI locus and identified that a missense mutation in *trpm4* (Transient receptor potential melastatin 4) is the cause of blunted cardiac conduction in several branches of a large Afrikaner family (Kruse et al, 2009). Afterwards, our group collaborated with scientists in France and identified another 3 mutants in *trpm4*, which are respectively from one Lebanese family and two French families with diverse conduction blocks transmitted with an autosomal dominant inheritance and incomplete penetrance (Liu et al, 2010).

## II.2 TRPM4 channel and its involvement in cardiac conduction disease

*Trpm4* encodes a non-selective cation channel, transient receptor potential melastatin 4 channel, which is activated by a rise in intracellular  $\text{Ca}^{2+}$  concentration (Launay et al, 2002; Xu et al, 2001). TRPM4 channel has been identified as a key modulator of numerous calcium-dependent mechanisms such as the immune response, insulin secretion, cerebral artery constriction, respiratory rhythm, and cardiac conduction (Cheng et al, 2007; Earley et al, 2004; Kruse et al, 2009; Liu et al, 2010; Mironov, 2008; Nelson et al, 2011; Stallmeyer et al, 2012; Vennekens et al, 2007; Weber et al, 2010). Recent evidence suggested that the cardiac TRPM4 channel mediates a  $\text{Ca}^{2+}$ -activated non-selective cationic current ( $I_{\text{NSCca}}$ ) detected in mouse sinoatrial node cells (Demion et al, 2007), rat ventricular (Colquhoun et al, 1981) and human atrial cardiomyocytes (Guinamard et al, 2004), respectively.

### Structure and expression of TRPM4 channel

TRPM4 is a member of transient receptor potential (TRP) superfamily of channel proteins. TRPM4 gene is located on human chromosome 19, and in mouse on chromosome 7. It consists of 25 exons, spanning 54kb in the human genome and 31kb in the mouse genome. TRPM4 possesses six transmembrane domains with a pore region between TM regions 5 and 6. Four subunits are required to form a functional channel (Fig II.3). Within its  $\text{NH}_2$ - and  $\text{COOH}$ - terminal regions, the channel possesses several PKC phosphorylation sites, two ATP-binding cassette transporter-like motifs, five calmodulin-binding sites, four Walker B sites (putative ATP-binding sites), a putative  $\text{PIP}_2$  binding site, and a coiled-coil domain (Fig II.4).

Within the TRPM subfamily, TRPM4 is most closely related to TRPM5, sharing approximately 50% homology. Interestingly, these channels also share most of their biophysical and regulatory properties such as single channel conductance, ionic selectivity,

and voltage-, calcium-,  $\text{PIP}_2$ -, and heat- sensitivity (Liman, 2007). However, TRPM5 is not inhibited by internal ATP and is mainly expressed in taste receptor cells and the digestive tract. According to this remarkable difference in expression, TRPM4 channel is considered the molecular support for most  $I_{\text{NSCca}}$  currents observed in native tissues.

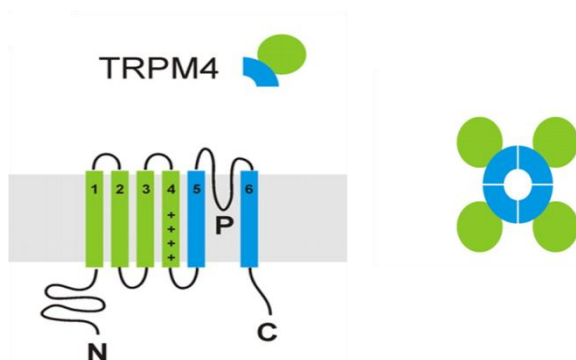


**Fig II.3 Membrane topology model of TRPM4 channel and predicted TRPM4 channel assembly.** Left, TRPM4 monomers consist of six TM helices with a pore region (p) between TM5 and TM6, and a voltage sensor in TM4 (indicated by plus signs). Right, functional TRPM4 channels are formed by oligomerization of four TRPM4 subunits. The pore-lining helices are surrounded by the voltage-sensing S1-S4 helices (Sala-Rabanal et al, 2012).

### Electrophysiological characteristic

Extensive electrophysiological analysis, based on human and mouse, full-length TRPM4 cDNA, overexpressed in HEK 293 cells, indicated that TRPM4 activation is calcium- and voltage-dependent. In TRPM4 overexpressing HEK 293 cells, cation currents can be measured in the whole-cell mode of the patch-clamp technique, upon loading cells with high intracellular  $\text{Ca}^{2+}$  concentrations through the pipette solution. The steady-state current-voltage relationship was reported to be either quasi-linear (Launay et al, 2002) or strongly outward rectifying (Nilius et al, 2003; Nilius et al, 2005a; Nilius et al, 2004; Nilius et al, 2005b; Ullrich et al, 2005). TRPM4 current slowly runs down within 30~120s and this run-down could be partly reversed or retarded in excised, cell-free patches, indicating that in the whole-cell mode an essential cytoplasmic factor for channel function is washed out of the cell (Launay et al, 2002; Nilius et al, 2003). The single channel conductance of TRPM4 is approximately 23 pS (Launay et al, 2002; Nilius et al, 2003).

## Physiology role of TRPM4 and its association with cardiac conduction disease

Calcium-activated nonselective cationic currents have been known for more than 30 years (Colquhoun et al, 1981), but their physiological significances have remained unclear until the recent cloning of the TRPM4 ion channel (Xu et al, 2001). Recent literatures based on *trpm4* gene targeting in mice have expanded our understanding by showing that TRPM4 regulates  $Ca^{2+}$  homeostasis and is involved in various physiological functions including myeloid cell migration (Barbet et al, 2008; Shimizu et al, 2009), insulin secretion (Cheng et al, 2007; Marigo et al, 2009; Nelson et al, 2011), and maintenance of myogenic tone in cerebral arteries (Crnich et al, 2010; Gonzales et al, 2010; Gonzales & Earley, 2012). Ablation of *trpm4* gene has also been demonstrated to induce hypertension by increasing catecholamine secretion (Mathar et al, 2010). Specifically, TRPM4 regulates  $Ca^{2+}$  homeostasis in a distinct way. Absence of TRPM4 elicited  $Ca^{2+}$  overload in Dendritic cells (DC) (Barbet et al, 2008), enhanced FcεRI-induced  $Ca^{2+}$  influx in mast cell (Vennekens et al, 2007). On the other hand, inhibition of TRPM4 in pancreatic  $\beta$ -cell lines significantly decreased intracellular  $Ca^{2+}$  concentration generated by agonist stimulation, thereby reducing insulin secretion (Marigo et al, 2009).

In recent years, our lab did some preliminary investigations on mutant TRPM4 channels which were discovered from familial cases with cardiac conduction disease. In 3 branches of a large South African Afrikaner pedigree with an autosomal-dominant form of PFHBI, the mutation c.19G-A in the TRPM4 gene at chromosomal locus 19q13.3 was identified. This mutation predicted the amino acid substitution p.E7K in the TRPM4 amino terminus (Kruse et al, 2009). Subsequently, heterozygous missense mutations of the TRPM4 gene (p.R164W, p.A432T and p.G844D) were also discovered from one Lebanese and two French families with autosomal dominant isolated cardiac conduction blocks (Liu et al, 2010). The affected family members showed prolonged QRS intervals with complete or incomplete RBBB, as main phenotypically characteristics. The highest penetrance of atrioventricular (AV) block was associated with members of the family carrying mutation TRPM4-p.R164W (Fig II.5).

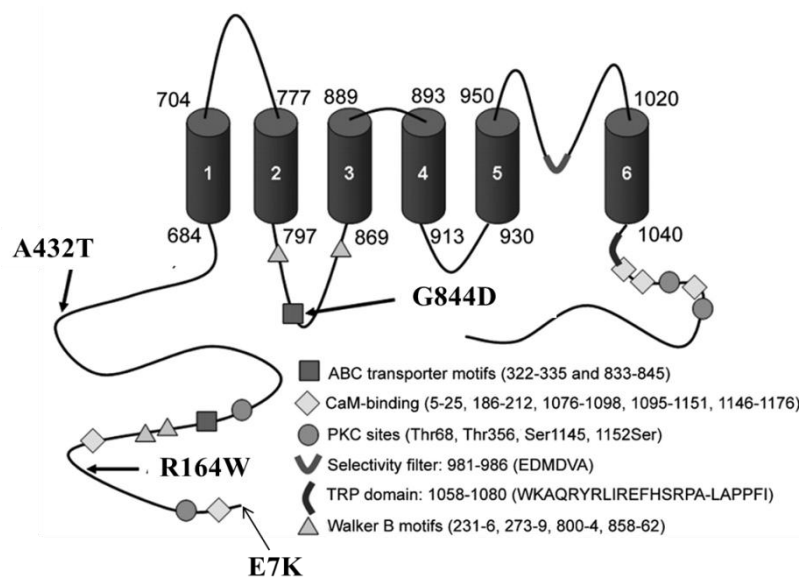


**Fig II.4 PFHBI- and ICCD-related mutations in TRPM4 protein.** E7K (Glu7Lys) is the mutant from a large South African Afrikaner pedigree with an autosomal-dominant form of PFHBI. R164W (Arg164Trp), A432T (Ala432Thr) and G844D (Gly844Asp) are respectively from one Lebanese family and two French families with autosomal-dominant ICCD. The intracellular segments contain several functional sites in N- or C-terminal (Adapted from Liu et al, 2010).

Interestingly, all four mutations result in distinct increased TRPM4 current densities when expressed in HEK 293 cells. Essentially, the same increase in current amplitude was observed after transfection of HEK 293 cells with a 1:1 mixture of wild-type and mutant TRPM4 cDNA. This is consistent with the observed dominant inheritance of PFHBI and ICCD phenotypes. The gain of TRPM4 function is not due to altered open probability or single channel conductance. Also, wild-type and mutant channels responded in an identical manner to changes in membrane voltage,  $PIP_2$ , and the ATP analogue (AMP-PNP) (Kruse et al, 2009; Liu et al, 2010).

Preliminary investigation suggested that TRPM4 current density was SUMOylation sensitive, whereas the ones of the mutant TRPM4 channels were not (Kruse et al, 2009; Liu et al, 2010). However, the precise mechanisms, that link SUMOylation and increase in TRPM4 current density, were poorly understood.

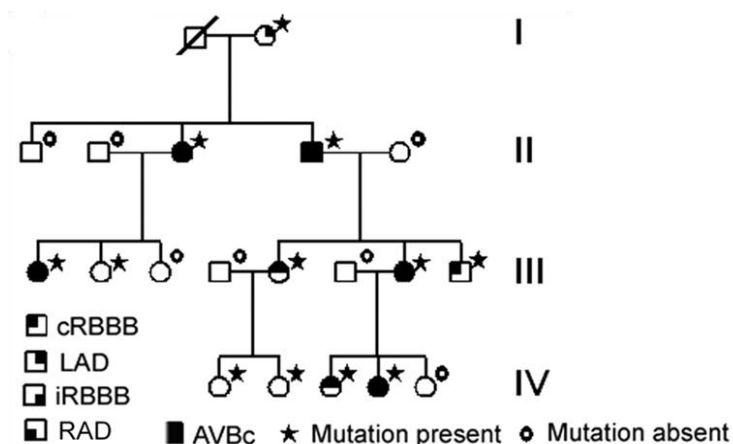


**Fig II.5 Pedigree of one French family carrying mutant R164W.** The legend indicates the type of cardiac conduction block and mutation status of family members (cRBBB, complete Right Bundle-Branch Block; iRBBB, incomplete RBBB; LAD, Left-Axis Deviation; RAD, Right Axis Deviation; AVB<sub>c</sub>, Atrioventricular Blocks) (Liu et al, 2010).

## II.3 SUMOylation and its regulation of ion channel

SUMO (Small ubiquitin-related modifier) was first identified as a reversible post-translational modification in 1997 (Mahajan et al, 1997). SUMO proteins are about 12kDa in size and resemble the three-dimensional structure of ubiquitin. It is ubiquitously expressed throughout the eukaryotic kingdom. The human gene encodes four distinct SUMO proteins: SUMO1-SUMO4. SUMO1-SUMO3 is ubiquitously expressed, whereas SUMO4 seems to be expressed mainly in kidney, lymph and spleen (Guo et al, 2005). Like ubiquitin, it is covalently and reversibly conjugated to specific lysine residues in the target protein. Apparently, SUMOylation stabilizes the target protein by blocking ubiquitination at the same lysine residue. A large body of publications showed that SUMO is a key regulator of several biological pathways (Geiss-Friedlander & Melchior, 2007; Guo et al, 2007; Wilkinson & Henley, 2010; Wilkinson et al, 2010).

### The SUMOylation cycle

All SUMO proteins are expressed in an immature form, in which they carry a C-terminal stretch of variable length (2-11 amino acids) after an invariant Gly-Gly motif that mask the

C-terminus of the mature protein. Removal of this C-terminus extension by SUMO-specific cysteine protease (SENP proteins) is a prerequisite for the conjugation of SUMO to targets. The first step is the activation of a mature SUMO protein at its C-terminus by the heterodimeric SUMO-specific E1 activating enzyme (Aos1-Uba2). This reaction is ATP-dependent. The formation of a SUMO-adenylate conjugate functions as an intermediate in the formation of a thioester bond between the C-terminal carboxyl group of SUMO and a cysteine residue in the catalytic center of Uba2. Next, SUMO is transferred from Uba2 to E2 conjugating enzyme Ubc9, forming a thioester bond between the catalytic cysteine residue of Ubc9 and the C-terminal carboxyl of SUMO. Finally, SUMO is transferred to the substrate through an isopeptide bond between C-terminal glycine residue of SUMO and a lysine side chain of the target. This process is facilitated by E3 ligase, which catalyses the transfer of SUMO from Ubc9 to a substrate. Although SUMOylation can be achieved without E3 activity *in vitro* (unlike ubiquitination), proteins like RanBP2, the polycomb family member, and members of the PIAS family (PIAS-1, -2, -3, -x- $\alpha$ , -x- $\beta$ , and -y) have E3-like activity and enhance SUMO conjugation, potentially by stabilizing the tripartite interaction between Ubc9, activated SUMO, and the target protein (Geiss-Friedlander & Melchior, 2007; Wilson & Rosas-Acosta, 2005). Interestingly, the K<sup>+</sup> channel associated protein KChAP (K<sup>+</sup> channel chaperone protein), which interacts directly with the N-terminus of Kv1.5 and serves to modulate the current density of many Kv channels (Wible et al, 1998), has recently been identified as PIAS3 $\beta$  (Wible et al, 2002). This observation raises the intriguing possibility that PIAS3 may have additional ion channel target, e.g. it serves to regulate the SUMO modification of TRPM4.

As with other ubiquitin-like proteins, the dynamic process of SUMOylation can be reversed by the action of the same cysteine proteases that are required for the maturation of pro-SUMO. One gene family has been identified so far that encodes SUMO-specific cysteine proteases. The corresponding protein in humans and mouse are called sentrin-specific protease (SENP1-3 and SENP5-7) and in yeast it is referred to as Ubl-specific proteases (Ulp). SENP proteins vary in their cellular distribution, SUMO prologue specificity and selectivity for SUMO maturation compared with de-conjugation activities (Kim & Baek, 2009).

SUMO conjugation is highly conserved in terms of target lysine residues. It usually occurs on lysine residues within the motif  $\Psi$ -K-X-E/D ( $\Psi$ , a large aliphatic acid; X, any amino acid). In most cases; SUMOylation induces the addition of single SUMO entities to individual acceptor lysine residues. However, the formation of polySUMO chains has also been observed both *in vivo* and *in vitro* (Bruderer et al, 2011).

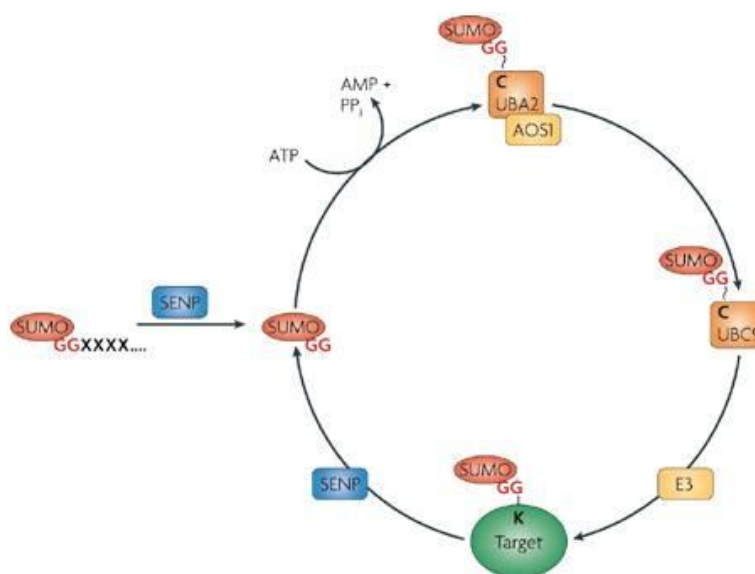


**Fig II.6 The SUMOylation cycle.** Before the first conjugation, nascent SUMO (small ubiquitin-related modifier) needs to be proteolytically processed to reveal its C-terminal Gly-Gly motif. This is accomplished by SUMO-specific isopeptidases (sentrin-specific proteases, SENPs), which remove 4 C-terminal amino acids from SUMO1, 11 amino acids from SUMO2 and 2 amino acids from SUMO3. Mature SUMO is activated by the E1 heterodimer AOS1–UBA2 in an ATP-dependent reaction, which results in a thioester bond between the C-terminal Gly residue in SUMO and C173 in Uba2. SUMO is then transferred to the catalytic Cys residue of the E2 enzyme Ubc9. Finally, an isopeptide bond is formed between the C-terminal Gly residue of SUMO and a Lys residue in the substrate. This step is usually aided by an E3 ligase. Sumoylated targets serve as substrates for SENPs, which ensures the reversible and dynamic nature of SUMO (Geiss-Friedlander & Melchior, 2007).

In addition of covalent SUMOylation through a specific lysine residue on substrate proteins, an increasing number of proteins has been identified which serve as non-covalent target of SUMO via SIMs/SBMs (SUMO-interacting motifs or SUMO-binding motifs). The SIM/SBM identified so far generally possesses a hydrophobic core surrounded by flanking acidic residues or phosphorylatable serine residues. NMR and X-ray studies revealed that the

SIM/SBM motif forms a  $\beta$ -strand that binds in parallel or anti-parallel orientation between the  $\alpha$ -helix and  $\beta$ -strand of SUMO (Song et al, 2004). A serine residue in the SIM/SBM is to regulate SUMO binding by phosphorylation, as negative charge to strengthen SUMO binding (Hannich et al, 2005; Hecker et al, 2006).

### **Molecular consequences of SUMOylation**

Three different effects have been described as functional consequence of SUMOylation. Firstly, SUMOylation can mask the binding site for substrate protein, essentially acting to occlude the interaction in a SUMOylation-dependent manner. A good example represents the SUMOylation of ubiquitin-conjugating enzyme E2-25K, which blocks E2 interaction with Ubiquitin E1 enzyme, leading to a decrease in its capability to conjugate ubiquitin to substrate proteins (Pichler et al, 2005). Secondly, the covalently attached SUMO moiety may act as an interaction “hub” that recruits new interacting proteins to the substrate either by a direct non-covalent interaction with the SUMO moiety or via a novel interaction domain created at the SUMO-substrate interface. Thirdly, SUMOylation can lead to a conformational change in the substrate, directly regulating its function (Wilkinson et al, 2010).

### **Cardiac ion channel and SUMOylation**

Since the discovery of SUMOylation, hundreds of SUMO targets are now known. The majority of SUMOylated proteins reside in the nucleus. Only a small proportion of membrane proteins especially ion channels e.g. Kv2.1, Kv1.5 and K2P1, have been implicated to be regulated by SUMOylation.

The Kv2.1 channel, which mediates sustained current ( $I_{\text{sus}}$ ) in cardiomyocytes (Bou-Abboud et al, 2000), is regulated by SUMOylation in overexpressed HEK 293 cells. SUMOylation leads to Kv2.1 current inhibition and alters Kv2.1 activation and recovery properties. This mechanism has been proposed to exert a modulatory effect on cellular excitability and AP firing (Dai et al, 2009). Kv1.5 is a voltage-gated potassium channel that mediates the

ultra-rapid delayed rectifier ( $I_{kur}$ ) current in human atrial myocytes (Wang et al, 1993). This channel harbors a conserved SUMOylation motif ( $\Psi$ -K-X-E/D), which is essential for SUMOylation transferred by the E2 enzyme Ubc9. The consequence of Kv1.5 modification is a biophysical alteration of Kv1.5 steady-state inactivation. However, Kv1.5 current density is unaffected. It was proposed that SUMOylation of Kv1.5 may potentially be involved in regulating the excitability of atrial myocytes (Benson et al, 2007). K2P1, also known as TWIK, is implicated in background membrane potassium conductance. Rajan et al succeeded in recording K2P1 current when a K2P1 mutant (lysine274 substituted by a glutamic acid) was overexpressed in *Xenopus oocytes*. Therefore, they suggested that K2P1 is potentially SUMOylated at a consensus motif, LK274KF (Rajan et al, 2005). By contrast, another group showed that K2P1 current was independent of SUMOylation (Felicangeli et al, 2007). In the above examples, SUMOylation affects the gating properties of these ion channels and down-regulates their activity. This contrasts with the observations on TRPM4 channel, where SUMOylation upregulates TRPM4 activity.

### III AIMS OF STUDY

The role of SUMOylation on ion channels is an emerging area of research. Although data in the literature showed that cardiac ion channels expressed *in vitro* can be regulated by SUMOylation, the role of SUMOylation of cardiac ion channels *in vivo* and its association with cardiac myopathies remain unknown. In this respect, the TRPM4 channel, which is implicated in the regulation of delayed after depolarization of cardiac action potential, offers an interesting opportunity to investigate in details how SUMOylation regulates the activity of a cardiac ion channel.

The specific aims of this study are:

- To study how SUMOylation regulates TRPM4 channel current in stably expressing TRPM4 wild-type and a cardiac conduction disease-related mutant channel cells.
- To investigate the specific localization of TRPM4 channel in plasma membrane and its interaction with other signaling regulators.
- To explore the potential physiological significance of TRPM4 channel in the cardiac conduction system, using a TRPM4 deficient mouse model.

## IV MATERIAL

### IV.1 Buffers and solutions

All the chemicals used in this study were of highest available quality and purchased from Merck (Darmstadt, Germany), Roche (Berlin, Germany), Roth (Karlsruhe, Germany), and Sigma & Aldrich (Munich, Germany) unless mentioned differently. Milli-Q ultrapure water ( $>18\text{M}\Omega\cdot\text{cm}$ ) was used for buffers and solutions preparation.

Name	Composition	
TAE buffer (50X)	Tris-acetate, pH8.0	2 M
	EDTA	100 mM
DNA sample buffer (5X)	Orange G	0.025% (w/v)
	glycerol	20% (v/v)
	in TAE buffer	
Blocking buffer (for immunoblot analysis)	5% (w/v) skimmed milk powder (Frema Reform) in PBS	
Phosphate buffered saline (PBS) pH7.4	NaCl	136 mM
	Na <sub>2</sub> HPO <sub>4</sub>	10 mM
	KCl	2.7 mM
	KH <sub>2</sub> PO <sub>4</sub>	1.8 mM
PBST (for immunoblot analysis)	PBS added with 0.05 % (v/v) Tween-20	
Lysis buffer (pH7.4)	Hepes	20mM
	EDTA	5mM
	NaCl	150mM
	Triton X-100	0.5~1%
	SDS	0.05~0.1%
Wash buffer (for Co-IP assay)	Tris.HCl (pH 7.9)	50mM
	NaCl	150mM
	MgCl <sub>2</sub>	5mM
	Triton-X 100	0.5%
Acid elution buffer (pH2.5)	Na-Citrate Buffer	0.1M
Neutralize buffer (pH8.7)	Tris.HCl	1M
Strip buffer (for Immunoblot analysis)	10% (w/v)SDS	3ml
	β-mercaptoethanol	117μl
	H <sub>2</sub> O	10.9ml
	Tris.HCl pH 7.4	975ul

Na <sub>2</sub> CO <sub>3</sub> -based Lysis buffer (for lipid raft isolation)	Na <sub>2</sub> CO <sub>3</sub> 0.5M added with 1% Protease Inhibitor Amplex (PIM (Sigma), pH about 11)
MBS buffer (for lipid raft isolation)	2-(N-Morpholino)ethanesulfonic acid 4-Morpholineethane, MES 25mM, NaCl 150mM, pH 6.5 adjusted with NaOH
90% sucrose buffer	90% sucrose in MBS buffer(w/v)
35% sucrose buffer	35% sucrose in MBS buffer with 250mM Na <sub>2</sub> CO <sub>3</sub> (w/v)
5% sucrose buffer	5% sucrose in MBS buffer with 250mM Na <sub>2</sub> CO <sub>3</sub> (w/v)

## IV.2 Primary antibodies

Name	Description and working condition
Anti-Myc	Rabbit polyclonal antibody (Abcam, ab9106), 1.000mg/ml, raised against EQKLISEEDL (C-Myc) conjugated with KLH.
Anti-Myc	Rabbit affinity isolated antibody (Sigma, C3956), raised against a peptide corresponding to amino acids 408-425 of the human <i>c-myc</i> proto-oncogene, conjugated to maleimide-activated KLH through a C-terminal added cysteine residue.
Anti-adaptin $\beta$ (AP2)	Mouse IgG1 monoclonal antibody (BD Transduction Laboratories, 610381), raised against amino acids 75-245 of the human adaptin $\beta$ .
Anti-caveolin-1	Mouse monoclonal antibody (Abcam, ab17052), raised against GLUT4-containing vesicles immunoadsorbed from low density microsomes of rat adipocytes (Sprague Dawley).
Anti-caveolin-1	Rabbit affinity isolated antibody (Sigma, C4490), raised against synthetic peptide corresponding to a region at the N-terminus of human caveolin-1 (amino acids 2-20).
Anti-caveolin-3	Mouse IgG1 monoclonal antibody (BD Transduction Laboratories, 610420), raised against amino acids 3-24 of rat caveolin-3.
Anti-caveolin-3	Rabbit polyclonal antibody (Abcam, ab2912), raised against synthetic peptide (MMTEEHTDLEARIIKDIH-C) corresponding to amino acids 1-18 of rat caveolin-3.
Anti-SUMO-1	Mouse IgG1-Kappa antibody (Invitrogen, 33-2400), raised against full-length recombinant SUMO-1.

---

Anti-SUMO-1	Rabbit IgG antibody (Sigma, S8070), raised against a synthetic peptide corresponding to amino acids 1-16 located at the N-terminus of human SUMO-1 conjugated to KLH.
Anti-pan SUMO	Rabbit polyclonal antibody (Abgent, AP1299a), raised against a recombinant protein encoding full length of human SUMO1. It recognizes all 3 SUMO isoforms, immunoblotting 1:1000 in blocking buffer.
Anti-SUMO2/3(FL-103)	Rabbit polyclonal antibody (Santa Cruz, SC-32873), raised against amino acids 1-103 representing full length SUMO-2 of human origin.
Anti- $\alpha$ -Na <sup>+</sup> /K <sup>+</sup> ATPase	Rabbit monoclonal antibody (Abcam, ab76020), raised against a synthetic peptide corresponding to residues near the N terminus of human Sodium Potassium ATPase.
Anti- $\alpha$ 1- Na <sup>+</sup> /K <sup>+</sup> ATPase	Mouse IgG1 fraction (Abcam, ab7691), raised against purified full length native protein (rabbit renal outer medulla).
Anti- $\alpha$ -Na <sup>+</sup> /K <sup>+</sup> ATPase	Mouse monoclonal antibody (Santa Cruz, sc-48345), raised against amino acids 551-850 mapping within an internal region of Na <sup>+</sup> /K <sup>+</sup> ATPase $\alpha$ of human origin.
Anti-TRPM4	Sheep polyclonal antibody (Thermo Scientific Pierce Products, OST00027W), raised against a synthetic peptide corresponding to a portion of rat and mouse transient receptor potential cation channel subfamily M member 4 (TRPM4) conjugated to immunogenic carrier protein.
Anti-Flotillin-1	Mouse IgG1 monoclonal antibody (BD Transduction Laboratories, 610821), raised against amino acids 312-428 of the mouse flotillin-1.
Anti-GAPDH	Mouse IgM monoclonal antibody (Sigma, G8795), raised against GAPDH from the rabbit.
Anti-Actin	Rabbit affinity isolated polyclonal antibody (Sigma-Aldrich, A 2066), raised against C-terminal actin fragment (C11 peptide attached to Multiple Antigen Peptide (MAP) backbone).
Anti-GFP	Mouse IgG2a monoclonal antibody (NeuroMab, clone N86/8), raised against fusion protein amino acid 1-238 (full length) of jellyfish green fluorescent protein.
IgG, rabbit	IgG from rabbit serum (Sigma-Aldrich)
IgG, mouse	IgG from mouse serum (Sigma-Aldrich)

---

### IV.3 Secondary antibodies

Secondary antibodies were purchased from Jackson ImmunoResearch laboratories (Danova, Hamburg, Germany). The antibodies were coupled to horse radish peroxidase (HRP) and purified by immunoaffinity chromatography. To analyze immunoblot of co-immunoprecipitation samples, preabsorbed antibodies were used to minimize cross-reactions to serum proteins of other species. The antibodies were used in dilutions of 1:5,000 or 1:10,000 in blocking buffer containing 0.05% Tween-20. Fluorescence 488-, Cy3- (or 546-) coupled secondary antibodies from Jackson ImmunoResearch Laboratories were used in a dilution of 1:500~1:1000 for immunocytochemistry.

### IV.4 DNA and protein standards

DNA/protein standards were used to indicate the molecular weight for electrophoresis.

Name	Company
1 kb DNA Ladder	Invitrogen
Novex® Sharp Pre-stained protein Standards (12 bands of 3.5-260 kDa, prestained in blue and red)	Invitrogen

### IV.5 Plasmids

pcDNA3	Invitrogen Inc., USA	mammalian expression vector, Ampicillin resistance
pGEM	Promega, USA	vector for subcloning of PCR amplified DNA fragments via T/A cloning. Ampicillin resistance

The following cDNAs were cloned into pcDNA3-vector: human TRPM4 (kindly provided by A. Guse, University Hospital Hamburg-Eppendorf), GFP-SUMO-3 (kindly provided by M.Schachner, Center for Molecular Neurobiology Hamburg), SENP1 and SENP1C603S

(kindly provided by P. O' Hare, Marie Curie Research Institute, Oxford) and HA-Ubc9 (kindly provided by S. Mueller, Max-Planck-Institute of Biochemistry). pCMV6 vector containing caveolin-1-GFP, caveolin-3-GFP, PIAS3 were purchased from Origene (USA).

Mutant and Myc-tagged hTRPM4-cDNAs were obtained by in vitro mutagenesis using the QuickChange® II site-directed mutagenesis kit (Stratagene, Amsterdam Netherland). Mutant cDNA clones were systematically sequenced before used in further experiments.

## IV.6 Bacterial strains

The following chemically competent bacterial strains were used for transformation with plasmid DNA.

Name	Description	Company
Escherichia coli DH5 $\alpha$	F- $\phi$ 80dlacZ $\Delta$ M15 $\Delta$ (lacZYA-argF)U169 deoR recA1 endA1 hsdR17(rk $^{-}$ ,mk $^{+}$ ) phoA supE44 $\lambda$ - thi-1 gyrA96 relA1	New England Biolabs
Escherichia coli Top10 cells	F- mcrA D(mrr-hsdRMS-mcrBC) f80lacZDM15 DlacX74 deoR recA1 araD139 D(ara-leu)7697 galU galK rpsL (StrR) endA1 nupG	Invitrogen

## IV.7 Bacterial media

Bacterial media were autoclaved and antibiotics were supplemented prior to use.

Name	Composition
LB-medium	10 g/l bacto-tryptone
pH 7.4	10 g/l NaCl 5 g/l yeast extract Antibiotic: 100 mg/l ampicillin
LB-agar	20 g/l agar in LB-medium Antibiotic: 100 mg/l ampicillin

## IV.8 Cell culture medium and materials

Sterile polystyrene cell culture plates and flasks were purchased from Greiner Bio-One GmbH. The material was free from heavy metal, non-pyrogenic and non-cytotoxic.

Name	Composition
Trypsin/EDTA (1:250)	0.5 mg/ml trypsin, 0.22 mg/ml EDTA, without $\text{Ca}^{2+}$ and $\text{Mg}^{2+}$ (PAA Laboratories)
HEK 293 cell Medium	DMEM/hanks without L-glutamine (PAA Laboratories), supplemented with: 10 % (v/v) Fatal calf serum (FCS) (PAA Laboratories) and 2mM L-glutamine (Invitrogen)
Flp In™ 293 cell Medium	Add 100µg/ml Zeocin (Invitrogen) in HEK 293 cell growth medium
TRPM4 Flp In cell Medium	Add 100µg/ml Hygromycin (Invitrogen) in HEK 293 cell growth medium
cell freezing medium	90 % (v/v) Fatal calf serum (FCS) (Invitrogen) and 10 % (v/v) DMSO (Sigma)

Patch clamp solutions:

Name	Composition
Bath Solution (Also used for $\text{Ca}^{2+}$ imaging of Flp In cells) pH 7.2	NaCl 156m CaCl <sub>2</sub> 5mM Hepes 10mM Glucose 10mM
Pipette Solution pH 7.4 (Free $\text{Ca}^{2+}$ in the pipette solution was 0.02 and 5.4µM by addition of CaCl <sub>2</sub> . $\text{Ca}^{2+}$ concentrations were measured with the $\text{Ca}^{2+}$ -sensitive dye Fluo4FF (Molecular Probes))	CsCl 156mM MgCl <sub>2</sub> 1mM EGTA 10mM Hepes 10mM
Pipette Solution (Resting membrane potential measurements) pH7.2 with KOH	KCl 140mM MgCl <sub>2</sub> 2mM CaCl <sub>2</sub> 1mM EGTA 2.5mM Hepes 10mM

## Solutions for cardiomyocytes isolation and culture:

Name	Composition	
Perfusion buffer pH 7.2 at 37°C	NaCl	135mM
	KCl	4mM
	MgCl <sub>2</sub>	1mM
	NaH <sub>2</sub> PO <sub>4</sub>	0.33mM
	Hepes	10mM
	Taurine	5mM
	Glucose	10mM
	BDM	10mM
Transfer buffer A pH 7.2 at 37°C	NaCl	135mM
	KCl	4mM
	MgCl <sub>2</sub>	1mM
	NaH <sub>2</sub> PO <sub>4</sub>	0.33mM
	Hepes	10mM
	Glucose	5.5mM
	BDM	10mM
	BSA	5mg/ml
Transfer buffer B pH 7.4 at 37°C	NaCl	137mM
	KCl	5.4mM
	CaCl <sub>2</sub> .2H <sub>2</sub> O	1.8mM
	MgCl <sub>2</sub>	0.5mM
	Hepes	10mM
	Glucose	5.5mM
Transfer buffer for use	0.06mM Ca <sup>2+</sup>	14.5mL A+ 0.5mL B
	0.24mM Ca <sup>2+</sup>	6.5mL A+ 1mL B
	0.60mM Ca <sup>2+</sup>	6mL A+ 3mL B
	1.20mM Ca <sup>2+</sup>	3mL A+ 6mL B
Culture medium (Filter and equilibrated in a 2%CO <sub>2</sub> culture incubator at 37°C for at least 2h prior to use )	MEM	9.3325mL
	BSA (100mg/mL)	0.01mL
	Pen/Strep	0.1mL
	500mM BDM	0.2mL
	Insulin (1mg/ml)	0.1mL
	Transferrin (1mg/ml)	0.055mL
	Na-selenite (6μM-Stock)	0.1mL
	Na-ascorbat (1mg/ml ascorbic acid)	0.0025ml
Heparin solution	16μl Heparin-Stock (250.000 iU/10mL) dissolved in 384μl PBS. Each mouse was injected 200μl.	
Enzyme buffer	34.5mL Perfusion buffer mixed with freshly prepared 0.5ml Liberase TM (5mg/mL in H <sub>2</sub> O)	

## IV.9 Inhibitors

Name	Function	Working Concentration
M $\beta$ CD	Cholesterol-depletion	5mM 30min at 37°C
Ouabain	Na, K-ATPase inhibitor	10 or 30 $\mu$ M for cardiomyocyte 100 $\mu$ M for TRPM4 Flp In cells
KB-R7943	Inhibitor of reverse mode of Na, Ca-exchanger	2 $\mu$ M for cardiomyocyte

## IV.10 Mouse strain

In this study, adult Myc-tagged TRPM4 knock in mice from our lab (generated by Frederik Flenner and Transgenic facility in ZMNH), TRPM4 deficient (TRPM4  $-/-$ ) mice kindly provided by Prof. Freichel (Universität Heidelberg) were utilized. In TRPM4  $-/-$  mice, Cre-loxP strategy was used to excise exons 15 and 16, which encode the first transmembrane-spanning domain of TRPM4. TRPM4  $-/-$  mice were viable and fertile, showed no obvious anatomical abnormalities, and were segregated with the expected mendelian frequency (Vennekens et al., 2007). All strains were repeatedly back-crossed into a C57BL/6J genetic background. TRPM4 wild type (TRPM4  $+/+$ ) animals from the same strain and breeding unit were used as controls. The genotype of mutant and wild-type mice was determined using polymerase chain reaction (PCR) with template DNA isolated from tails.

Mice were kept under a standard 12h/12h (light/dark) cycle with food and water *ad libitum*. They were housed under specific pathogen free conditions, at a temperature of 19-25 °C and a humidity of 45-60%. All experiments were conducted in accordance with the national law and guidelines (Animal Welfare Committee of the University of Hamburg and University of Saarland).

## V METHODS

### V.1 Molecular biological methods

#### V.1.1 Molecular cloning

To generate the expression constructs encoding the full length hTRPM4–myc mutations, QuickChange® II XL-Site-Directed Mutagenesis kit from Agilent Technologies was used.

##### V.1.1.1 Site directed mutagenesis

Primers are designed according to the DNA sequence of pcDNA3-hTRPM4-wt-myc.

TRPM4 Mutation	Primer	DNA sequence
S255A	Forward	5'-CTTGCGCCTGGAGGCCTACATCTCACAGC-3'
	Reverse	5'-GCTGTGAGATGTAGGCCTCCAGGCGCAAG-3'
S255D	Forward	5'-CTTGCGCCTGGAGGACTACATCTCACAGC-3'
	Reverse	5'-GCTGTGAGATGTAGTCCTCCAGGCGCAAG-3'
F223A	Forward	5'-CCGGAGGACGGGGTCCAGGCTCCCCTGGACTACAACACTAC-3'
	Reverse	5'-GTAGTTGTAGTCCAGGGGAGCCTGGACCCCGTCCTCCGG-3'
F232A	Forward	5'-CTACAATACTCGGCCGCTTCCTGGTGGACGACG-3'
	Reverse	5'-CGTCGTCCACCAGGAAGGCGGCCGAGTAGTTGTAG-3'
K341A	Forward	5'-CAGGCGTTTTCTTTCCCGCAGGGGACCTTGAGGTCC-3'
	Reverse	5'-GGACCTCAAGTCCCCTGCGGGAAAGAAACGCCTG-3'
K492N	Forward	5'-CAAAGCCCCAGCCCTAAATGGGGGAGCTGCGGAGC-3'
	Reverse	5'-GCTCCGCAGCTCCCCATTTAGGGCTGGGGCTTTG-3'
K618A	Forward	5'-GAGGAAAGACCTGGCGTTCGCGTTTGAGGGGATGG-3'
	Reverse	5'-CCATCCCCTCAAACGCGAACGCCAGGTCTTTCCTC-3'
K1140A	Forward	5'-TGGCACGCGCTAGGGACGCGCGGGAGAGCGACTCCG-3'

	Reverse	5'-CGGAGTCGCTCTCCCGCGCGTCCCTAGCGCGTGCCA-3'
K1154A	Forward	5'-AACGCACGTCCCAGGCGGTGGACTTGGCACTGAAAC-3'
	Reverse	5'-CGGAGTCGCTCTCCCGCGCGTCCCTAGCGCGTGCCA-3'

The reaction mixture:

Component	Amount per reaction
H <sub>2</sub> O	37.5 µl
10x Reaction buffer	5µl
dNTP mix	1µl
QuickSolution reagent	3µl
100ng/µl primer forward primer	1.25µl
100ng/µl primer reverse primer	1.25µl
10 ng/µl template DNA	1µl
Pfu Ultra HF DNA polymerase	1µl

#### V.1.1.2 PCR program

Cycles	Temperature	Time
1	95°C	1 min
18	95°C	50 sec
	60°C	50sec
	68°C	9 min 45 sec
1	68°C	7 min
1	4°C	∞

Add 1 µl of Dpn I to the reaction tube and mix it gently. Afterwards spin it down for 1min and incubate the reaction mixture at 37 °C for 1 hour. .

## V.1.2 Transformation of bacteria

After a 10 min treatment with 2  $\mu$ l  $\beta$ -Mercaptoethanol, 45  $\mu$ l ultra-competent cells (*E. coli*) were mixed with 2  $\mu$ l of Dpn I-treated DNA and incubated on ice for 10 min. Then the heat shock (42  $^{\circ}$ C for 30 s) followed by chilling on ice (for 2 min) was performed. After 1 hour incubation at 37  $^{\circ}$ C with 500  $\mu$ l of NZY+ Broth medium in shaking incubator, 250  $\mu$ l of transformed bacteria were plated on LB agar plates containing the appropriate antibiotics.

## V.1.3 Purification of plasmid DNA

### V.1.3.1 Small scale plasmid DNA purification

3 ml LB medium containing appropriate selective antibiotic (100  $\mu$ g/ml ampicillin) was inoculated with a single colony and incubated overnight at 37  $^{\circ}$ C with vigorous shaking (225 rpm). Each clone was also plated on a selective plate with appropriate selective antibiotic. Then bacteria were harvested by centrifugation at 11,000 g for 3 min at room temperature. The plasmid was isolated according to the manufacturer's instructions of the NucleoSpin Plasmid QuickPure Kit (Macherey-Nagel) and eluted by 40  $\mu$ l of 10mM Tris.HCl (pH 8.0)

### V.1.3.2 Large scale plasmid DNA purification

A culture of 50 ml LB medium containing appropriate selective antibiotic (100  $\mu$ g/ml ampicillin) was inoculated with a single colony from the isolated clones and incubated overnight at 37  $^{\circ}$ C with vigorous shaking (120rpm). Then bacteria were harvested by centrifugation at 6,000 g for 15 min at 4  $^{\circ}$ C. The plasmid was isolated according to the manufacturer's instructions of the NucleoBond<sup>®</sup> PC 100 plasmid purification Kit (Macherey-Nagel) and eluted by 50  $\mu$ l of 10mM Tris.HCl (pH 8.0).

### V.1.3.3 Determination of DNA concentration

DNA concentration was determined spectroscopically by Amersham-Pharmacia

spectrometer, which measures the absorbance at 260nm, 280nm and 320nm. Absorbance at 260nm was between 0.1 and 0.6 for reliable determinations by appropriate dilution of DNA. The ratio of the DNA absorbance at 260nm and 280nm was used to monitor the purity of DNA. A ratio of A<sub>260</sub>/A<sub>280</sub> between 1.8 and 2.0 indicated sufficient purity of DNA for further experiments.

#### V.1.3.4 Sequencing of DNA

DNA sequencing was performed by the sequencing facility of the ZMNH, Hamburg. For preparation, 0.5 µg of DNA was diluted in distilled water along with 1 µl sequencing primer (10 pmol/µl). The final volume was 8 µl.

#### V.1.4 Restriction digestion of DNA

The mutations (See Methods V.1.1.1) were inserted into a new vector of pcDNA3-TRPM4-wt-Myc to avoid other mutations made by PCR. Therefore a part of the new clone including the mutation and the vector was digested into different fragments by restriction enzymes. All restriction digestions were made using restriction enzyme in accordance with the Fermentas catalogue and technical reference.

#### V.1.5 Horizontal agarose gel electrophoresis of DNA

To determine the purity of DNA, the horizontal agarose-gel electrophoresis was used. 1% (w/v) agarose gels with 0.57 µg/ml ethidiumbromide was prepared in 1xTAE buffer. The DNA-sample buffer was added to the DNA samples, before they were loaded on the gel. Load DNA samples to the gel and run the gel at the constant voltage. In case the DNA fragment of interest was needed for further cloning, it was cut out for purification and processed using protocol V.1.6.

## V.1.6 Gel purification and Ligation

The DNA was purified according to the manufacturer's instructions of the illustrate GFX PCR DNA and Gel Band Purification Kit (GE Healthcare). The ligation was performed according to the manufacturer's instructions of the Rapid DNA Ligation kit (Roche). Afterwards, the product was transformed into bacteria. The new construct was purified and sequenced to make sure no new unexpected mutation happen.

## V.2 Protein biochemical methods

### V.2.1 SDS-PAGE electrophoresis

#### V.2.1.1 Determination of protein concentration

For the determination of the protein concentration, the Pierce<sup>®</sup> BCA Protein Assay Kit (Pierce Biotechnology, USA) was used. 25  $\mu$ l samples were placed on a microplate and incubated for 30 min at 37  $^{\circ}$ C with 200  $\mu$ l of the solution which was prepared according to the kit manual. BSA standards ranging from 62.5  $\mu$ g/ml to 1000  $\mu$ g/ml were simultaneously incubated. Samples and standards were analyzed in triplicate. Copper ions in the reagent are reduced by proteins in the sample proportional to the amount of protein. The reduced copper ions form a purple colored complex with bicinchoninic acid (BCA). Its absorbance was measured at 562 nm using the  $\mu$ Quant Microplate spectrophotometer (BioTek Instruments Inc., Winooski, Vermont, USA, KC junior software). Protein concentration was then determined by correlating the relative absorbance to the BSA standards.

#### V.2.1.2 SDS-PAGE

Proteins were separated by discontinuous SDS-PAGE using an *Xcell SureLock Mini-Cell* chamber (Invitrogen Inc., USA). The chamber was assembled according to the manufacturer's protocol. Protein samples were diluted with appropriate amount of 4X SDS sample buffer followed by heating for 10 minutes at 70  $^{\circ}$ C and a suitable amount of total

protein of each sample was loaded per well. Run the gel at constant voltage of 120 V for 20 min and then 150 V until the bromphenol blue line migrated to the bottom of the gel. Gel was subjected to immunoblot analysis.

## V.2.2 Immunoblot analysis

### V.2.2.1 Electrophoretic transfer of proteins

Proteins were transferred from SDS-polyacrylamide gel onto a *Protran*<sup>®</sup> *nitrocellulose Transfer membrane* (Schleicher & Schuell, Deutschland) using a *Mini Transblot*<sup>®</sup>-*apparatus* (Bio-Rad Inc., USA). After equilibration of the polyacrylamide gel in transfer buffer for approximately 5 minutes, a blotting “sandwich” was assembled as described in the manufacturer’s protocol. Proteins were transferred at 4 °C in transferring buffer at constant voltage or current (100 V for 2 h or 40 mA overnight).

### V.2.2.2 Immunochemical detection of transferred proteins

After electrophoretic transfer, the nitrocellulose membranes were removed from the blotting sandwiches and placed protein-bound side-up in glass vessels. Membranes were washed once in PBST for 5 minutes and were subsequently blocked for 1 h in blocking buffer under gentle shaking at room temperature. Incubation with an appropriate antibody diluted in blocking buffer, was performed overnight at 4 °C on a shaking platform or 2h at room temperature. The primary antibody solution was removed and membranes were washed 3 x 5 min with PBST under constant shaking. The appropriate horseradish peroxidase (HRP)-conjugated secondary antibody was applied in blocking buffer with 0.05% Tween-20 for 40 minutes at room temperature, followed by washing with PBST 4 X 10min. Immunoreactivity was visualized by *SuperSignal West Dura Chemiluminescent Substrate* (Thermo Fisher Scientific,. USA). The membrane was covered with detection solution (1:1 mixture of solution I and II) for 2 min, and placed between two plastic foils and exposed to X-ray film (Kodak Biomax-XL, Sigma-Aldrich) for various time periods followed by development and fixation of film. Alternatively, the membrane can be exposed under LAS-4000 imaging

---

system (Fujifilm, USA) for various time periods to achieve a linear and sensitive exposure.

#### V.2.2.3 Densitometric evaluation of band density

Chemiluminescence was quantified using the image processing software Image J (NIH,USA) .The film was scanned and the digitized picture was exported to the image processing program. The quantified data was analyzed using Microsoft Excel software.

#### V.2.2.4 Stripping and re-probing of immunoblot

For detection of an additional protein on the immunoblot, the nitrocellulose membranes were stripped from bound antibodies by shaking blots in stripping buffer for 50 minutes at 50 °C then wash 3 x 5 min with PBST, subjected to re-probing.

#### V.2.2.5 Co-immunoprecipitation

For co-immunoprecipitation experiments, samples containing 1 mg of total protein were lysed with cold lysis buffer, containing 1% protease inhibitor cocktail (PIM, Sigma) and 20mM N-Ethylmaleimide (NEM), for 30min at 4 °C. Lysates were centrifuged for 5 min at 3,000 g at 4 °C. Supernatants were pre-cleared with protein A / G-agarose beads (Dynabeads® protein G, Invitrogen) for 2 h at 4 °C to reduce unspecific binding. Afterwards, beads were removed by magnetic stack. The supernatant was incubated with the corresponding antibodies or non-specific IgG overnight at 4 °C, followed by precipitation with protein A / G-agarose beads for 3 h at 4 °C. The beads were pelleted and washed 5 times with wash buffer. The proteins were finally eluted from beads with 34.8µl pH 2.5 Sodium-Citrate buffers and then immediately neutralized with 14µl 1M pH8.7 Tris.HCl buffer. The eluted solutions were heated in 70 °C with 4X LDS buffer (Invitrogen Inc., USA) and 10X Reducing buffer (Invitrogen Inc., USA) for 10min and then were analyzed by immunoblotting. Alternatively, the proteins can be directly eluted in 70 °C with 4X LDS buffer (Invitrogen Inc., USA) and 10X Reducing buffer (Invitrogen Inc., USA).

### V.2.3 Lipid-raft fractionation

#### V.2.3.1 Non-detergent-based isolation of lipid rafts from total lysate of TRPM4 Flp In cells

TRPM4 Flp In cells were cultured in DMEM medium supplemented with 10% (v/v) FCS and 1% penicillin/Streptomycin. Before using, put flasks in 4 °C for 30min .Wash cells with cold PBS twice to remove the medium, add ice cold 0.5M Na<sub>2</sub>CO<sub>3</sub> buffer containing protease inhibitor cocktail (Sigma), and rotate in 4 °C for 30min.Cells were further disrupted by repeated aspiration through 23 gauge needle. Pellet cellular debris by centrifugation at 3000 g for 5 min at 4 °C and supernatant was taken for following steps (Song et al, 1996a).

Make the homogenate up to 45% sucrose by the addition of an equal volume of ice cold 90% sucrose in MBS buffer and load the resulting 4mL into a thin-walled ultracentrifuge tube .Overlay the sample with 4mL of 35% sucrose prepared in MBS buffer with 250-mM Na<sub>2</sub>CO<sub>3</sub> and then 4mL of 5% sucrose again prepared in MBS with 250mM Na<sub>2</sub>CO<sub>3</sub>.

Separate the buoyant and the non-buoyant membrane fractions by centrifugation of the sucrose gradient at 28000 RPM for 18h at 4 °C using an ultracentrifuge (Surespin 630) equipped with swing-out rotor.

By carefully placing a pipette tip just under the surface at the very top of the gradient, collect consecutive 1-mL fractions and place these in pre-labeled tubes on ice. If the centrifuge tube is held up to light, the buoyant, cholesterol-enriched membranes are sometimes visible as a milky, light scattering band at the 5~35% sucrose interface. Store the fractions at -20 °C until required for SDS-PAGE or cholesterol/protein assay.

#### V.2.3.2 Detergent-based isolation of lipid rafts from total lysate of TRPM4 Flp In cells

The protocol is similar to V.2.3.1, except that the lysis buffer is replaced by ice cold MBS buffer containing 1% Triton X-100. And sucrose was dissolved in MBS buffer without 250mM

---

Na<sub>2</sub>CO<sub>3</sub> to generate concentration of 90%, 35%, 5%.

#### V.2.3.3 Non-detergent-based isolation of lipid rafts from membrane lysate of Myc-tagged TRPM4 knock-in mouse

Heart was cut from adult Myc-tagged TRPM4 knock-in Mouse, washed in cold TE buffer containing 1% PIM to remove blood and tissue as much as possible. Cut heart into small pieces and homogenized for 1min in ice. Collect supernatant after 1000g 10min and further high speed centrifuge at 35000rpm for 30 min at 4°C. Discard supernatant (cytosolic part), and dissolve pellet in 0.5M Na<sub>2</sub>CO<sub>3</sub> plus 1% PIM. Further centrifuge 3000g 5min to remove undissolved part, and remaining supernatant were processed as described in Methods V.2.3.1.

#### V.2.3.4 Cholesterol assay

Cholesterol levels in each fraction can be quantified according to fluorometric kit-based protocol by using Amplex Red Cholesterol Assay Kit (Molecular Probes). Measure the fluorescence in a fluorescence microplate reader using excitation in the range of 530-560 nm and emission detection at -590 nm.

### V.3 Cell biological methods

#### V.3.1 Cell culture

##### V.3.1.1 Maintenance of HEK 293 cells and Flp In cells

HEK 293 cells were either grown in 75 cm<sup>2</sup> flasks (Greiner Bio-One) with 20 ml cell growth medium or 25 cm<sup>2</sup> flasks (Greiner Bio-One) with 5 ml cell growth medium or six-well plates (d=35 mm; area=9.69 cm<sup>2</sup>, Greiner Bio-One) with 2 ml medium under constant conditions at 37 °C, 5 % CO<sub>2</sub> and 90 % relative humidity. Cells were passaged as they reached confluence after 3-5 days. The medium was removed and the cell layer was detached by trypsin/EDTA treatment for 5 min at 37 °C. Detached cells were suspended in fresh medium. For

maintenance, cells were split 1:5 in fresh medium and seeded in new flask or six-well plates.

### Cryopreservation

The cell layer was trypsinized and collected in cell growth medium. The cell pellet, obtained by centrifugation at 1000 RPM for 5 min at room temperature, was suspended in freezing medium containing 90% FCS and 10% DMSO and transferred into cryotubes (Biochrom). The cryotubes were frozen in a -80 °C freezer. After at least 24 h; the cryotubes were removed from the freezing container and stored at liquid N<sub>2</sub>.

To culture cryopreserved cells, thawed cell solutions from 37 °C water bath were immediately diluted with pre-warmed medium without antibiotics, centrifuge at 1000 RPM for 5 min at room temperature. Discard supernatants and suspended pellets with pre-warmed medium and then transfer them into flasks. When cells attached to the bottom of flask, medium was replaced by fresh medium on the following day.

#### V.3.1.2 Transient transfection

Cells were transfected using the Lipofectamine 2000 reagent (Invitrogen). Transfection was performed according to the manufacturer's protocol. One day prior transfection, cells were seeded in six-well plates or 25/75 cm<sup>2</sup> flasks. When cell density reached 60-80%, the cells were ready for transfection. Specific amount of DNA and Lipofectamine 2000 reagent (1:2-1:4) were used to form DNA-lipid complexes in serum free Opti-MEM (GIBCO). After at least 20min incubation, the DNA-lipid complexes were added to six-well plates or 25/75 cm<sup>2</sup> flasks. The DNA-lipid complexes solution was replaced by medium without antibiotics after 4-6h incubation. After 24 h post-transfection cells were ready for biochemical analysis or electrophysiology measurement.

#### V.3.1.3 Generating TRPM4 stably-expressing cell line

Flp-In<sup>TM</sup>-293 cells stably express the *lacZ-Zeocin*<sup>TM</sup> fusion gene from pFRT/*lacZeo* were co-transfected with pcDNA5/FRT expression vector containing full length

Myc-tagged-hTRPM4 and pOG44 using Lipofectamine 2000 reagent according to the manufacturer's instructions. pOG44 Vector is a plasmid for expression of Flp recombinase in mammalian cells. Flp recombinase catalyzes the integration of the Myc-tagged TRPM4 gene into the genome of Flp-In-HEK cells at the FRT (Flp recombination target) site to generate a stably expressing cell line. Successful integration confers resistance to Hygromycin B. After 24h post-transfection, cells were selected in the medium with 200 µg /ml Hygromycin B (Invitrogen) for 3 to 4 weeks. Single clones were selected and verified by immunoblot analysis and current density measured via whole-cell patch clamp. The cell clone which stably express Myc-tagged TRPM4 was named TRPM4 Flp In cell, and clone which stably express Myc-tagged TRPM4<sup>R164W</sup> was named TRPM4<sup>R164W</sup> Flp In cells.

### V.3.2 FACS analysis

TRPM4 Flp In cells or mock Flp In cells transfected with agent using Lipofectamine 2000 (Invitrogen, USA) grown in 6-well plates. Cells were harvested by Accutase (PAA Laboratories GmbH), washed once by cold PBS and resuspended at a density of  $1 \times 10^6$  cells/ml in FACS buffer (PBS plus 1% BSA). Cells were stained with FITC-coupled Myc-specific antibody (Miltenyi Biotec, Germany) at a dilution of 1:50 for 30 minutes at 4 °C. Subsequently, cells were washed with 1 ml FACS buffer, resuspended in 400 µl FACS buffer, and directly analyzed for FITC fluorescence.

For the analysis of intracellular fluorescence signal, cell suspensions were first fixed in 4% PFA for 10 minutes and permeabilized in PBS containing 0.5% Triton X-100 for 10 minutes at 4 °C. Afterwards, cells were stained as described above.

### V.3.3 Cell surface biotinylation

TRPM4 Flp In cells or HEK 293 cells transfected with agent using Lipofectamine 2000 (Invitrogen, USA) grown in 6-well plates. After washing cells twice with ice-cold PBS, biotinylation was initiated by adding 0.25 mg/ml of EZ-Link Sulfo-NHS-LC-Biotin (Pierce

Biotechnology) and incubated on a shaker for 30 min at 4 °C. Reactions were stopped by adding 50 mM glycine for 10 min at 4 °C. After washing twice with ice cold PBS, cells were scrapped into lysis buffer with 1% PIM. The lysates were put on ice for 30min, centrifuged at 3,000 g for 5 min at 4 °C. To precipitate biotinylated proteins, supernatants containing equal amounts of protein were mixed with 30 µl NeutrAvidin<sup>®</sup> Ultralink<sup>®</sup> Resin (Pierce Biotechnology) and incubated overnight at 4 °C with rotation. After washing 4 times with PBS, the precipitates were heated in 4x SDS sample buffer and 10 x reducing buffer at 70 °C for 10min, subjected to SDS-PAGE and Western-blot analysis. The immunoreactivity of actin or GAPDH was used as control of contamination with intracellular protein.

## V.4 Electrophysiology

### V.4.1 Experimental set up

A conventional patch clamp set up was used for electrophysiological recordings. The petri dish was placed under inverted light microscope Axiovert 25 (Zeiss, Oberkochen, Germany). The patch pipette with a reference electrode was connected to the head stage that was mounted on a micromanipulator Patchman (Eppendorf GmbH, Hamburg, and Germany). Patch pipettes were made of borosilicate capillaries (GB 150F-10, Science products, HARVARD APPARATUS GmbH, Germany) and pulled using an automatic puller (DMZ – Universal Puller, Zeitz, and Augsburg, Germany). Suction system was connected to the chamber to remove the continuous perfusion of the solution. The bath chamber, microscope, micromanipulator and head stage were placed on air table with pressure cylinders to eliminate vibrations. The whole set up was placed in a faraday cage and connected to the ground to reduce electrical noise. Recordings and data acquisition were controlled by an EPC-9 patch clamp amplifier and combined with pulse/pulse fit software (HEKA Electronic, Germany).

## V.4.2 Procedure for whole-cell recording

### V.4.2.1 Whole-cell patch clamp configuration

The patch-clamp technique, first invented by Neher and Sakmann in 1980's (Hamill et al, 1981; Neher & Sakmann, 1992), represents a particular voltage-clamp procedure. The electrical activity of a single ion channel, or the ensemble activity of a large number of channels within a small patch of membrane, or the activity of all channels within a cell can be measured via using various configurations.

The cell-attached configuration is obtained by lowering the tip of the pipette onto the cell followed by the application of negative pressure to the recording pipette to create the gigaohm seal (in the order of  $10^9 \Omega$ , gigaohms). The whole-cell configuration was obtained by applying negative pressure and/or high voltage pulse to the recording pipette after attaining the cell-attached configuration. The whole-cell configuration allows the study of the ensemble response of all ion channels within the cell's membrane..

### V.4.2.2 Electrode

Recording patch pipettes were capillaries made of borosilicate glass, which were pulled and polished with an electrode puller. The pipette resistance was between 2-4 M $\Omega$  when filled with intracellular solution. Because voltage drops proportionally to the series resistances in an electrical circuit, the pipette resistance should ideally be at least two orders of magnitude the cell membrane's resistance after obtaining the whole-cell configuration. Therefore, the pipette series resistance should ideally be below 10 M $\Omega$ . Part of the pipette series resistance can be automatically compensated by the patch-clamp amplifier by increasing the command voltage. The reference electrode consisted of a silver wire with an AgCl pellet which insures a low resistance.

### V.4.2.3 Measurement and data analysis

Whole-cell recordings were performed with an EPC9 patch-clamp amplifier (HEKA Electronic)

---

at a sampling rate of 20 kHz. Patch electrodes had a DC resistance between 2-4 M $\Omega$  when filled with intracellular solution for whole-cell patches. Capacitance and access resistance were monitored continuously, and cell membrane capacitance values were used to calculate current densities. Holding potential was -60 mV, and current traces were elicited by voltage ramps for 250 ms from -120 to +100 mV (Fliegert et al, 2007).

For the measurement of resting membrane potential (RMP), the initial steps are as same as whole-cell patch clamp. After obtaining cell-attached configuration, applying negative pressure and/or high voltage pulse to the recording pipette to disrupt membrane, the mode was switched to current-clamp mode. The RMP was recorded in 0 pA, the mean value of RMP in 1 min was used for analysis.

## V.5 Calcium imaging

### V.5.1 Principle of the method

In this study the dual-wavelength ratio metric dye fura-2 (Grynkiewicz et al, 1985) was used to monitor and measure global changes in the intracellular Ca<sup>2+</sup> concentration ([Ca<sup>2+</sup>]<sub>i</sub>). To load the cells with the dye, the acetoxymethyl (AM) ester form (fura-2AM) of the indicator was used to mask the negatively charged carboxyl groups. After entering the cell, AM esters of the indicator are cleaved by cytoplasmic esterase trapping fura-2 inside the cell and the carboxyl groups are now able to bind Ca<sup>2+</sup> and to trap the fluorescent indicator inside the cell (Kao, 1994).

The Ca<sup>2+</sup>-free and Ca<sup>2+</sup>-bound forms of this dye have emission peaks at two different spectral excitation wavelengths. A Ca<sup>2+</sup> increase causes an increase of emission intensity at 340 nm but a decrease of the emission intensity at 380 nm excitation. Calculating the ratio between the emission intensities at these two excitation wavelengths minimizes artifacts unrelated to changes in [Ca<sup>2+</sup>]<sub>i</sub>, like bleaching.

## V.5.2 Measurement of fura-2 AM fluorescence

Cultured cells were loaded with fura-2 AM (Merck chemicals, Darmstadt, Germany) in the dark for 30min at 37 °C. Fura-2 AM was dissolved in DMSO (stock 1 mM) with 5 µM final concentration in cell culture medium. In order to elicit and monitor the fura-2 fluorescence, a polychromator V (TILL Photonics, Gräfelfing, Germany) and a Sensicam camera (PCO Imaging, Kelkheim, Germany) were used. Images were acquired every 500 ms with 10 ms exposure time using TILLVision software (TILL Photonics). Emission at 510 nm was measured with alternating excitations at 340/380 nm. The experiments were carried out at 35 °C under a water-immersed objective of an Axioskop2 FS plus microscope (Carl Zeiss SMT, Göttingen, Germany). 100 µM Ouabain dissolved in bath solution was perfused at 3 ml/min, finally, 0.5% Triton X-100 in bath solution was perfused to permeabilize cells and achieve maximal  $[Ca^{2+}]_i$ .

## V.5.3 Data analysis

Ratio images (340/380 nm) of matching frames of the two movies were calculated after background subtraction of the fluorescence in an area with no cells and no fura-2AM loaded formations. The ratio fluorescence intensity is called R. The changes in R averaged from the area of individual cells, were analyzed in Igor (WaveMetrics, Lake Oswego, OR). Cytoplasmic  $Ca^{2+}$  is calculated according to this formula,

$$[Ca^{2+}]_i = K_d (R - R_{min}) / (R_{max} - R)$$

$R_{max}$  can be achieved by perfusion cells with 0.5% Triton X-100 to obtain maximal  $[Ca^{2+}]_i$ ,  $R_{min}$  can be achieved by perfusion cells with EGTA/Tris. The maximal  $[Ca^{2+}]_i$  by Ouabain application and  $[Ca^{2+}]_i$  before Ouabain application were used to calculate changed  $[Ca^{2+}]_i$ . Significance was tested by unpaired Student's *t* tests.

---

## V.6 Studies on adult murine cardiomyocytes

### V.6.1 Cardiomyocytes isolation

#### V.6.1.1 Setup procedure

Prior to the isolation, clean and sterilize all dissection tools as well as perfusion buffer, digestion buffer, and transfer buffers. Perfusion buffer and digestion buffer should be equilibrated to 37 °C prior to use. Medium should be equilibrated in a 2% CO<sub>2</sub> culture incubator at 37 °C for at least 2h prior to use.

Clean and sterilize the perfusion system with 50 ml 70% ethanol and then thoroughly rinse with 100 ml sterile water. Finally, prime the perfusion system with 20 ml perfusion buffer for another 5min. Remove any residual air bubbles from system. Switch on water circulator to make sure that buffer coming out of cannula is 37 °C at a constant flow rate of 3 ml/min.

#### V.6.1.2 Heart excision and aorta cannulation

Inject the mouse with 200 IU heparin via i.p (intraperitoneal injection). After 10min, anesthetize the mouse with isoflurane. Once the mouse is fully anesthetized, clip excess animal chest hair and wipe the chest with 70% ethanol. Expose the rib cage, cut the rib cage along the mid-sternal axis using fine surgical scissors and separate the ribs to expose the thoracic cavity. Using fine forceps and surgical scissors lift the heart and cut the aorta 2-3 mm from the aortic valve, freeing the heart from the thoracic cage. Immediately place the heart in a culture dish containing 10 ml pre-chilled perfusion buffer. Make sure that the entire heart and aortic root is entirely submerged to prevent air from entering the aorta. With the aid of a dissection microscope, attach the heart to the perfusion cannula through the aorta, and then firmly tie the aorta to the cannula using suture.

### V.6.1.3 Heart perfusion and mechanical isolation

Connect the cannula with perfusion system, perfuse the heart with perfusion buffer for 5 min and switch to perfusion buffer containing digestion enzyme (Liberase™, Roche, Germany). Following about 8 min of perfusion with the digestion buffer, the heart will become progressively edematous and appear pale and flaccid. Remove the heart from cannula and place in a 60-mm × 15-mm culture dish containing 5 ml room temperature transfer buffer A. All subsequent steps should be performed in a strictly sterile environment under a laminar flow culture hood.

Cut the heart into 4-5 sections and gently tease the tissue apart with forceps, dissociating the cells. Pipette the suspension several times with a sterile plastic transfer pipette to further allow cardiomyocytes dissociation. Transfer the cell suspension to a 50-ml polypropylene conical tube, straining through a 250-µm filter top. Rinse the dish with another 3 ml transfer buffer A and transfer the remaining solution to the same tube. Place the conical tube upright and allow the cells to settle by gravity for 13 min.

Subsequently, collect the cells pellet and transfer to a 15-ml polypropylene conical tube containing 5 ml 0.06 mM calcium transfer buffer. Place the conical tube upright and allow the cells to settle by gravity for 13 min. Again pipette the cell pellet and transfer to next 15-ml polypropylene conical tube containing 5 ml 0.24 mM calcium transfer buffer. Repeat this step using 0.6 and 1.2 mM calcium transfer buffer.

### V.6.2 Cell culture

Finally, transfer the cardiomyocytes pellet from the 1.2 mM calcium transfer buffer to a new 15-ml polypropylene conical tube containing 6ml cell culture medium. Evenly separate them into 6 × 1.5-ml tubes, put into the 2% CO<sub>2</sub> incubator with the lid open.

### V.6.3 Immunocytochemistry

The subcellular localization of TRPM4 channel and Caveolin-3 in cultured cardiomyocyte was examined using immunofluorescence confocal microscopy. Sterile coverslips were firstly coated with 10ug/ml Laminin (Sigma,Germany) in incubator for at least 2h, then washed by sterile PBS. Add freshly dissociated cardiomyocyte into coverslips and incubated in 2% CO<sub>2</sub> incubator for at least 2h.

After at least 2h culture, most of rod-shaped cardiomyocytes were already attached into coverslips. Cells were washed in PBS and fixed in ice-cold 4% formaldehyde plus 4% sucrose in PBS for 15min at RT. After quickly rinsed with PBS for twice, cells were permeabilized in 0.2% Triton plus 0.2% BSA in PBS for 10min at RT. Next, cells are blocked in PBS containing 10% Donkey serum and 0.2% Triton for at least 30min or overnight. After removal of the blocking solution, cells were incubated with primary antibodies diluted in blocking buffer for 1h at RT. Unbound primary antibodies were washed away with PBS for 3 times, 5 minutes each. The secondary antibodies coupled with 488 or Cy3(546) diluted in 0.05% Tween-PBS containing 10% donkey serum were added to cells and incubated for 45min at RT in the dark. Cells were washed 3 times with 0.05% Tween-PBS. Afterwards, DAPI was added to label nuclei for 5 min at RT in the dark, followed by once with PBS. Coverslips were mounted on glass slides with Fluoromount G (SouthernBiotech, USA). Glass slides were stored in darkness at 4°C after they were dry. Photographic documentation was made on confocal laser-scanning microscope (Leica SP2, Leica Microsystem Heidelberg GmbH; Fluroview 1000, Olympus).

### V.6.4 Measurement of cardiomyocyte [Ca<sup>2+</sup>]<sub>i</sub> transients

This part was carried out in Würzburg by Dr. Michael Klaiber (Institut für Physiologie, Universität Würzburg). Adult ventricular myocytes were isolated and whole cell Ca<sup>2+</sup> transients together with simultaneously recorded cell length were measured in INDO-1 loaded electrically paced (0.5 Hz) cardiomyocytes. Excitation was at 365 nm, and the

emitted fluorescence was recorded at 405 and 495 nm. The ratio of fluorescence at the two wavelengths was used as an index of the cytosolic  $\text{Ca}^{2+}$  concentration. Data were collected at 20 Hz, and acquisition and processing were supported by Felix software (Felix version 1.1, Photon Technologies, Seefeld, Germany). After obtaining basal recordings for 10 min, myocytes were sequentially exposed to 10  $\mu\text{M}$  Ouabain, 30  $\mu\text{M}$  Ouabain and 30  $\mu\text{M}$  Ouabain in the presence of 2  $\mu\text{M}$  KB-R7943.

## V.7 Statistical analysis

All data analysis and calculations were performed by using Excel (Microsoft software, USA) and Igor Pro (version 5.0, Wave Metrics, USA). If not otherwise stated; data are expressed as mean  $\pm$  S.E.M and number of observations (n). Statistically significant differences were assessed by unpaired student T-test.

## VI RESULTS

### VI.1 Expression of TRPM4 and TRM4<sup>R164W</sup> channel

Previously, it was shown that mutations associated with idiopathic cardiac conduction disease (PFHBI/ICCD) increase TRPM4 current density in transiently transfected HEK 293 cells. The increase in current density was correlated with an altered sensitivity to enzymes involved in SUMOylation, e.g. the SUMO conjugating enzyme Ubc9 (Ubiquitin- conjugating enzyme 9) and the SUMO-protease SENP1 (Sentrin-specific protease 1). This observation was used to interpret the effect of PFHBI mutations as insensitivity to deSUMOylation associated with impaired endocytosis (Kruse et al, 2009). However, how cardiac ICCD-related mutations affect sensitivity to SUMOylation is still unclear (Liu et al, 2010).

Through targeted site-specific recombination, I generated Flp-In<sup>TM</sup> HEK 293 cell lines stably expressing wild-type TRPM4 channel (TRPM4 Flp In cell) and ICCD-associated mutant TRPM4<sup>R164W</sup> channel (TRPM4<sup>R164W</sup> Flp In cell) (See Method V.3.1). As previously described (Kruse et al, 2009; Liu et al, 2010), a Myc-tag was inserted into an external loop of the TRPM4 protein. The external Myc-tag did not affect TRPM4 channel properties and facilitated detection of TRPM4 protein in immunochemical experiments. A ramp protocol ranging from -120mV to +100mV was used to record TRPM4-mediated current on TRPM4 Flp In cells in the whole-cell patch-clamp configuration (See Method V.4.2). Current traces exhibited a voltage-dependent outward rectification (Fig VI.1A), which is typical for TRPM4-mediated current (Nilius et al, 2003). In agreement with previous transient transfection results (Liu et al, 2010), TRPM4 and TRPM4<sup>R164W</sup> channels responded in an essentially identical manner to change in membrane voltage (Fig VI.1B), but TRPM4<sup>R164W</sup> Flp In cell produced significantly higher TRPM4 current amplitudes than the TRPM4 Flp In cell. TRPM4<sup>R164W</sup> current density ( $82.1 \pm 13.2$  pA/pF at +80mV and  $-22.38 \pm 3.38$  pA/pF at -80mV, n=18) was approximately four-fold higher than TRPM4 current density ( $20.6 \pm 2.5$  pA/pF at +80 mV and  $-5.62 \pm 1.71$  pA/pF at -80mV, n=16; Fig VI.1C).

Next, I investigated whether the increased TRPM4<sup>R164W</sup> current density correlated with an increased amount of TRPM4 protein at the plasma membrane. Membrane proteins were biotinylated, and purified by NeutrAvidin resin (See Method V.3.3). Immunoblots of biotin-labeled surface protein and total lysates showed similar expression level of TRPM4 and TRPM4<sup>R164W</sup> protein (Fig VI.1D and E). Subsequently, I employed FACS analysis to investigate fluorescence intensity of non-permeabilized and permeabilized cells labelled with FITC-coupled anti-Myc antibodies (See Method V.3.2). TRPM4 and TRPM4<sup>R164W</sup> Flp In cells displayed similar mean fluorescence intensities (MFI) of surface and total signal (Fig VI.1F). This data further confirmed that TRPM4 and TRPM4<sup>R164W</sup> Flp In cells have similar TRPM4 protein levels at the surface membrane and in the cytoplasm, respectively.

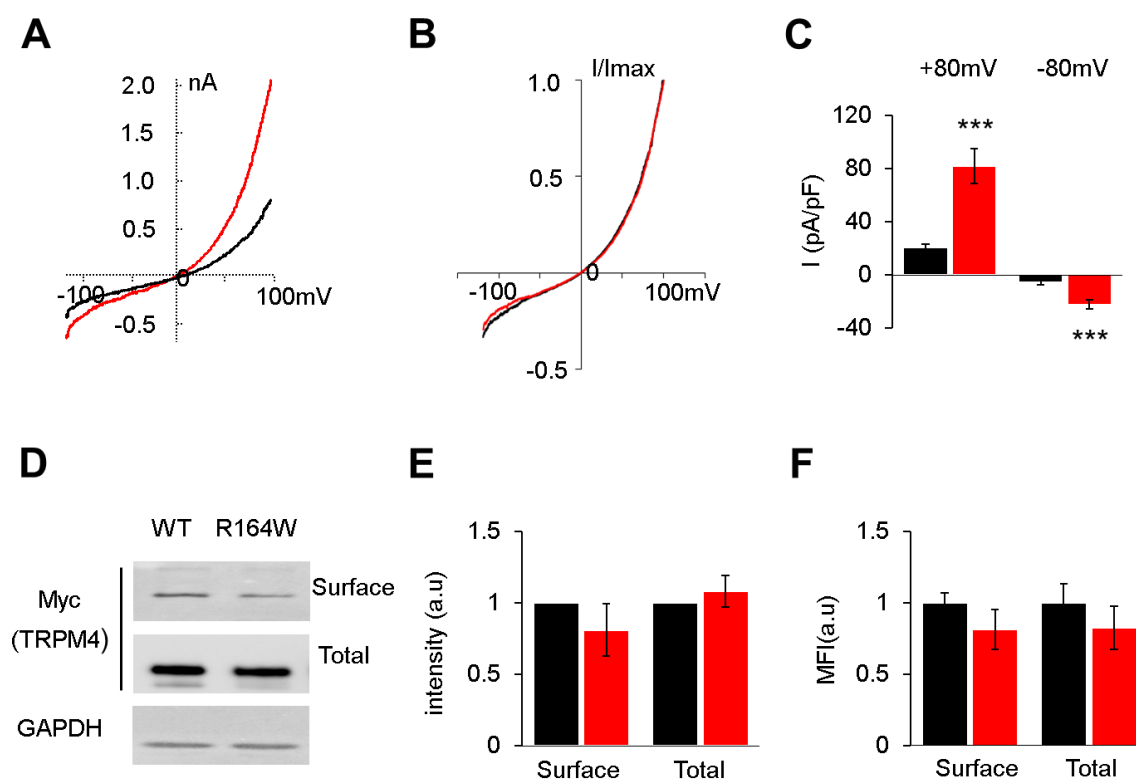


**Fig VI.1 TRPM4<sup>R164W</sup> increases current density, but not TRPM4 surface expression.** Unless otherwise indicated, black traces denote TRPM4, red traces denote TRPM4<sup>R164W</sup>. **A.** Representative current traces obtained from 250-ms voltage ramps (voltage range: -120 to +100mV) for TRPM4 and TRPM4<sup>R164W</sup> Flp In cells. Current traces were measured in the whole-cell patch-clamp configuration. Holding potential was -60mV. **B.** Normalized current-voltage relationship for TRPM4 and TRPM4<sup>R164W</sup> channel obtained as A. **C.** Current

densities of TRPM4 (n=16) and TRPM4<sup>R164W</sup> (n=18) determined at +80mV and -80 mV, respectively (\*\*p<0.001). **D.** Immunoblots comparing the amount of biotinylated Myc-tagged TRPM4 (WT) or TRPM4<sup>R164W</sup> (R164W) at the cell surface versus total lysates of Flp In cells. Myc-tagged TRPM4 and TRPM4<sup>R164W</sup> protein was stained with anti-Myc antibodies. Staining with anti-GAPDH antibody served as loading control. **E.** Bar diagram summarizing densitometric analysis of immunoblots such as shown in D. Values are given in arbitrary units (a.u) (n=3; p>0.05). **F.** Non-permeabilized (surface) or 0.2%Triton X-100-permeabilized cells (total) were stained with FITC-coupled anti-Myc antibodies for FACS analysis of cellular distribution of TRPM4 and TRPM4<sup>R164W</sup>. Mean fluorescence intensity (MFI) was normalized to wild-type TRPM4 (n=3~5; p>0.05).

## VI.2 SUMOylation regulates TRPM4 current via a non-covalently conjugating

SUMOylation is a multi-step protein modification reaction in which SUMO (small ubiquitin-like modifier) molecules are covalently attached to lysine residues of substrate proteins. E1-Activating enzyme (Aos1-Uba2), E2-SUMO conjugating enzyme (Ubc9) and E3-SUMO ligase (PIAS3) are involved in this cascade (Geiss-Friedlander & Melchior, 2007). Previous results showed that wild-type TRPM4 current in transiently expressed HEK 293 cells was sensitive to Ubc9, but not TRPM4<sup>R164W</sup> (Liu et al, 2010). Now, I checked TRPM4 current density in Flp In cells transfected with Ubc9 or PIAS3 cDNA. The current density of wild-type increased to approximately 2-fold when Ubc9 (56.58 ± 7.34 pA/pF at +80mV, n=16; p<0.01) or PIAS3 (67.14±10.06 pA/pF at +80mV, n=41; p<0.01) were separately transfected into cells compared to cells transfected with empty vectors (30.6±3.42 pA/pF at +80mV, n=36). Strikingly, co-transfection of Ubc9 and PIAS3 further increased wild-type TRPM4 current density (126.3 ± 19.47 pA/pF at +80mV, n=29; p<0.001) in an additive manner (Fig VI.2A). By contrast, TRPM4<sup>R164W</sup> current density was insensitive to coexpression of Ubc9 and PIAS3 (134.56±38.31 pA/pF at +80mV, n=10) compared to cells transfected with empty vector (116.09±36.5 pA/pF at +80mV, n=9; p>0.05) (Fig VI.2A). The data clearly showed that TRPM4<sup>R164W</sup> had lost the sensitivity of TRPM4 to SUMOylation.

Next, I explored whether Ubc9/PIAS3 increased current density was associated with an

increased channel number in the plasma membrane. Non-permeabilized TRPM4 Flp In cells before and after transfection with Ubc9 and PIAS3 cDNA were labeled with biotin. Biotin-labeled surface proteins and, respectively, total proteins from lysates of TRPM4 Flp In cells were separated by SDS-PAGE. Subsequent immunoblots were probed with anti-Myc antibodies (See Method V.3.3). As shown in Fig VI.2B, similar band intensities of TRPM4 protein were seen in immunoblots of membrane and total lysate preparations. This result indicated that SUMO conjugating enzyme Ubc9 and SUMO ligase PIAS3 increased TRPM4 channel current densities, but not TRPM4 protein levels at the cell surface.

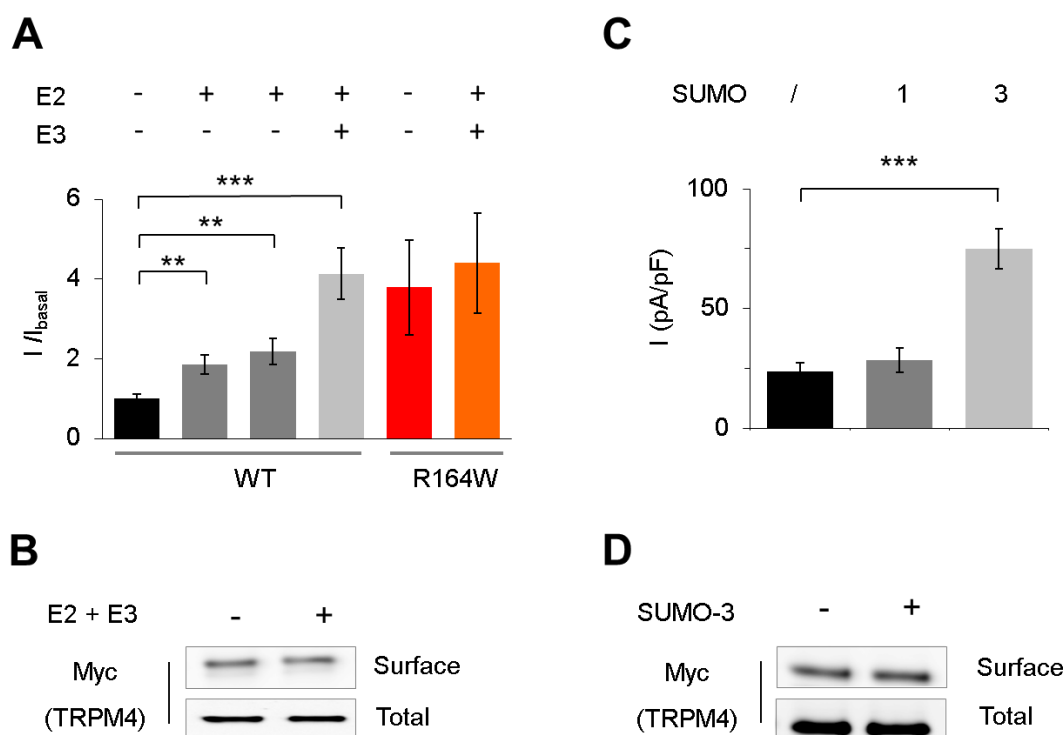


**Fig VI.2 SUMOylation increases TRPM4 current density without changing TRPM4 cell-surface expression.** **A.** TRPM4 and TRPM4<sup>R164W</sup> Flp In cells were transfected with SUMO enzymes as indicated on top of bar graph (E2, Ubc9; E3, PIAS3). Current densities were obtained at +80mV as described in Fig VI.1C and normalized to TRPM4 cells transfected with empty vector DNA (n=9~41; \*\*p<0.01, \*\*\*p<0.001). **B.** Immunoblot analysis of surface and total Myc-tagged TRPM4 proteins isolated from TRPM4 Flp In cells. Transfection with E2 and E3 is indicated on top of immunoblot. **C.** Transfection of TRPM4 Flp In cells with GFP-SUMO-3, but not with HA-SUMO-1 increased TRPM4 current density. Current densities were obtained at +80mV (n=14~23; \*\*\*p<0.001). **D.** Immunoblot analysis of surface and total Myc-tagged TRPM4 proteins isolated from TRPM4 Flp In cells transfected with empty vector (-) or GFP-SUMO-3 (+) cDNA.

SUMO ligase may use three SUMO isoforms (SUMO-1, SUMO-2, SUMO-3) in human cells; SUMO-1 is distinct from SUMO-2 and SUMO-3, which show a high degree of similarity to each other (Guo et al, 2007). In order to clarify if SUMO-1 or SUMO-2/3 was involved in the regulation of TRPM4 activity, I transfected TRPM4 Flp In cells with HA-tagged SUMO-1 (HA-SUMO-1) or GFP-tagged SUMO-3 (GFP-SUMO-3). Because of the similarity between SUMO-2 and SUMO-3, I only used SUMO-3 in my experiments. The results showed that expression of SUMO-3 significantly increased TRPM4 current density ( $75.0 \pm 8.5$  pA/pF at +80mV,  $-21.78 \pm 8.5$  pA/pF at -80mV, n=17) without affecting outward rectification, while expression of SUMO-1 had no effect ( $28.3 \pm 5.1$  pA/pF at +80mV,  $-8.61 \pm 1.61$  pA/pF at -80mV, n=23; Fig VI.2C). The data showed that SUMOylation-evoked stimulation of TRPM4 current density specifically involves SUMO-3, but not SUMO-1. Again, the TRPM4 current increase in cells transfected with SUMO-3 was accompanied neither with an increase of TRPM4 protein at the cell surface nor with an increase in total amount of TRPM4 protein (Fig VI.2D).

SUMO ligases link SUMO to target proteins through a covalent isopeptide bond between a C-terminal glycine residue of SUMO and a lysine side chain of the target (Geiss-Friedlander & Melchior, 2007). This leads to an increase in molecular weight of the target protein by 10~20 kDa resulting in protein bands that migrate slower than unmodified target protein in SDS-PAGE/immunoblotting analysis. However, the SUMOylation experiments consistently failed to display an additional protein band on top of unmodified TRPM4 (Fig VI.1D, Fig VI.2B, D; Fig VI.3A). Nevertheless, anti-SUMO-2/3 antibodies co-immunoprecipitated Myc-tagged TRPM4 protein as revealed in immunoblots of anti-SUMO-2/3 precipitates stained with anti-Myc antibodies to detect TRPM4 protein (Fig VI.3A). Moreover, expression of GFP-SUMO-3 in TRPM4 Flp In cells enhanced the quantity of TRPM4 proteins that could be co-immunoprecipitated with anti-SUMO-2/3 antibodies (Fig VI. 3A), whereas expression of the deSUMOylation protease SENP1 markedly reduced TRPM4 band intensity in immunoblots of respective co-immunoprecipitates (Fig VI. 3A). It should be noted that the apparent molecular weight of co-immunoprecipitated TRPM4 protein always corresponded to the one of unmodified TRPM4.

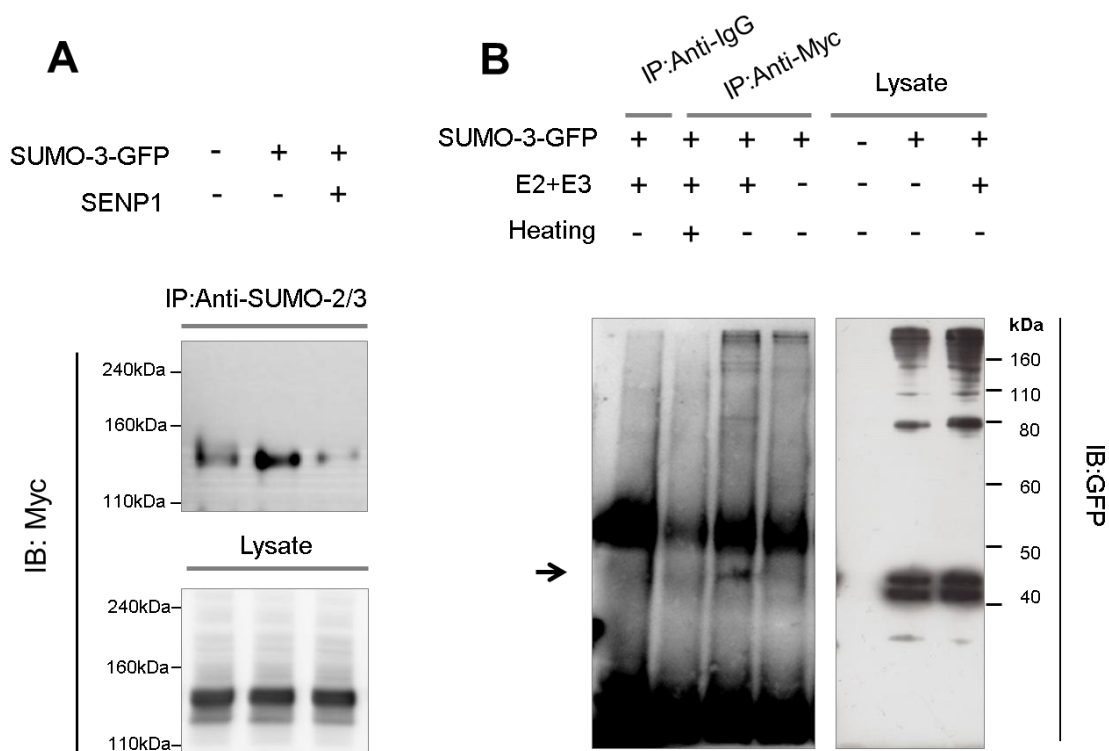


**Fig VI.3 Anti-SUMO-3 antibodies precipitate TRPM4 protein.** **A.** Immunoblot (IB) of lysates of TRPM4 Flp In cells 24h post-transfection with constructs as indicated on top of blot. Immunoprecipitation (IP) was with anti-SUMO-2/3 antibodies. Blots were stained with anti-Myc antibodies (Myc). **B.** Immunoblot (IB) of lysates of TRPM4 Flp In cells 24h post-transfection with constructs as indicated on top of blot. Immunoprecipitation (IP) was with anti-IgG or anti-Myc antibodies as indicated on top of immunoblot. Blots were stained with anti-GFP antibodies for GFP-tagged SUMO-2/3. Heating: Lysate was heated at 70° for 5min in the presence of 0.5%SDS before immunoprecipitation. Arrowhead indicates GFP-SUMO-3.

Alternatively, I used anti-Myc antibodies to precipitate Myc-tagged TRPM4 and its associated protein(s). The respective immunoblots were then stained with anti-GFP antibodies to detect GFP-SUMO-3. Co-IP assays with lysate of TRPM4 Flp In cells co-transfected both with E2 enzyme/E3 ligase and GFP-SUMO-3 showed that anti-Myc antibodies co-immunoprecipitated GFP-SUMO-3 (Fig VI.3B left panel). The immunoblot showed polypeptides corresponding to high-molecular weight aggregates as well as to free GFP-SUMO-3. Heating the lysate to 70 °C for five minutes before immunoprecipitation, made all GFP-SUMO-3 positive bands disappear. Altogether, the Co-IP assays revealed a non-covalent interaction of TRPM4 protein and SUMO-3.

I considered several likely explanations for the failure to detect a protein band corresponding to a TRPM4-SUMO-3 conjugate: i) only a minor fraction of TRPM4 protein is localized to the membrane. However, the biotinylated surface protein did not reveal a higher molecular weight corresponding to SUMO-modified TRPM4 protein; ii) only a minor fraction of TRPM4 protein at the plasma membrane is SUMOylated, i.e. less than 10%. Otherwise I would have detected a corresponding protein band. If TRPM4 current density is directly correlated with SUMOylation, I would have expected to see a TRPM4-SUMO-3 conjugate under stimulation conditions; iii) the SUMO-modification may not be detectable in immunoblot. Taking into account comparable literature data on SUMOylated proteins, this possibility also seemed unlikely; iv) SUMO-3 and TRPM4 make a non-covalent complex. In this case, the co-immunoprecipitation results should remain unaffected by expression of a deconjugating enzyme, such as SENP1, but this was not the case; v) combining SENP1- and heat-sensitivity of the Co-IP results, suggested as a most likely explanation that an as yet unknown ancillary protein of the TRPM4 channel is modified by SUMO. Based on these considerations, the second and fifth explanation seemed to be the most likely ones. Therefore, I designed further experiments to explore the two possibilities.

In order to further investigate whether SUMO-3 is covalently attached to TRPM4 protein, I firstly mutated lysine residues in putative SUMOylation sites of TRPM4. Using the programme SUMOplot™ Prediction to identify potential SUMOylation sites in the TRPM4 protein sequence, five lysine residues were identified; they were mutated to alanine (K341A, K618A, K1140A, and K1154A) or asparagine (K492N). Transfection of HEK 293 cells with the mutant TRPM4 constructs together with GFP-SUMO-3 cDNA showed that TRPM4 mutants were expressed like wild-type. Immunoblots of the mutants displayed the same apparent molecular weight as wild-type TRPM4 (Fig VI.4A). Furthermore, electrophysiological recordings showed similar current densities for wild-type and mutant TRPM4 channels without affecting outward rectification (Fig VI.4B). Apparently, the five lysine-residues (K314, K492, K618, K1140, and K1154) are unimportant for the SUMO-3-evoked stimulation of TRPM4 channel activity. A likely interpretation of this result was that SUMOylation affects TRPM4 channel activity indirectly. Therefore, I looked for an

ancillary protein as a potential SUMOylation target.

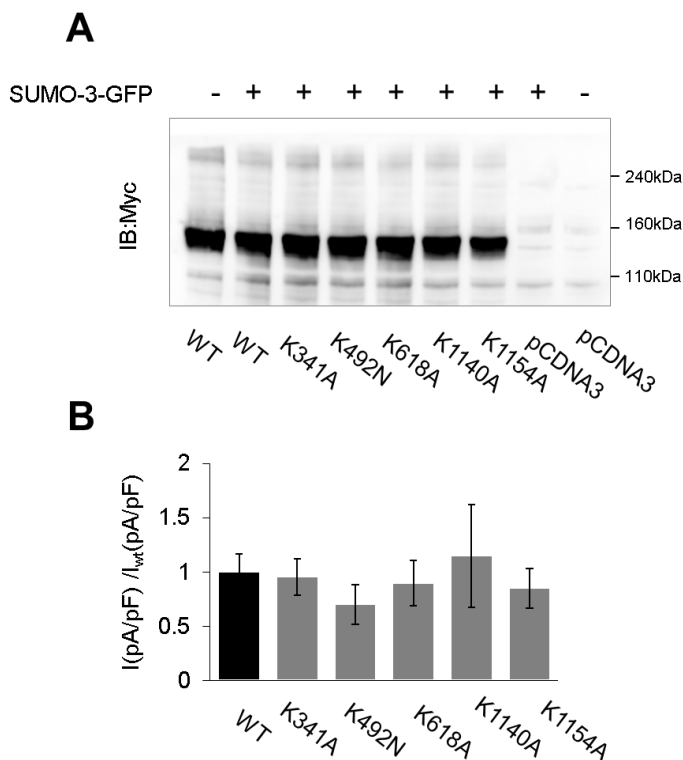


**Fig VI.4 Expression and current densities of TRPM4 channels with a mutated SUMOylation consensus motif.** **A.** TRPM4 wild-type (WT) or potential SUMO-deficient mutants (K341A, K492N, K618A, K1140A, and K1154A) were transfected with or without GFP-SUMO-3. Lysates were analyzed by immunoblotting with anti-Myc antibodies. **B.** Relative current densities of TRPM4 wild-type and potential SUMO-deficient mutants expressed in HEK 293 cells. Current densities were obtained at +80mV as described in Fig VI.1C and normalized to TRPM4 wild-type.

### VI.3 Caveolin-1 binding affects TRPM4 channel activity

Because the observed SUMOylation-evoked stimulation of TRPM4 channel activity took place at the plasma membrane, I looked for potential interaction partners known to be associated with plasma membrane. Screening of the TRPM4 protein sequence for protein binding motifs revealed a potential caveolin-binding motif (222FPLDYNYSAFF232) within the TRPM4 N-terminus. This was very interesting because caveolins have conserved SUMOylation consensus motifs within their N-terminus near the caveolin-scaffolding domain (CSD), and caveolin-3 becomes SUMOylated in transfected mammalian cells expressing SUMO-3 (Fuhs & Insel, 2011).

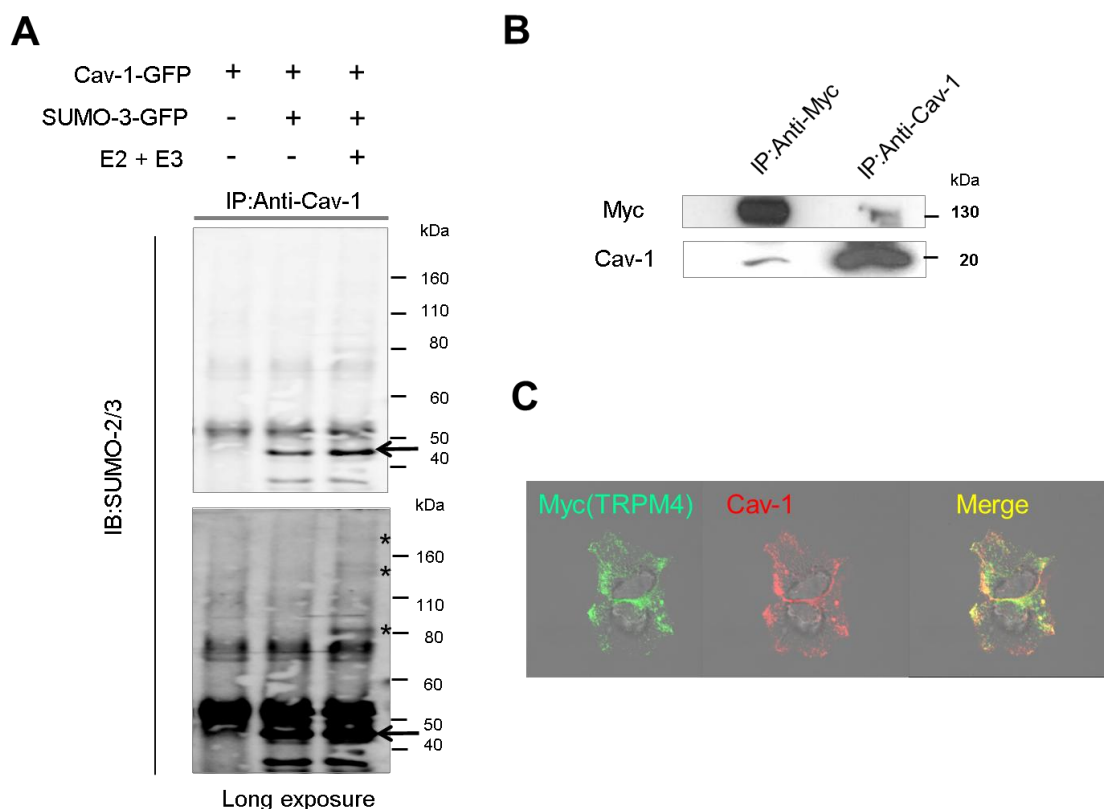


**Fig VI.5 Caveolin-1 associated with SUMO-3 and TRPM4. A.** Lysates from TRPM4 Flp In cells transfected with constructs indicated as top of blot. Immunoprecipitation (IP) was with anti-Caveolin-1 antibodies, blots were stained with anti-SUMO-2/3 antibodies. Arrowhead indicates GFP-SUMO-3, and asterisk indicates SUMO-3 conjugates. **B.** Co-IP assay of Myc-tagged TRPM4 and caveolin-1. Lysates of TRPM4 Flp In cells were incubated with anti-Myc and anti-caveolin-1 antibodies as indicated. Resulting immunoprecipitates were immunoblotted and probed with anti-caveolin-1 (Cav-1) and anti-Myc antibodies (Myc), respectively. **C.** Immunocytochemical staining of caveolin-1 (Cav-1) and Myc-tagged TRPM4 (Myc(TRPM4)) in TRPM4 Flp In cells. Cells were fixed, permeabilized and then labeled by anti-Myc and anti-caveolin-1 antibodies.

I obtained comparable results for caveolin-1 and SUMO-3. Fig VI.5A shows immunoblotting results of caveolin-1 immunoprecipitates obtained from lysates of TRPM4 Flp In cells overexpressing caveolin-1-GFP and GFP-SUMO-3. Staining of the immunoblot with anti-SUMO2/3 antibodies produced a band corresponding to the free GFP-SUMO-3 form (~45 kDa). The intensity of this band became stronger when E2 enzyme/E3 ligase were co-expressed with GFP-SUMO-3. Long exposure of the immunoblot revealed caveolin-1-SUMO-2/3 conjugates (See asterisks in Fig VI.5A). This result demonstrated that SUMOylation takes

place in the TRPM4 Flp In cells and that it is possible to detect SUMO-3- protein conjugates in immunoblots.

Because HEK 293 cells *per se* express caveolin-1, I investigated a possible interaction of TRPM4 protein and caveolin-1 in co-immunoprecipitation experiments with lysates of TRPM4 Flp In cells. As shown in Fig VI. 5B, anti-Myc antibodies pulled down endogenous caveolin-1 as revealed in immunoblots stained with anti-caveolin-1 antibodies. Conversely, anti-caveolin-1 antibodies pulled down TRPM4 protein as revealed in immunoblots stained with anti-Myc antibodies. The result showed that the two proteins are in close association. Their association was also verified by immunocytochemistry experiment. An apparent co-localization of Myc staining indicated TRPM4 protein and caveolin-1 staining was observed especially near or at the plasma membrane in TRPM4 Flp In cells (Fig VI.5B).

In order to test whether caveolin-1 and TRPM4 are direct binding partners, I mutated Phenylalanine223 and Phenylalanine232, key aromatic amino acids in the caveolin-binding motif of TRPM4, to alanine. After transfection of HEK 293 cells with TRPM4<sup>F223A</sup>, TRPM4<sup>F223A</sup> or wild-type cDNA, protein expression level and current densities were compared. TRPM4<sup>F223A</sup> showed slightly decreased expression level, while expression of TRPM4<sup>F223A</sup> was significantly lower than wild-type (Fig VI.6A). Co-immunoprecipitation experiments indicated that the two TRPM4 mutants apparently had a decreased binding affinity for caveolin-1 in comparison to wild-type TRPM4 (Fig VI.6B). Subsequently, comparison of current densities showed that HEK 293 cells expressing TRPM4<sup>F223A</sup> exhibited slightly increased current densities ( $29.58 \pm 5.08$  pA/pF at +80mV, n=21). On the other hand, HEK 293 cells expressing TRPM4<sup>F232A</sup>, albeit the low TRPM4<sup>F232A</sup> protein-expression level, displayed significantly increased current densities ( $41.90 \pm 6.70$  pA/pF at +80mV, n=22;  $p < 0.01$ ) in comparison to wild-type TRPM4 ( $18.20 \pm 3.26$  at +80mV, n=19, Fig VI.6C). Taken together the data suggested that a weakened caveolin binding leads to an increase in TRPM4 current density.

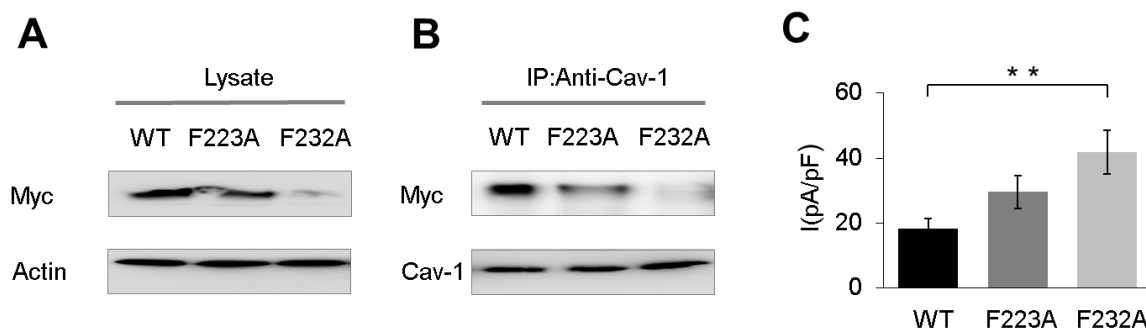


**Fig VI.6 Comparison of caveolin-binding mutations.** **A.** Immunoblots comparing expression of Myc-tagged TRPM4 wild-type (WT), two caveolin-binding mutations TRPM4<sup>F223A</sup> (F223A) and TRPM4<sup>F232A</sup> (F232A) in HEK 293 cells. Staining with anti-Actin antibody served as loading control. **B.** Co-IP assay of WT, F223A and F232A with caveolin-1. **C.** Current densities of TRPM4 (WT, n=19), TRPM4<sup>F223A</sup> (F223A, n=21), and TRPM4<sup>F232A</sup> (F232A, n=22) expressed in HEK 293 cells. Current densities were obtained at +80mV as Fig VI.1C (\*\* p<0.01).

Based on this notion, I hypothesized that TRPM4<sup>R164W</sup> channels, which give rise to a higher current density than wild-type TRPM4 channels, have a weaker interaction with caveolin-1 than wild-type. Consistent with this hypothesis was that, in comparison to wild-type control, anti-caveolin-1 antibodies pulled down less quantities of TRPM4<sup>R164W</sup> protein (Fig VI.7A). Thus, I concluded that the interaction of caveolin-1 with TRPM4 negatively regulates TRPM4 channel activity. Therefore, I hypothesized that overexpression of caveolin-1 in Flp-In cells augments the interaction of caveolin-1 with TRPM4<sup>R164W</sup> leading to a decrease in TRPM4<sup>R164W</sup> current density.

When I measured TRPM4<sup>R164W</sup> current density after transfection of Flp-In cells with caveolin-1-GFP, I saw indeed a marked decrease of TRPM4<sup>R164W</sup> current density (Fig VI.7C). However, overexpression of caveolin-1 in TRPM4 Flp In cells increased TRPM4 current density. Furthermore, TRPM4 and TRPM4<sup>R164W</sup> I-V relations were almost linear due to a relative increase in inward current (Fig VI.7B) in comparison to untransfected cells, where TRPM4 I-V relations exhibit an outward rectification (Fig VI. 7B, gray traces). The altered rectification properties of the TRPM4 channel in caveolin-1 overexpressing cells indicated that overexpression of caveolin-1 affected TRPM4 channel activity in more than one way, making the interpretation of the data difficult. Some of the effects may be

associated with the observation that caveolin, as an important cholesterol-binding protein, transfers newly synthesized cholesterol from the endoplasmic reticulum (ER) to the plasma membrane (Smart et al, 1996), and that overexpression of caveolin affects cholesterol metabolism (Fu et al, 2004) (see section VI.4). Nevertheless, the data shows that overexpression of caveolin-1 in TRPM4<sup>R164W</sup> Flp In cells, a relatively weak caveolin binder, leads to a decrease in TRPM4<sup>R164W</sup> current density. This observation supports the idea that caveolin binding and TRPM4 current density are inversely correlated with each other.

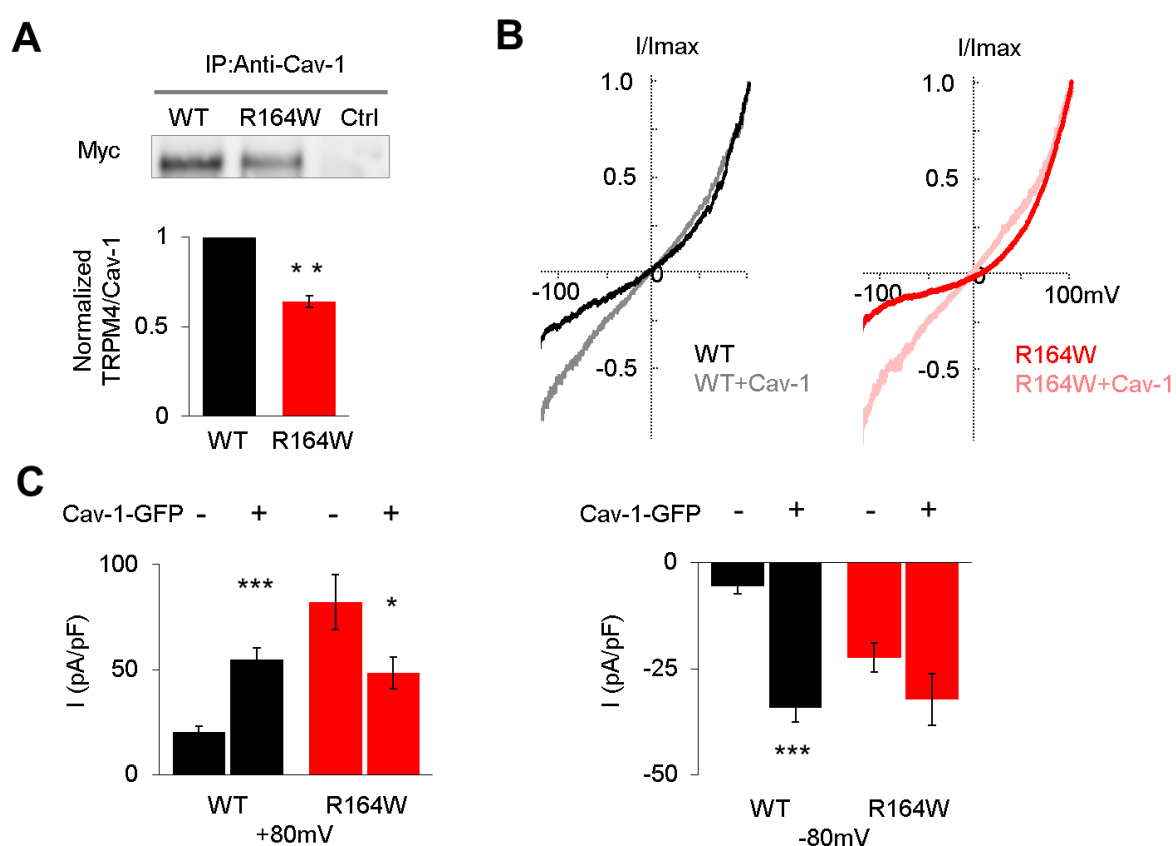


**Fig VI.7 Caveolin-1 affects TRPM4 current density and outward rectification.** **A.** Co-IP assay of Myc-tagged TRPM4<sup>R164W</sup> (R164W) and endogenous caveolin-1 from Flp In cells. Bottom is Co-IP band intensity normalized to wild-type (WT) (n=3; \*\*p<0.01). **B.** Normalized current-voltage relationship for TRPM4 and TRPM4<sup>R164W</sup> channel in Flp In cells transfected with caveolin-1-GFP. **C.** Current densities of TRPM4 (n=11) and TRPM4<sup>R164W</sup> (n=8) channel in Flp In cells transfected with caveolin-1-GFP at +80 or -80mV were obtained as described in Fig VI.1C (\*\* p<0.01, \*\*\* p<0.001).

## VI.4 TRPM4 channels reside in cholesterol- and caveolin-rich membrane microdomains

Caveolins are considered as a major cholesterol interacting protein involved in the traffic of cholesterol to the plasma membrane (Thiele et al, 2000). Moreover, cholesterol is considerably more abundant in caveolae than in the surrounding plasma membrane (Simionescu, 1983). Interestingly, it has been previously reported that members of the TRP channel family are associated with cholesterol-rich microdomains, known as lipid rafts, and exert distinct activities in or outside of lipid raft (Morenilla-Palao et al, 2009). Thus, I hypothesized that the caveolin-overexpression results are in part due to an altered cholesterol-metabolism and that TRPM4 channel may be localized to cholesterol and caveolin-rich microdomains.

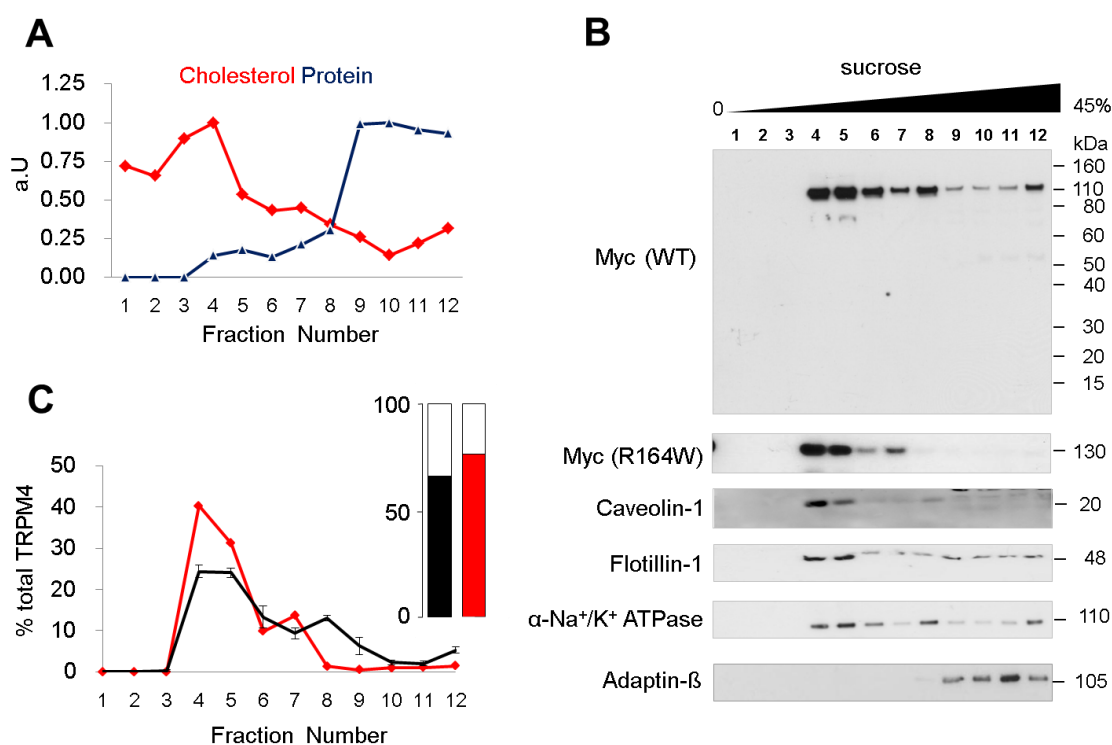


**Fig VI.8 TRPM4 channels reside in low density, cholesterol and caveolin-rich membrane compartment.** **A.** Relative cholesterol and protein levels in each of 12 1-ml fractions collected from the top to the bottom of Na<sub>2</sub>CO<sub>3</sub>-based sucrose density gradient. Values are given in arbitrary units (a.u.) normalized to maximum. **B.** Sucrose density gradient fractions were prepared from Myc-tagged TRPM4 (WT) and TRPM4<sup>R164W</sup> (R164W) Flp In cells, separated on SDS-PAGE, and

probed with anti-Myc antibodies and other antibodies for marker protein. **C.** Densitometric quantitative analysis of relative abundance (%) of WT (black, n=3) and R164W (red, n=2) in 12 fractions or in high cholesterol (lower of stacked column) and low cholesterol (upper of stacked column) fractions.

In order to test this hypothesis, Na<sub>2</sub>CO<sub>3</sub>-based sucrose gradient centrifugation was performed to investigate distribution of TRPM4 and TRPM4<sup>R164W</sup> from Flp In cells in high and low cholesterol membrane fractions (See Method V.2.3). After 18h-ultra speed centrifugation, cholesterol was mainly enriched in low-density fractions (Fraction 1-5), while protein was mainly enriched in high-density fractions (Fraction 9-12 in Fig VI.8A). As shown in Fig VI.8B, strongly immunoreactive bands corresponding to wild-type TRPM4 protein were mainly detected in low density but high cholesterol fractions; the pattern of TRPM4<sup>R164W</sup> protein was even more concentrated in low density but high cholesterol fractions. Caveolin-1 (principal component of caveolae membranes) and flotillin-1 (caveolae-associated integral membrane protein) were all found exclusively in low-density fraction. Notably, distribution of Na<sup>+</sup>/K<sup>+</sup> ATPase  $\alpha$ -subunit (caveolae related membrane protein) was quite similar to that of wild-type TRPM4, whereas adaptin- $\beta$  (marker of clathrin-coated vesicles) was found exclusively in high-density, caveolin-1 free fractions. Quantitation of TRPM4 protein in each fraction clearly showed for TRPM4<sup>R164W</sup> protein a higher concentration (see also red stacked column) than for wild-type TRPM4 (black stacked column, Fig VI.8C) in high cholesterol fractions. The results imply that TRPM4 and TRPM4<sup>R164W</sup> distributions in high-cholesterol membrane fraction differ. The predominant distribution in high cholesterol fraction reflects a higher preference of TRPM4<sup>R164W</sup> for cholesterol-enriched plasma membrane microdomains.

In order to deplete membrane cholesterol from TRPM4 Flp In cells, I applied a low concentration (5mM) of methyl-beta-cyclodextrin (M $\beta$ CD) for 30 minutes. The M $\beta$ CD-treatment remarkably increased TRPM4 current density ~14 fold at +80mV (358.2 $\pm$ 41.9 pA/pF) and ~10 fold at -80mV (-83.99 $\pm$ 17.38 pA/pF, n=22; Fig VI.9A). Importantly, after normalizing TRPM4 current to -120mV, it was evident that M $\beta$ CD-treatment of TRPM4 Flp In cells had two effects. Firstly, the treatment markedly enhanced outward rectification of TRPM4 current. This produced a ~1.4 fold increase at +80 mV in current density.

Secondly, current density *per se* increased by approximately 10 fold. The effect of M $\beta$ CD on TRPM4 current density was reversible. When cholesterol-depleted cells were replenished with cholesterol by using a 1:10 mixture of cholesterol and M $\beta$ CD (mol/mol), TRPM4 current density was nearly back to basal level ( $48.94 \pm 10.45$  pA/pF at +80mV, n=9; Fig VI.9A).

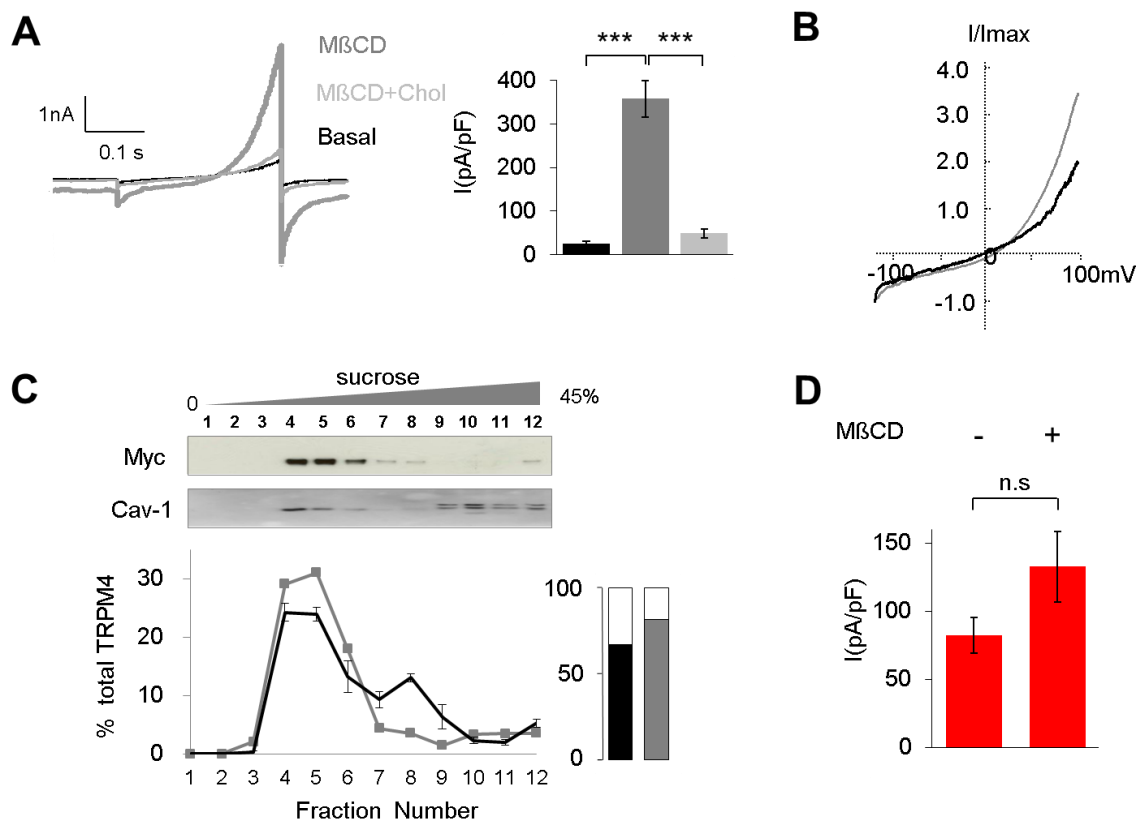


**Fig VI.9 Cholesterol depletion alters TRPM4 but not TRPM4<sup>R164W</sup> channel current density and membrane distribution.** **A.** TRPM4 Flp In cells were treated with 5mM M $\beta$ CD (n=22) for 30min and replenished with cholesterol-saturated M $\beta$ CD (n=9) for 30min. Representative currents are shown left, with average current densities obtained at +80mV as described in Fig VI.1C shown on the right (\*\*\*p<0.001). **B.** Normalized current-voltage relation for TRPM4 channel in presence (gray) or absence of M $\beta$ CD (black). **C.** Upper panels: Immunoblots to detect Myc-tagged TRPM4 and caveolin-1 in Na<sub>2</sub>CO<sub>3</sub>-based sucrose density gradient fractions from lysate of M $\beta$ CD-treated TRPM4 Flp In cells. Lower panel: Quantitative densitometric analysis of relative abundance of TRPM4 protein (% total TRPM4) in 12 fractions from M $\beta$ CD-treated (gray) or non-treated (black) cells. Right bar diagram illustrates relative abundance of TRPM4 protein in high cholesterol (lower of stacked column) and low-cholesterol (upper of stacked column) fractions (n=2~3). **D.** Current densities of TRPM4<sup>R164W</sup> measured on 5mM M $\beta$ CD treated (n=17) or non-treated (n=18) Flp In cells, obtained at +80mV as described in Fig IV.1C (P>0.05).

Next, I checked the TRPM4 protein distribution in Na<sub>2</sub>CO<sub>3</sub>-based sucrose gradient after

treatment of TRPM4 Flp In cells with 5mM M $\beta$ CD. Immunoblot analysis of the gradient fractions (Fig VI.9B) showed that M $\beta$ CD treatment caused relocalization of caveolin-1 to the low-cholesterol and high sucrose density fractions (Fig VI.9B). The result was in agreement with a report that cholesterol-depletion causes caveolae disassembly and relocalization of caveolin-1 membrane microdomains with low cholesterol content (Rodal et al, 1999). By contrast, TRPM4 protein was found relocated to low sucrose density, high-cholesterol fraction. Since the low sucrose density fractions are rich in PIP<sub>2</sub> (Pike & Casey, 1996), this somehow counterintuitive observation may indicate that TRPM4 after dissociation of caveolin moves to a lipid raft rich in PIP<sub>2</sub>, known to activate the TRPM4 channel (Nilius et al, 2006). Clearly, the data corroborated the observation in RESULT VI.3 that an increase in TRPM4 current density is associated with dissociation of caveolin-1-TRPM4 complex. The M $\beta$ CD data suggest that the effects of caveolin-1 overexpression on TRPM4 current density (Fig VI.7) are correlated in part with an altered cholesterol metabolism. In contrast to TRPM4 Flp In cells, M $\beta$ CD treatment of TRPM4<sup>R164W</sup> Flp In cells had no effect on TRPM4<sup>R164W</sup> current density and I-V relationship (132.52 $\pm$ 25.88 pA/pF at + 80mV, -36.36 $\pm$ 6.81 pA/pF at -80mV, n=17; Fig VI.9D). Combining the data indicated that TRPM4 channel activity is low when the channel resides in a high cholesterol/caveolin-1 plasma membrane microdomain, and that the TRPM4<sup>R164W</sup> channel stays away from such plasma membrane microdomain.

## VI.5 SUMOylation regulates TRPM4 channel via altered TRPM4 distribution in membrane microdomains

Cellular cholesterol concentration exerts an important influence on stability and trafficking of caveolin-1, which has an essential role on TRPM4 channel activity. As SUMOylation also influences TRPM4 channel activity, I hypothesized that SUMOylation of caveolin causes a redistribution of TRPM4 in the plasma membrane. Therefore, after Ubc9 and PIAS3 were transfected into TRPM4 Flp In cells, the distribution of TRPM4 channel in Na<sub>2</sub>CO<sub>3</sub>-based sucrose gradient fraction was investigated. The quantitative analysis of every fraction clearly exhibited a more concentrated distribution of TRPM4 channel in low

sucrose density, high cholesterol fractions in comparison to controls (Fig VI.10A). The data implied that enhanced SUMOylation alters TRPM4 membrane localization, similar to the redistribution observed upon cholesterol-depletion by M $\beta$ CD treatment.

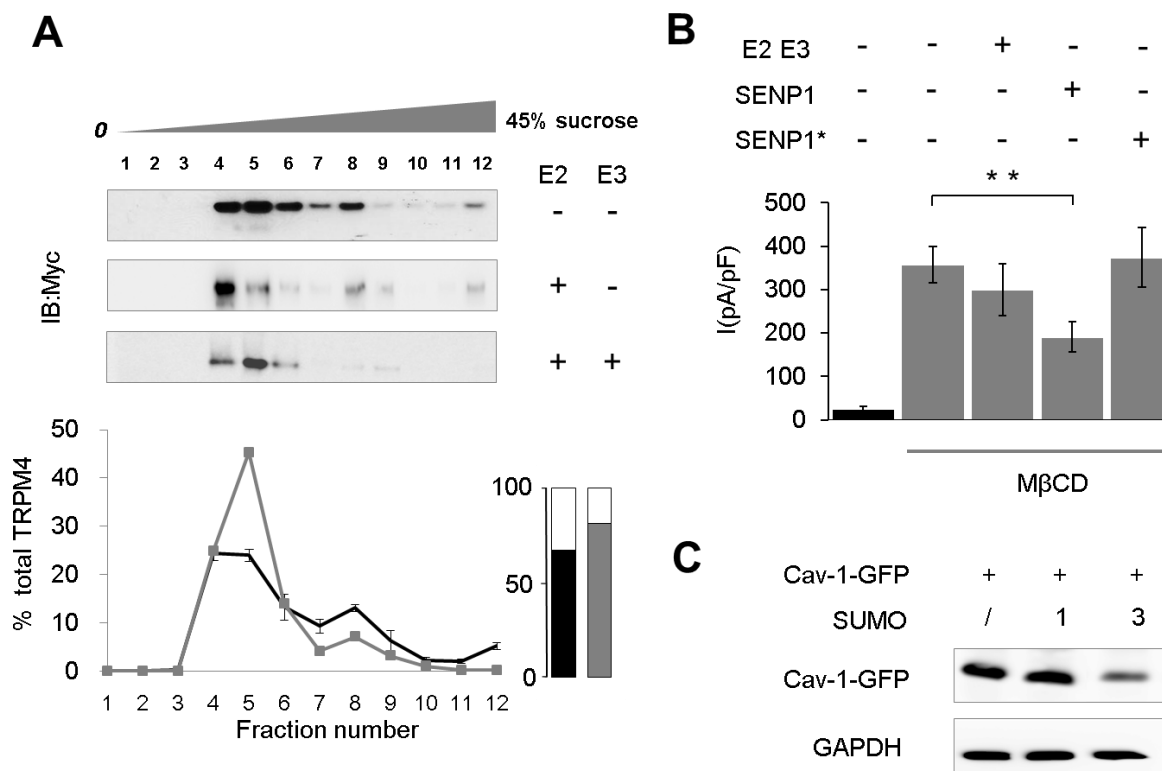


**Fig VI.10 SUMOylation altered TRPM4 channel distribution between high cholesterol and low cholesterol microdomains. A.** TRPM4 Flp In cells were transfected with Ubc9 (E2) or Ubc9 and PIAS3 (E2+E3) and processed as Fig VI.8B. Fractionations of Myc-tagged TRPM4 probed with anti-Myc antibodies were shown above, with densitometric quantitative analysis of relative abundance (%) of TRPM4 as described in Fig VI.8C shown below. Gray curve denotes cells transfected with E2 and E3 (n=2), black curve denotes basal condition (n=3). **B.** TRPM4 Flp In cells were transfected with or without SUMO enzymes (as indicated on top of bar graph, SEN1\* indicate inactive form SENP1C603S), then treated with 5mM M $\beta$ CD for 30min. Current densities were obtained at +80mV as described in Fig VI.1C (n=6~27; \*\*p<0.01). **C.** TRPM4 Flp In cells were transfected with caveolin-1-GFP as well as either HA-SUMO-1 or GFP-SUMO-3, after at least 24h post-transfection, lysates were collected and analyzed by immunoblotting with anti-caveolin-1 antibodies. Staining with anti-GAPDH-antibody served as loading control (n=3).

Subsequently, TRPM4 Flp In cells expressing Ubc9 and PIAS3 as well as SENP1 overexpressing cells were treated with M $\beta$ CD, and then their current densities were measured. The aim was to check if SUMOylation and cholesterol-depletion have

coordinated or antagonistic effect on TRPM4 activity. Compared to controls (empty vector transfected cells treated with M $\beta$ CD), M $\beta$ CD treatment of Ubc9 and PIAS3 (E2+E3) co-transfected cells ( $299.06 \pm 59.53$  pA/pF, n=11) had no further effect. However, enhanced deSUMOylation by overexpression of SENP1 partially reduced the effect of M $\beta$ CD on TRPM4 current density ( $191.0 \pm 34.4$  pA/pF at +80mV,  $-41.95 \pm 8.95$  pA/pF at -80mV, n=27;  $p < 0.01$ ) without affecting M $\beta$ CD-induced enhanced outward rectification. Inactive SENP1 isoform, SENP1C603S (Xu et al, 2006), was unable to decrease current density ( $373.8 \pm 68.8$  pA/pF, n=10; Fig VI.10B).

In order to explore whether SUMOylation has a direct effect on caveolin-1 to stimulate TRPM4 current, I coexpressed caveolin-1-GFP with HA-SUMO-1 or GFP-SUMO-3 in TRPM4 Flp In cells. Subsequently prepared immunoblots showed for caveolin-1-GFP a significantly decreased protein level in SUMO-3, but not in SUMO-1 transfected cells (Fig VI.10 C). This indicated that SUMO-3 expression in TRPM4 Flp In cells had a direct effect on caveolin-1.

Altogether, the data implied that cholesterol depletion and SUMOylation of caveolin are part of a signaling pathway to relocate the TRPM4 channel to a more favorable membranous environment for TRPM4 channel activity. By contrast, the ICCD mutation TRPM4<sup>R164W</sup> renders channel activity insensitive to SUMOylation and cholesterol-depletion, and enhances the residence of the TRPM4 channel in microdomains more favorable for its activity.

Caveolin trafficking is affected by serum. In the absence of serum, caveolin-1 accumulates in the LE/lysosomes of CHO cells stably expressing caveolin-1-GFP (Mundy et al, 2012). Serum withdrawal and cell stress are closely related. Therefore, cell stress may be an important trigger for TRPM4 channel activity. Indeed, serum withdrawal for 30 min markedly increased TRPM4 current density, both for wild-type ( $128.1 \pm 30.1$  pA/pF at +80mV, n=5;  $p < 0.01$ ) and for TRPM4<sup>R164W</sup> ( $255.0 \pm 48.9$  pA/pF at +80mV, n=10;  $p < 0.05$ ). Notably, in the absence of serum, inward current was enhanced for TRPM4<sup>R164W</sup> ( $-142.29 \pm 29.5$  pA/pF at

-80mV) but not for wild-type TRPM4 channel ( $38.65 \pm 9.74$  pA/pF at -80mV)(Fig VI.11A).

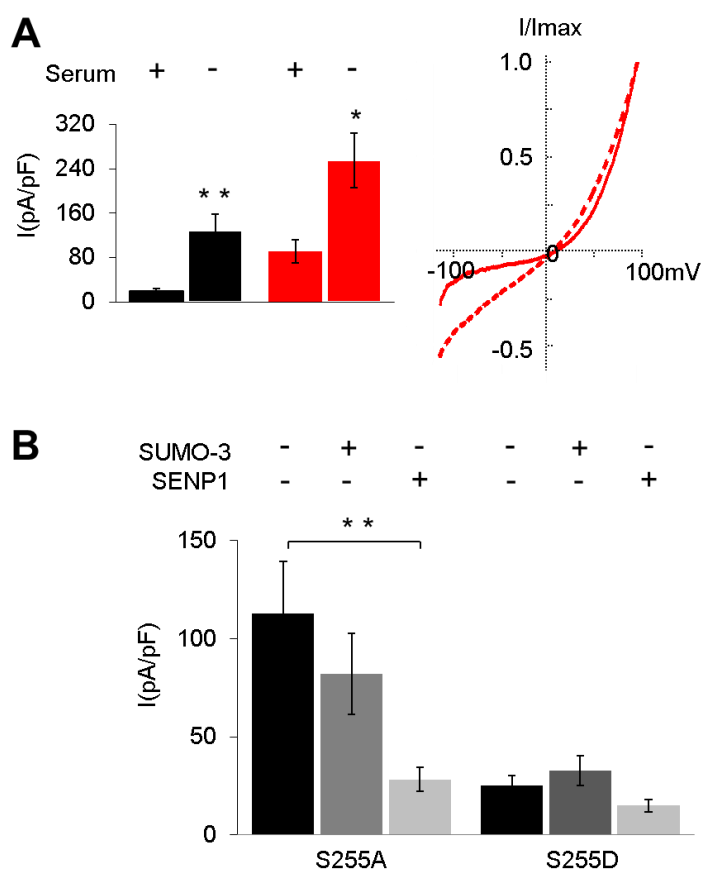


**Fig VI. 11 TRPM4 current sensitivity to serum withdrawal. A.** Current densities of wild-type TRPM4 (black) and TRPM4<sup>R164W</sup> (red) in the absence of serum, were obtained at +80mV as described in Fig VI.1C (n=5~14; \*\*p<0.01, \*p<0.05). Normalized current-voltage relationship for TRPM4<sup>R164W</sup> channel in presence (solid) or absence of serum (dotted) is shown on the right. **B.** Current densities of TRPM4<sup>S255A</sup> (S255A) and TRPM4<sup>S255D</sup> (S255D) with (+) or without (-) SUMO-3 and SENP1 overexpression were obtained at +80mV as described in Fig VI 1.C (n=11~21; \*\*p<0.01).

Serum withdrawal attenuates expression of serum-glucocorticoid-regulated protein kinase (SGK) at the transcriptional level (Webster et al, 1993). Screening the TRPM4 protein sequence for a potential SGK-phosphorylation site (Seeböhm et al, 2005) revealed one SGK-consensus motif (RXRXXS) within the TRPM4 N-terminus (amino acids 250RLRLES255). Substitution of TRPM4 serine255 by alanine (TRPM4<sup>S255A</sup>) abolished the TRPM4 SGK-phosphorylation site. After transfection of HEK 293 cells with the phosphorylation null mutant TRPM4<sup>S255A</sup>, TRPM4 current measurements showed that the

increase in TRPM4<sup>S255A</sup> current density (112.7±25.9 pA/pF at +80mV) was similar to the one observed for TRPM4 upon serum withdrawal. Conversely, substitution of TRPM4 serine255 by aspartic acid (TRPM4<sup>S255D</sup>) to create a pseudo-phosphorylated TRPM4 yielded similar current densities (25.3±4.90 pA/pF at +80mV, n=16) as wild-type TRPM4 (20.19±3.52 pA/pF at +80mV, n=17). The combined data indicates that TRPM4 channel activity is augmented by serum withdrawal, i.e. cell stress. Coexpression experiments of TRPM4<sup>S255A</sup> and TRPM4<sup>S255D</sup> with SUMO-3 demonstrated that both TRPM4<sup>S255A</sup> and TRPM4<sup>S255D</sup> current densities were insensitive to SUMO-3, however co-expression SENP1 significantly decreased TRPM4<sup>S255A</sup> current densities to similar level as wild-type at basal condition (28.25±6.23 pA/pF at +80mV, n=12; p<0.01) but has no effect on TRPM4<sup>S255D</sup> (14.87±3.30 pA/pF at +80mV, n=11; p>0.05) (Fig VI. 11B). The result strongly suggests that SGK-phosphorylation/dephosphorylation of TRPM4 is upstream of the SUMOylation effect on TRPM4 activity.

## VI.6 Association of TRPM4 and caveolin-3 in murine heart

So far, the biochemical and electrophysiological data were obtained for TRPM4 expressed in a tissue cultured cell line. To validate the major conclusions of the above studies for primary cardiac tissue cells, cardiac tissue preparations were subjected to biochemical and immunohistochemical analysis. For these analyses, however, suitable anti-TRPM4 antibodies were not available. Therefore, I took advantage of a knock in mouse line (generated by Frederik Flenner and Transgenic facility in ZMNH), which expressed TRPM4 protein; Myc-tagged the same way as TRPM4 Flp In cell line. Thus, I analyzed the distribution of TRPM4 in plasma membrane microdomains of primary mouse cardiomyocytes using anti-Myc antibodies (Fig VI.12A). Firstly, Na<sub>2</sub>CO<sub>3</sub>-based sucrose gradient centrifugation experiment was performed to investigate distribution of TRPM4 protein in high versus low cholesterol fractions (See Method V.2.3). Lysate was prepared from freshly isolated and minced cardiac tissue of adult TRPM4 knock-in mice. A membrane pellet was collected by high-speed centrifugation. The pellet was suspended in

0.5M Na<sub>2</sub>CO<sub>3</sub> and submitted to ultra-speed sucrose gradient centrifugation. As shown in Fig VI.12A, Myc-tagged TRPM4 protein was exclusively detected in high cholesterol sucrose-gradient fraction. A substantial amount of caveolin-1 and -3, which are both expressed in cardiac tissue (Song et al, 1996b; Volonte et al, 2008) , as well as flotillin-1 and Na, K-ATPase  $\alpha$  subunit co-migrated in the sucrose gradient with TRPM4 (Fig VI. 12 A). The data indicates that cardiac TRPM4 protein is localized to cholesterol- and caveolin-rich microdomains of the plasma membrane.

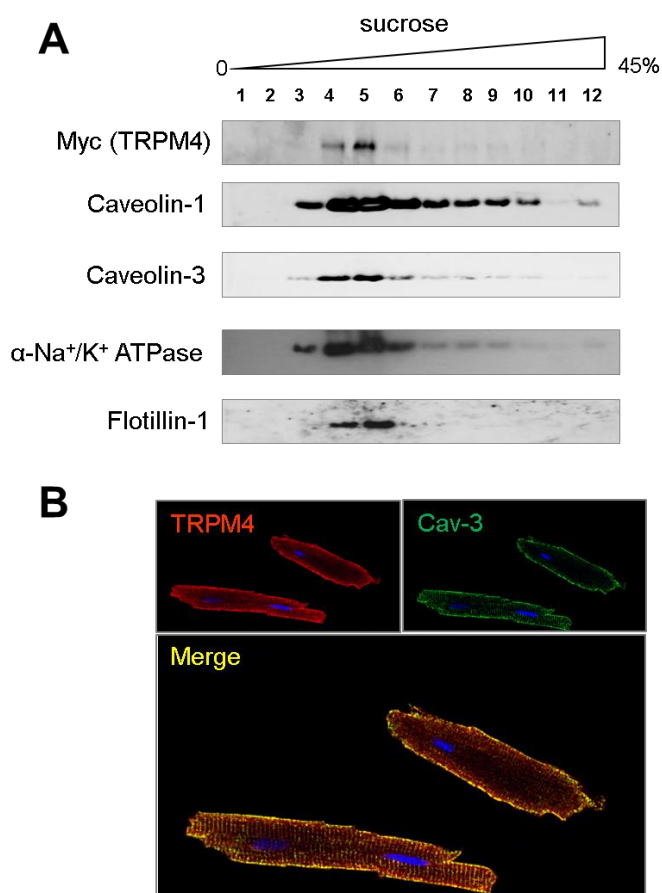


**Fig VI. 12 Associations of TRPM4 channel and caveolin in murine heart. A.** Immunoblot of cardiac membrane proteins isolated from lysate of cardiac tissue of Myc-tagged TRPM4 knock in mouse and subjected to Na<sub>2</sub>CO<sub>3</sub>-based sucrose gradient centrifugation as described in Fig VI.8. Twelve fractions were probed with antibodies against Myc-tagged TRPM4 (Myc (TRPM4)), caveolin-1, caveolin-3,  $\alpha$ -Na<sup>+</sup>/K<sup>+</sup> ATPase, and flotillin-1 as indicated at left. **B.** Immunohistochemical co-localization of TRPM4 (red) and caveolin-3 (green) in dissociated ventricular cardiomyocytes. Blue is DAPI nuclear staining.

Next, localization of cavolin-3 and TRPM4 protein within acutely isolated cardiac myocytes was visualized. Anti-caveolin-3 mouse antibodies and anti-TRPM4 sheep antibodies were

used to perform immunofluorescent co-localization analysis (Fig VI 12.B). The results showed that caveolin-3 and TRPM4 protein, which are both expressed in ventricular cardiomyocytes, co-localized at the plasma membrane. The immunohistochemical staining pattern strongly supports the earlier conclusion that the TRPM4 channel and caveolin form a complex.

## VI.7 Ouabain activates TRPM4 channel and alters its distribution in membrane microdomains

The membrane-bound  $\text{Na}^+/\text{K}^+$ -ATPase are abundantly localized to caveolae, a plasma membrane domain enriched in caveolin (Liu et al, 2003). From above results (Fig VI.8B and 12A), it was evident that the distribution of TRPM4 in sucrose gradients was similar to that of  $\text{Na}^+/\text{K}^+$ -ATPase. Interestingly, caveolar  $\text{Na}^+/\text{K}^+$ -ATPase interacts with cholesterol (Chen et al, 2009; Chen et al, 2011), and its  $\alpha$ -subunit also harbors caveolin-binding motifs (Wang et al, 2004). Inhibition of the  $\text{Na}^+/\text{K}^+$ -ATPase depolarizes cardiac myocytes and subsequently increases intracellular  $\text{Ca}^{2+}$  via the  $\text{Na}^+/\text{Ca}^{2+}$ -exchanger (NCX), thus increasing contractile force (Lingrel, 2010). Since TRPM4 is activated by a rise in intracellular  $\text{Ca}^{2+}$ , I wonder if inhibition of  $\text{Na}^+/\text{K}^+$ -ATPase by Ouabain will affect TRPM4 channel activity. To inhibit endogenous  $\text{Na}^+/\text{K}^+$ -ATPase in HEK 293 cells, a concentration of 100  $\mu\text{M}$  Ouabain was applied (Kockskamper et al, 1997) and TRPM4 current was measured before and after a 30 min application of Ouabain. TRPM4 currents were recorded as described in Fig VI.1C. Ouabain application significantly increased TRPM4 current ( $160.56 \pm 25.81$  pA/pF at +80mV, n=16;  $p < 0.001$ ) compared with control ( $34.58 \pm 6.32$  pA/pF at +80mV, n=16) without affecting TRPM4 current rectification. By contrast, TRPM4<sup>R164W</sup> currents were insensitive to Ouabain treatment ( $102.17 \pm 31.55$  pA/pF at +80mV without Ouabain, n=6;  $113.1 \pm 32.17$  pA/pF at +80mV with Ouabain, n=6;  $p > 0.05$ ) (Fig VI. 13A). Co-IP assays performed with lysates from TRPM4 Flp In cells treated with or without 100  $\mu\text{M}$  Ouabain showed that  $\text{Na}^+/\text{K}^+$ -ATPase  $\alpha$ -subunit co-immunoprecipitated with Myc-tagged TRPM4. Apparently, application of Ouabain augmented significantly the

amount of co-immunoprecipitated  $\text{Na}^+/\text{K}^+$ -ATPase  $\alpha$ -subunit (Fig VI.13B, n=3). By contrast, Co-IP assays with  $\text{TRPM4}^{\text{R164W}}$  showed, in comparison to wild-type  $\text{TRPM4}$ , already higher amounts of co-immunoprecipitated  $\text{Na}^+/\text{K}^+$ -ATPase  $\alpha$ -subunit (Fig VI.13C, n=3). The Co-IP result is a likely explanation for the observation that  $\text{TRPM4}^{\text{R164W}}$  current density was insensitive to Ouabain application.

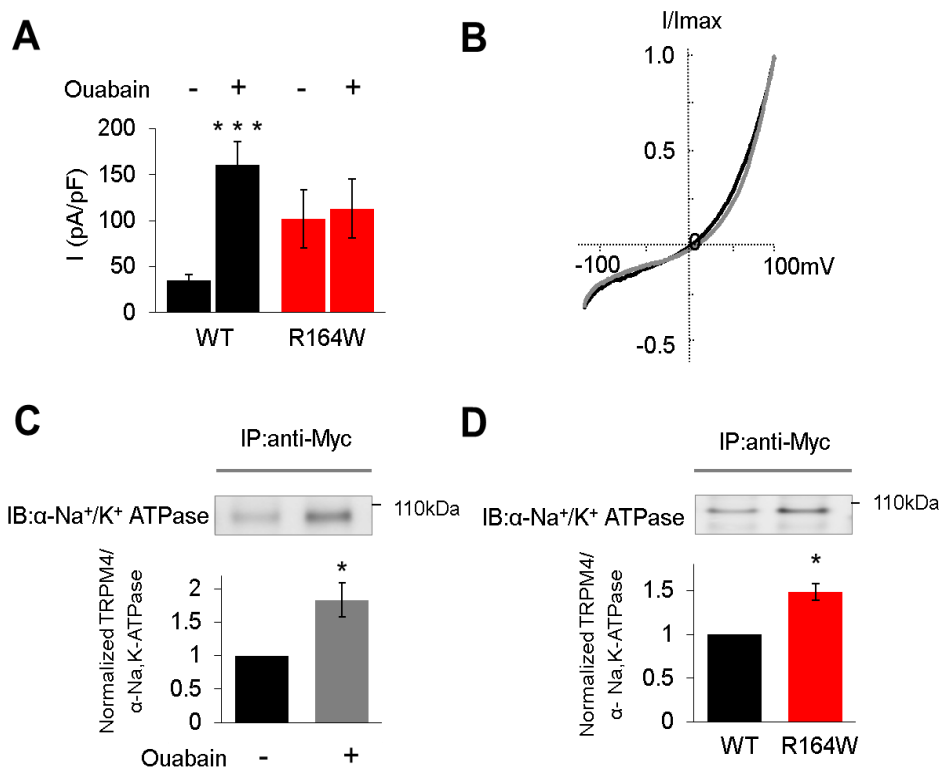


**Fig VI.13 Ouabain activates TRPM4 current and stabilizes TRPM4 and  $\text{Na}^+/\text{K}^+$ -ATPase complex.** **A.**  $\text{TRPM4}$  and  $\text{TRPM4}^{\text{R164W}}$  Flp In cells were treated with  $100\mu\text{M}$  Ouabain for 30min. Current densities of  $\text{TRPM4}$  (n=16) and  $\text{TRPM4}^{\text{R164W}}$  (n=6), obtained at  $+80\text{mV}$  as described in Fig VI.1C (\*\*\*) $p < 0.001$ ). **B.** Normalized current-voltage relations for  $\text{TRPM4}$  wild-type channel treated with (gray) or without Ouabain (black). **C.** Co-IP assays of Myc-tagged  $\text{TRPM4}$  protein and endogenous  $\text{Na}^+/\text{K}^+$ -ATPase  $\alpha$ -subunit from Flp In cells with (+) or without (-)  $100\mu\text{M}$  Ouabain treatment. Bottom is Co-IP band intensity normalized to basal condition (n=3;  $*p < 0.05$ ). **D.** Co-IP assays of Myc-tagged  $\text{TRPM4}$  and  $\text{TRPM4}^{\text{R164W}}$  with endogenous  $\text{Na}^+/\text{K}^+$ -ATPase  $\alpha$ -subunit from Flp In cells. Bottom is Co-IP band intensity normalized to wild-type (n=3;  $*p < 0.05$ ).

There is evidence that Ouabain inhibition of  $\text{Na}^+/\text{K}^+$ -ATPase induces  $\text{Na}^+/\text{K}^+$ -ATPase endocytosis in porcine proximal tubular cells (LLC-PK1) by a clathrin-dependent mechanism (Liu et al, 2004). Therefore, I performed biotinylation experiment to investigate whether

Ouabain will affect trafficking of TRPM4 channel. As shown in Fig VI.14A, Ouabain treatment resulted in a relatively small, but significant decrease of  $\text{Na}^+/\text{K}^+$ -ATPase  $\alpha$ -subunits residing at the cell surface ( $n=3$ ;  $p<0.05$ ), whereas the cell surface residence of TRPM4 was insensitive to Ouabain ( $n=3$ ;  $p>0.05$ ). On the other hand, ouabain treatment affected the distribution of TRPM4 and  $\text{Na}^+/\text{K}^+$ -ATPase  $\alpha$ -subunit in  $\text{Na}_2\text{CO}_3$ -based sucrose gradients in a similar way. Both proteins were shifted to lower-density sucrose fractions (Fig VI.14B). The data suggests a close functional association of TRPM4 channel and ouabain-inhibited  $\text{Na}^+/\text{K}^+$ -ATPase in specific membrane compartments, which are rich in cholesterol and possibly  $\text{PIP}_2$ .

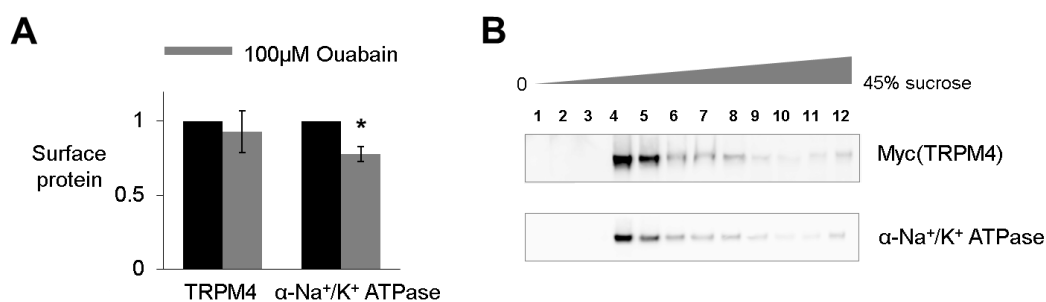


**Fig VI.14 Ouabain alters TRPM4 channel distribution in plasma membrane.** **A.** Surface proteins (TRPM4 and  $\text{Na}^+/\text{K}^+$ -ATPase  $\alpha$ -subunit) from TRPM4 Flp In cells treated with or without 100  $\mu\text{M}$  Ouabain for 1h were analyzed by biotinylation ( $n=3$ ;  $*p<0.05$ ). **B.** Distribution of TRPM4 and  $\text{Na}^+/\text{K}^+$ -ATPase  $\alpha$ -subunit from Flp In cells incubated with 100  $\mu\text{M}$  Ouabain in  $\text{Na}_2\text{CO}_3$ -based sucrose gradient fraction, processed as Fig VI.8B.

## VI.8 $\text{Ca}^{2+}$ response in TRPM4 deficient mice

Considering that  $\text{Na}^+/\text{K}^+$ -ATPase plays an essential role to maintain resting membrane potential (RMP), and Ouabain is able to activate TRPM4 channel and enhance association of TRPM4 and  $\text{Na}^+/\text{K}^+$ -ATPase in TRPM4 Flp In cells, I explored the physiological significance of TRPM4 channel to membrane potential. Firstly, I utilized mock Flp In cells and TRPM4 Flp In cells to compare their RMP, especially in the condition of Ouabain treatment. As shown in Fig VI.15A, in basal condition, Flp In cells had an average RMP at  $-14.07 \pm 1.17 \text{mV}$  ( $n=14$ ) in good agreement with the RMP reported for HEK 293 cells

(Sogaard et al, 2001). However RMP of TRPM4 Flp In cells was found to be significantly more depolarized ( $-6.17 \pm 1.64$  mV,  $n=11$ ;  $p<0.001$ ). 100  $\mu$ M Ouabain treatment increased RMP of mock Flp In cells to comparably positive potentials ( $-9.13 \pm 1.33$  mV,  $n=8$ ;  $p<0.05$ ). By contrast, RMP of TRPM4 Flp In cells was insensitive to ouabain treatment ( $-7.66 \pm 2.77$  mV,  $n=6$ ;  $p>0.05$ ). The data suggests that expression of TRPM4 channel in Flp In cells increases RMP and attenuates the effect of Ouabain on RMP.

In heterogenous expression system, the cardiac glycoside Ouabain stabilized a TRPM4- $\text{Na}^+/\text{K}^+$ -ATPase complex, induced their redistribution into specific cholesterol-rich membrane compartments, and resulted in a significant increase in TRPM4 current density. Cardiac  $\text{Na}^+/\text{K}^+$ -ATPase inhibition by ouabain leads to accumulation of  $\text{Na}^+$  in the cytoplasm, which may allow NCX into a reverse mode transporting  $\text{Na}^+$  out and  $\text{Ca}^{2+}$  into the cell (Iwamoto et al, 2007). It is reasonable to assume that this cellular condition increases intracellular  $\text{Ca}^{2+}$ , and thereby, activates  $\text{Ca}^{2+}$ -activated TRPM4 channel to balance membrane potential and  $\text{Ca}^{2+}$  influx. From this hypothesis it follows that cardiomyocytes of TRPM4 knock-out mice should respond differently to ouabain compared to wild-type mice.

Before investigating primary cardiomyocytes, I performed  $\text{Ca}^{2+}$ -imaging experiment on TRPM4 Flp In cells in comparisons to mock Flp In cells. Fura-2AM loaded cells were measured at 35°C, Ouabain in bath solution was perfused at 3ml/min. Compared with Flp In cells, expression of TRPM4 channel induced an obvious  $[\text{Ca}^{2+}]_i$  increase with Ouabain treatment. Finally, the cells were perfused with 0.5% Triton X-100 to achieve a maximal rise in  $[\text{Ca}^{2+}]_i$ . The ratio of maximal, minimal and baseline fluorescence was used to estimate changes in relative  $\text{Ca}^{2+}$  concentration (see Methods V.5.2). As shown in Fig VI.15B,  $\text{Ca}^{2+}$  response to Ouabain in TRPM4 Flp In cells ( $n=15$ ) was significantly higher than in mock Flp In cells ( $n=14$ ,  $p<0.05$ ), and under basal condition, they have no difference in  $[\text{Ca}^{2+}]_i$  ( $p>0.05$ ). The results suggested that TRPM4 channel is contributing to the increased  $\text{Ca}^{2+}$  influx in response to Ouabain. Combined with data from TRPM4 deficient mice would be an important observation to elucidate role of TRPM4 channel in heart.

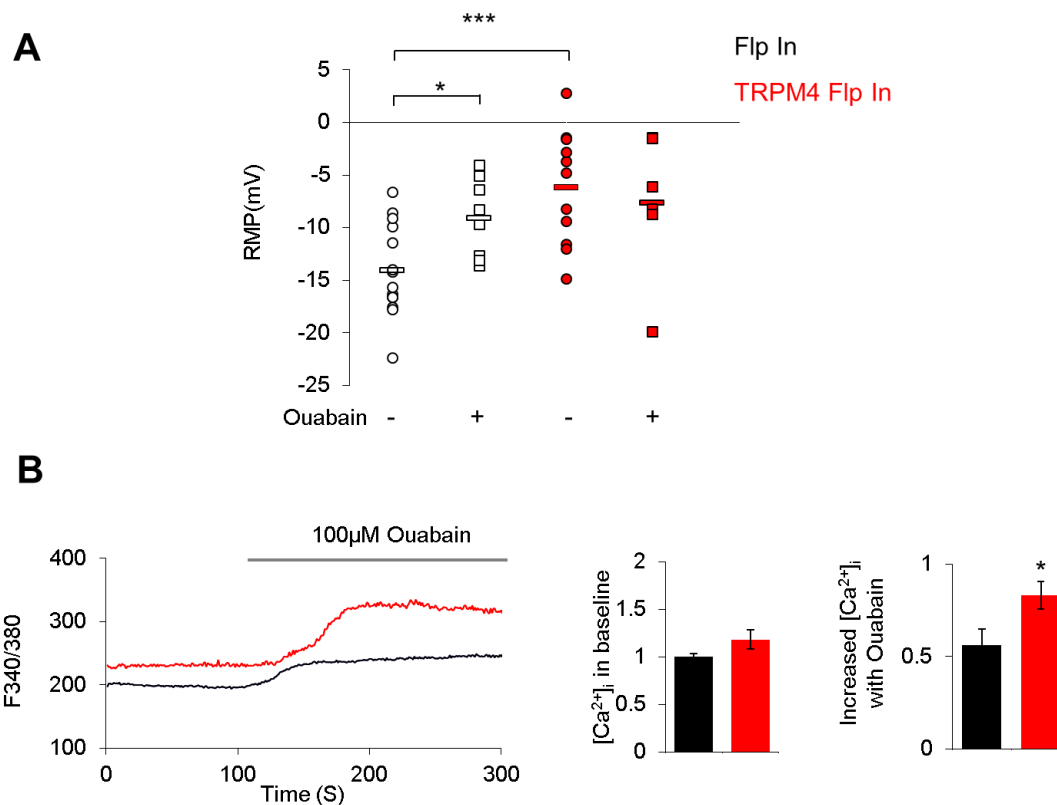


**Fig VI.15 Resting membrane potential and Ca<sup>2+</sup> response to Ouabain in TRPM4 Flp In cells.** **A.** Resting membrane potential (RMP) of mock Flp In cells (black) and TRPM4 Flp In cells (red) was measured at 0 pA in current clamp mode with (+) or without (-) Ouabain treatment (n=6~14; \* p<0.05, \*\*\* p<0.001). **B.** Fura-2AM loaded cells were perfused with 100μM Ouabain and their ratio fluorescence intensity (340nm/380nm) was recorded. Left is one representative experiment, right histograms are comparisons of intracellular Ca<sup>2+</sup> in baseline and after Ouabain treatment (n=14~15; \* p<0.05).

TRPM4 knock-out mice were obtained from Prof. Freichel (Universität Heidelberg), Ca<sup>2+</sup> measurements were carried out in Würzburg by Dr. Michael Klaiber (Institut für Physiologie, Universität Würzburg). As shown in Fig VI.16A, in the basal condition, peak amplitudes of Ca<sup>2+</sup><sub>i</sub> transients (Indo-1 Ratio<sub>405/495nm</sub>, systolic-diastolic) from cardiomyocytes in TRPM4 +/+ (n=21) and TRPM4 -/- mice (n=15) were similar (0.128±0.005 for TRPM4 +/+, 0.122±0.005 for TRPM4 -/-). When the cells were exposed to 10μM Ouabain and then 30μM Ouabain, significantly increased Ca<sup>2+</sup><sub>i</sub> amplitudes were observed both in cardiomyocytes of TRPM4 +/+ (10μM: 0.190±0.009, n=21; 30μM: 0.243±0.016, n=21; p<0.001) and TRPM4 -/- mice (10μM: 0.167±0.006, n=15; 30μM: 0.199±0.009, n=15; p<0.001). Importantly, TRPM4 +/+ mice exhibited stronger Ca<sup>2+</sup> response to Ouabain either at low or high concentration

compared with TRPM4  $-/-$  mice ( $p < 0.05$ ). Notably, subsequent addition of  $30 \mu\text{M}$  Ouabain and  $2 \mu\text{M}$  KB-R7943, a selective inhibitor of NCX in reverse mode (Iwamoto et al, 2007), efficiently decreased  $[\text{Ca}^{2+}]_i$  and there is no difference between TRPM4  $+/+$  ( $0.082 \pm 0.010$ ,  $n=12$ ) and TRPM4  $-/-$  mice ( $0.098 \pm 0.008$ ,  $n=11$ ). This indicated that reverse mode of NCX is involved in this process, inhibition of reverse mode of NCX is able to counteract the effect of Ouabain on cardiomyocyte.

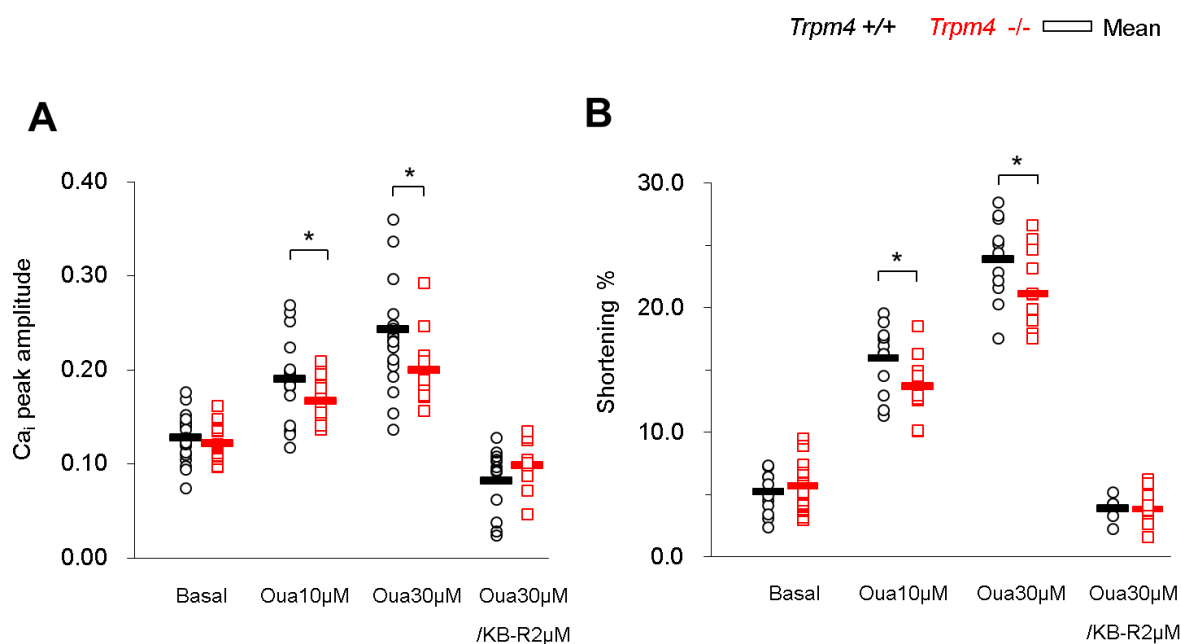


**Fig VI.16  $\text{Ca}^{2+}$  response and shortening of cell length.** Indo-1 Ratio $_{405/495\text{nm}}$ , systolic-diastolic (A) and simultaneously recorded cell length ( $L_{\text{max}}-L_{\text{min}}$ , expressed as percent from  $L_{\text{max}}$ ) in field-stimulated myocytes (B) at baseline and during perfusion with  $10 \mu\text{M}$  Ouabain,  $30 \mu\text{M}$  Ouabain and mixture of  $30 \mu\text{M}$  Ouabain and  $2 \mu\text{M}$  KB-R7943 ( $n=6\sim 21$  cells from 6 TRPM4  $+/+$  mice and 3 TRPM4  $-/-$  mice; \*  $p < 0.05$ ).

In agreement with  $\text{Ca}^{2+}$  amplitude measurements, increased  $[\text{Ca}^{2+}]_i$  transients accompanied increased sarcomere shortening. TRPM4  $+/+$  and TRPM4  $-/-$  mice both showed significantly increased shortening when cells were perfused with  $10 \mu\text{M}$  Ouabain ( $15.96 \pm 0.78\%$  for TRPM4  $+/+$ ,  $n=12$ ;  $13.70 \pm 0.68\%$  for TRPM4  $-/-$ ,  $n=12$ ;  $p < 0.001$ ), and then  $30 \mu\text{M}$  Ouabain ( $23.88 \pm 0.92\%$  for TRPM4  $+/+$ ,  $n=12$ ;  $21.13 \pm 0.92\%$  for TRPM4  $-/-$ ,  $n=12$ ;  $p < 0.001$ ). Finally this effect was reversed by addition of  $30 \mu\text{M}$  Ouabain and  $2 \mu\text{M}$  KB-R7943 ( $3.87 \pm 0.41\%$  for TRPM4  $+/+$ ,  $n=6$ ;  $3.87 \pm 0.52\%$  for TRPM4  $-/-$ ,  $n=9$ ;  $p < 0.001$ ). Notably, TRPM4  $+/+$  mice

showed more significant higher shortening in 10  $\mu$ M and 30  $\mu$ M Ouabain treatment compared with TRPM4  $-/-$  mice ( $p < 0.05$ ).

Taken together, the data suggested a potential role of TRPM4 channel in  $\text{Ca}^{2+}$  homeostasis and cardiac contraction. TRPM4 channel serves as an amplifier of Ouabain effect on  $\text{Na}^+/\text{K}^+$ -ATPase, and it contributes to more  $\text{Ca}^{2+}$  influx and stronger cardiac contraction, which are absent in the TRPM4 deficient mice.

## VII DISCUSSION

The purpose of this study was to explore regulatory mechanisms of TRPM4 channel activity and its physiological significance in relation to cardiac conduction using TRPM4 stably-expressing cell lines and TRPM4 deficient mice. The major findings were that caveolin, a caveolae structure protein, binds to TRPM4 and thereby regulates TRPM4 channel activity. SUMOylation, a post-translational modification, is involved in this regulation. SUMOylation of caveolin-1, leads to an altered localization of TRPM4 within the plasma membrane to activate TRPM4 channel. Furthermore, analysis of wild-type and TRPM4 knock out mice revealed a functional association of TRPM4 and Na<sup>+</sup>/K<sup>+</sup>-ATPase in caveolae of murine cardiomyocytes. TRPM4 channel activity apparently contributes to intracellular Ca<sup>2+</sup> homeostasis, which is essential for cardiac contraction.

### VII.1 SUMOylation stimulates TRPM4 current indirectly

Target protein modified by SUMOylation is a transient and reversible reaction; only a small fraction of substrate is in the SUMOylated form (Ulrich, 2005). This leads to difficulty in detecting SUMOylated target especially *in vivo*. With the exception of a SUMO to substrate branched-peptide being identified by mass spectrometry from an immunoprecipitation of an endogenous protein, no single experiment is sufficient to prove that a protein is SUMO modified (Tatham et al, 2009). Most targets were identified through *in vitro* SUMOylation assay with assist of SUMO enzymes and ATP (Fuhs & Insel, 2011). TRPM4 channel is a membrane protein, whereas majority of SUMO molecules reside in the nucleus. On the other hand, the effect of SUMOylation on TRPM4 is related with activity of channel rather than turnover of channel on the membrane, this likely implies an indirect regulation of TRPM4 by SUMOylation.

Current densities of TRPM4 channel are sensitive to SUMO conjugation enzyme, Ubc9, and SUMO ligase, PIAS3, and overexpression of both Ubc9 and PIAS3 can coordinately

increase current density. However, mutant TRPM4<sup>R164W</sup> is still insensitive to SUMOylation enzymes. Besides, I found out the SUMOylation-evoked stimulation of TRPM4 current is specifically observed with SUMO-3 (highly similarity with SUMO-2) not SUMO-1 (only 50% similarity with SUMO-2/3). However, I failed to detect any additional band on the top of TRPM4 protein band (~130kDa) in immunoblots, which is supposed to correspond to SUMO covalently-modified TRPM4 protein. Also, five potential SUMOylation-deficient mutations (K341A, K492N, K618A, K1140A, and K1154A) showed no obvious defect in TRPM4 channel function and protein expression level. These observations substantially decreased the possibility that SUMO is directly conjugated to TRPM4 protein. Possibly, there is a non-covalent binding between SUMO molecules and TRPM4 protein. Alternatively, TRPM4 associated with a SUMO target, not SUMO itself. This may explain the observations that TRPM4 protein can be co-immunoprecipitated with SUMO-3, and this interaction is attenuated by SENP1 overexpression.

Next, caveolae structure protein, caveolin was identified as an important binding partner of TRPM4 channel and its interaction with TRPM4 negatively regulates TRPM4 channel activity. This was firstly proved by Co-IP assay of TRPM4 protein and endogenous caveolin-1 as well as immunocytochemistry experiment, which showed an apparent co-localization especially near or at the plasma membrane in TRPM4 Flp In cells and murine cardiomyocytes.

Interaction with caveolin has been shown to directly modulate the activity or trafficking of a number of ion channels (Barbuti et al, 2004; McEwen et al, 2008). Caveolin scaffolding domain (CSD), which is responsible for association with other signaling molecules, is known to bind to specific sequences (caveolin-binding motif) on target proteins ( $\Phi X \Phi X X X X \Phi$ ,  $\Phi X X X X \Phi X X \Phi$  and  $\Phi X \Phi X X X X \Phi X X \Phi$ ), where  $\Phi$  is an aromatic amino acid (tryptophan, phenylalanine or tyrosine) and X is any amino acid (Couet et al, 1997). Two caveolin-binding mutations (TRPM4<sup>F223A</sup> and TRPM4<sup>F232A</sup>) based on consensus caveolin-binding motif from intracellular sequence of TRPM4 protein, showed attenuated association with caveolin-1 but enhanced current densities in comparison with wild-type

TRPM4. Consistent with this investigation, ICCD-related mutations, TRPM4<sup>R164W</sup>, ~four-fold current density of wild-type TRPM4 channel, showed weakened binding with caveolin-1 compared with wild-type. Moreover, overexpression of caveolin-1 augments interaction of caveolin-1 and induces a significantly decreased TRPM4<sup>R164W</sup> current and an obvious linear I-V relation instead of typical outward rectification, due to a relative increased inward current.

Notably, caveolin-1 and -3 both have conserved SUMOylation consensus motifs within their N-terminus near the caveolin-scaffolding domain (CSD), and caveolin-3 becomes SUMOylated in transfected mammalian cells expressing SUMO-3 (Fuhs & Insel, 2011). In TRPM4 Flp IN cells, Cav-1-SUMO-3 conjugates were also observed, which further corroborated the hypothesis that SUMOylation regulates TRPM4 current via caveolin-1, which acts as an ancillary protein.

## VII.2 TRPM4 activity associated with high cholesterol microdomain

In this part, I provided the first evidence that TRPM4 channel expressed in mammalian cell or murine heart, is highly localized to cholesterol and caveolin-rich membrane rafts. Depletion of cellular cholesterol content in TRPM4 Flp In cells, which significantly increased current amplitude of TRPM4 channel and enhance outward current as well, altered the distribution of TRPM4 channel between high and low-cholesterol domains. Together with the observations that excessive caveolin-1, disrupts cholesterol metabolism, alters TRPM4 outward rectification, I propose that TRPM4 channel I-V relations differ in membrane microdomains having different cholesterol concentration.

On the other hand, enhanced SUMOylation was also correlated with TRPM4 altered distribution in membrane microdomains. In the case of a boost in SUMOylation, more TRPM4 channels are segregated into low sucrose density and high-cholesterol microdomains, without affecting amount of channels at the plasma membrane. This

observation is similar to the effect of cholesterol-depletion. The two manipulations (cholesterol-depletion and enhanced SUMOylation) have no coordinated effect, nevertheless, enhanced deSUMOylation attenuated effect of cholesterol-depletion on TRPM4 current rather than on I-V relations, indicating consequence of SUMOylation on TRPM4 channel current occurs via a pathway similar to cholesterol-depletion.

M $\beta$ CD at high concentration rapidly removes cholesterol from plasma membrane and stops caveolin-1 trafficking completely, lower concentration induces accumulated caveolin-1 in LE/lysosome (Mundy et al, 2012), which also stimulates TRPM4 current. This is in line with the investigation that caveolin-1 negatively regulates TRPM4 channel current. Furthermore, the decreased protein level of caveolin-1 in the case of SUMO-3-evoked SUMOylation unveiled how SUMO-3- specific-SUMOylation regulates TRPM4 channel in a caveolin-1 dependent way. However, the decreased protein level of caveolin-1 in the case of SUMO-3-evoked SUMOylation due to enhanced degradation or alternatively, to altered trafficking, needs more study.

The known data implied that cholesterol depletion and SUMOylation of caveolin-1 are part of a signaling pathway to relocate the TRPM4 channel to a membranous environment more favorable for TRPM4 channel activity. By contrast, the ICCD mutation TRPM4<sup>R164W</sup> renders channel activity insensitive to SUMOylation and cholesterol-depletion, and enhances the residence of the TRPM4 channel in microdomains more favorable for its activity. Cholesterol is reported to regulate ion channels via down-regulation of PIP<sub>2</sub> (Chun et al, 2010), an activator of most TRP channels. PIP<sub>2</sub>-activated TRP channels (like TRPM8, TRPV1, and TRPC1 channel) are regulated by cholesterol-depletion in distinct ways (Bergdahl et al, 2003; Morenilla-Palao et al, 2009; Szoke et al, 2010). It is likely that TRPM4 activity-favorable microdomains is a PIP<sub>2</sub>-enriched one, and the effects on increased TRPM4 current are related to an increased affinity of TRPM4 for PIP<sub>2</sub> (Fig VII.1).

Finally, I unveiled that serum withdrawal is an efficient cell-stress to trigger SUMOylation

effects on TRPM4 channel current. This mechanism is related with a phosphorylation of TRPM4 by SGK, which is reported to regulate a series of ion channel, e.g. ENac and voltage-gated potassium channels (Pearce, 2003; Schuetz et al, 2008). However, the detailed mechanism how cell stress regulates SUMOylation is so far unclear.

Taken together, these observations suggested that TRPM4 hyperactivity in cardiac conduction diseases is probably caused by altered channel localization in the plasma membrane microdomains.

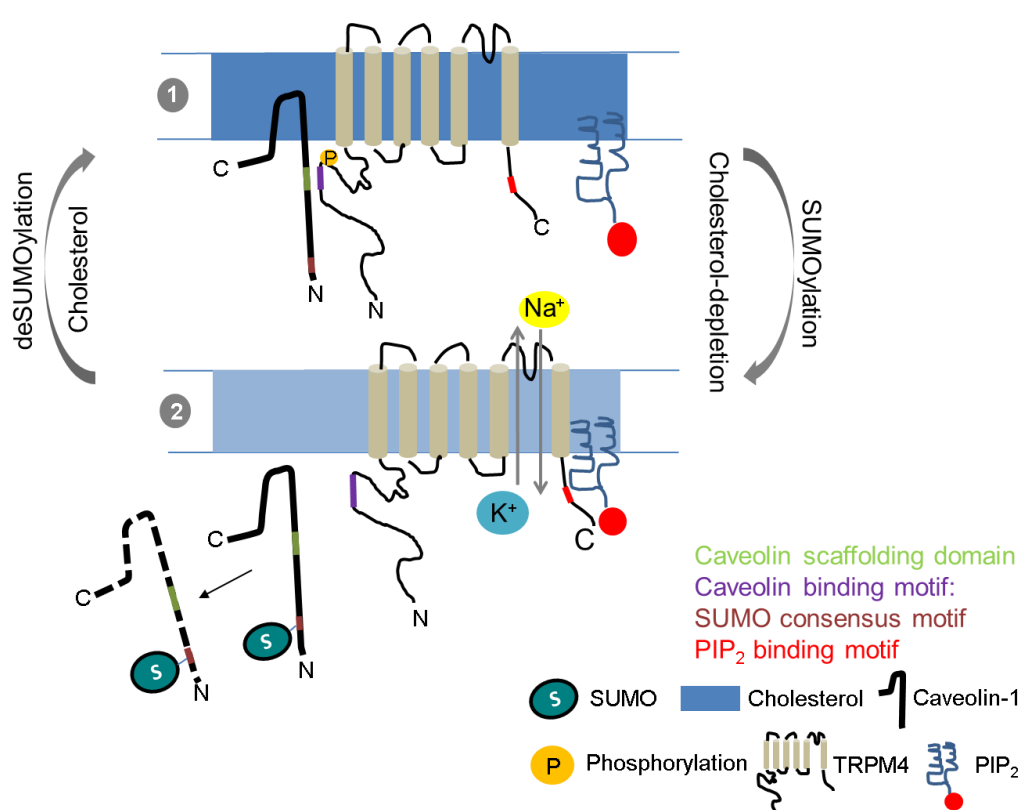


**Fig VII.1 Proposed models illustrating regulation of TRPM4 channel activity.** (1) TRPM4 channel is preferably localized to cholesterol and caveolin-1-enriched microdomains. TRPM4 channel interacts with caveolin-1 through caveolin binding motif. Caveolin-1 acts as a negative regulator of TRPM4. (2) SUMOylation (or cholesterol depletion) induces caveolin to dissociate of the TRPM4 channel, which relocates to a PIP<sub>2</sub>-enriched microdomains more favorable for TRPM4 channel activity. deSUMOylation reverses this process. N, N-terminus; C, C-terminus.

### VII.3 TRPM4 promotes $\text{Ca}^{2+}$ influx via inhibition of $\text{Na}^+/\text{K}^+$ -ATPase by Ouabain in cardiomyocytes

The  $\text{Na}^+/\text{K}^+$ -ATPase is an abundant protein in the plasma membrane of all animal cells that shuttles  $\text{Na}^+$  out of and  $\text{K}^+$  into the cytoplasm to maintain electric resting potential. Its regulation by cardiac glycosides is highly conserved across evolution and has been utilized to improve heart function since long before the rise of modern medicine. Inhibition of the  $\text{Na}^+/\text{K}^+$ -ATPase depolarizes cardiac myocytes and subsequently increases intracellular calcium via the  $\text{Na}^+/\text{Ca}^{2+}$ -exchanger (NCX), thus increasing contractile force (Lingrel, 2010). The cardiac TRPM4 channel conducts  $\text{Na}^+$  inward and  $\text{K}^+$  outward currents, making it a natural antagonist of the  $\text{Na}^+/\text{K}^+$ -ATPase. However, how the opposing activities of  $\text{Na}^+/\text{K}^+$ -ATPase and TRPM4 channel are coordinated in heart is so far unknown.

The distribution of  $\text{Na}^+/\text{K}^+$ -ATPase, a known caveolae-related membrane protein, in detergent-free based sucrose gradient is quite similar to that of TRPM4 protein. In line with this, the two proteins from mammalian cells can be co-immunoprecipitated and they are also co-localized in dissociated cardiomyocytes, suggesting a close spatial association. Moreover, when endogenous  $\text{Na}^+/\text{K}^+$ -ATPase in TRPM4 Flp In cells was inhibited by  $100\mu\text{M}$  Ouabain, TRPM4 channel current increased significantly and the binding between TRPM4 and  $\alpha$ -subunit of  $\text{Na}^+/\text{K}^+$ -ATPase was enhanced. I also observed that more TRPM4 proteins and  $\alpha$ -subunit of  $\text{Na}^+/\text{K}^+$ -ATPase were recruited in low sucrose density and high cholesterol fractions. These observations suggested a close functional association of TRPM4 channel and  $\text{Na}^+/\text{K}^+$ -ATPase in specific membrane compartments in the case of Ouabain.

To investigate physiological significance of TRPM4 channel combined with  $\text{Na}^+/\text{K}^+$ -ATPase in heart, especially whether inhibition of  $\text{Na}^+/\text{K}^+$ -ATPase will lead to activation of TRPM4 channel *in vivo*, intracellular  $\text{Ca}^{2+}$  response in cardiomyocytes were measured in TRPM4 deficient mice. TRPM4 deficient mice showed an unaltered  $\text{Ca}^{2+}$

response and shortening under basal conditions. When Ouabain with low or high concentration was applied, strongly increased  $\text{Ca}^{2+}$  amplitudes and sarcomere shortenings were observed in wild-type mice and TRPM4 deficient mice. However, TRPM4 deficiency showed a significantly attenuated  $\text{Ca}^{2+}$  response and contraction compared with wild-type mice. Besides, KB-R7943, blocker of reverse mode of NCX, completely reversed effect of Ouabain on  $\text{Ca}^{2+}$  amplitude and sarcomere shortening, suggesting  $\text{Ca}^{2+}$  influx by reverse mode of NCX is involved in this process and increased  $[\text{Ca}^{2+}]_i$  is indispensable for TRPM4 activation. Increased intracellular  $\text{Ca}^{2+}$  by NCX leads to activation of TRPM4 and TRPM4 transports more  $\text{Na}^+$  into cytoplasm, which enhances  $\text{Na}^+$  accumulation in cytoplasm, thereby more  $\text{Ca}^{2+}$  are transported into cytoplasm in place of  $\text{Na}^+$  by NCX. TRPM4 is supposed to work as an amplifier of Ouabain on  $\text{Ca}^{2+}$  response and heart contraction (Fig VII.2).

Recent literature based on *trpm4* gene targeting in mice showed that TRPM4 regulates  $\text{Ca}^{2+}$  homeostasis in distinct ways, depending on cell types. Absence of TRPM4 elicited  $\text{Ca}^{2+}$  overload in dendritic cells (Barbet et al, 2008), similarly, deletion of TRPM4 enhanced FcεRI-induced mast cell  $\text{Ca}^{2+}$  influx (Vennekens et al, 2007). In contrast, inhibition of TRPM4 in pancreatic  $\beta$ -cell lines by a dominant-negative effect significantly decreased the magnitude of the  $\text{Ca}^{2+}$  generated by agonist stimulation, therefore reducing insulin secretion (Marigo et al, 2009). My preliminary result unveiled a possible role of TRPM4 in  $\text{Ca}^{2+}$  homeostasis of cardiomyocytes. Notably, in basal condition, TRPM4 deficiency showed unaltered physiological behavior of murine heart; the difference only happened in the pharmacological status, in which TRPM4 channel was largely activated. Consistently, those PFHBI/ICCD-related mutations all induce gain of function in current densities compared with wild-type TRPM4 channel. Therefore, it may be more worthwhile to investigate behaviors of genetically-modified mice with overexpressed TRPM4. Besides,  $\text{Na}^+/\text{K}^+$ -ATPase plays an essential role in maintaining membrane potential, and TRPM4 channel is a voltage-dependent channel, it remains to be determined whether TRPM4 channel coordinates with  $\text{Na}^+/\text{K}^+$ -ATPase to maintain membrane potential.

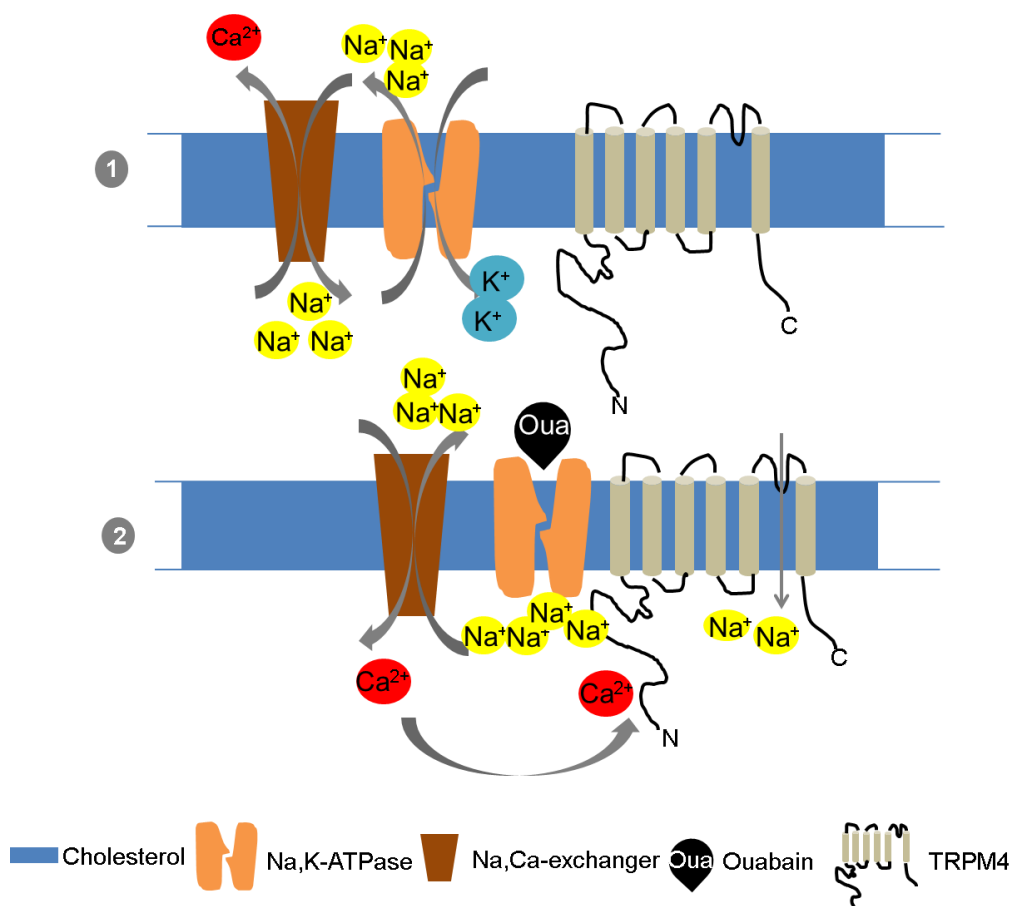


**Fig VII. 2 Proposed models illustrating the functional association of Na<sup>+</sup>/K<sup>+</sup>-ATPase and TRPM4 channel.** (1) Under basal condition, Na<sup>+</sup>/K<sup>+</sup>-ATPase cooperates with Na,Ca-exchanger to maintain ion homeostasis. (2) When Na<sup>+</sup>/K<sup>+</sup>-ATPase is inhibited by Ouabain, Na<sup>+</sup> accumulates in cytoplasm. Reverse mode of NCX is activated (Ca<sup>2+</sup> is transported into cytoplasm in place of 3 Na<sup>+</sup>). Increased [Ca<sup>2+</sup>]<sub>i</sub> activates TRPM4 channel, which transports more Na<sup>+</sup> into cytoplasm to amplify effect of Ouabain on Ca<sup>2+</sup> influx.

In conclusion, this thesis elucidated regulation of TRPM4 activity and its potential role for cardiac conduction. These observations provide the first evidence that TRPM4 channel activity is associated with its distribution in membrane microdomains, and its localization could be affected by either mutant channel, cholesterol content in membrane and interaction with caveolins. SUMOylation is one pathway to stimulate TRPM4 channel activity via regulating caveolins and altering its distribution. Moreover, TRPM4 channel has close functional association with Na<sup>+</sup>/K<sup>+</sup>-ATPase in Ca<sup>2+</sup> homeostasis and cardiac contraction *in vivo*. The results should provide a new insight into understanding physiological and pathological significance of TRPM4 channel in cardiac conduction.

## VIII REFERENCE

Barbet G, Demion M, Moura IC, Serafini N, Leger T, Vrtovsnik F, Monteiro RC, Guinamard R, Kinet JP, Launay P (2008) The calcium-activated nonselective cation channel TRPM4 is essential for the migration but not the maturation of dendritic cells. *Nat Immunol* **9**: 1148-1156

Barbuti A, Gravante B, Riolfo M, Milanesi R, Terragni B, DiFrancesco D (2004) Localization of pacemaker channels in lipid rafts regulates channel kinetics. *Circ Res* **94**: 1325-1331

Bardien-Kruger S, Wulff H, Arieff Z, Brink P, Chandy KG, Corfield V (2002) Characterisation of the human voltage-gated potassium channel gene, KCNA7, a candidate gene for inherited cardiac disorders, and its exclusion as cause of progressive familial heart block I (PFHBI). *Eur J Hum Genet* **10**: 36-43

Benson MD, Li QJ, Kieckhafer K, Dudek D, Whorton MR, Sunahara RK, Iniguez-Lluhi JA, Martens JR (2007) SUMO modification regulates inactivation of the voltage-gated potassium channel Kv1.5. *Proc Natl Acad Sci U S A* **104**: 1805-1810

Bergdahl A, Gomez MF, Dreja K, Xu SZ, Adner M, Beech DJ, Broman J, Hellstrand P, Sward K (2003) Cholesterol depletion impairs vascular reactivity to endothelin-1 by reducing store-operated Ca<sup>2+</sup> entry dependent on TRPC1. *Circ Res* **93**: 839-847

Bou-Abboud E, Li H, Nerbonne JM (2000) Molecular diversity of the repolarizing voltage-gated K<sup>+</sup> currents in mouse atrial cells. *J Physiol* **529 Pt 2**: 345-358

Boukens BJ, Christoffels VM (2012) Electrophysiological Patterning of the Heart. *Pediatr Cardiol*

Brink AJ, Torrington M (1977) Progressive familial heart block--two types. *S Afr Med J* **52**: 53-59

Brink PA, Ferreira A, Moolman JC, Weymar HW, van der Merwe PL, Corfield VA (1995) Gene for progressive familial heart block type I maps to chromosome 19q13. *Circulation* **91**: 1633-1640

Bruderer R, Tatham MH, Plechanovova A, Matic I, Garg AK, Hay RT (2011) Purification and identification of endogenous polySUMO conjugates. *EMBO Rep* **12**: 142-148

Chen Y, Cai T, Wang H, Li Z, Loreaux E, Lingrel JB, Xie Z (2009) Regulation of intracellular cholesterol distribution by Na/K-ATPase. *J Biol Chem* **284**: 14881-14890

Chen Y, Li X, Ye Q, Tian J, Jing R, Xie Z (2011) Regulation of alpha1 Na/K-ATPase expression by cholesterol. *J Biol Chem* **286**: 15517-15524

Cheng H, Beck A, Launay P, Gross SA, Stokes AJ, Kinet JP, Fleig A, Penner R (2007) TRPM4 controls insulin secretion in pancreatic beta-cells. *Cell Calcium* **41**: 51-61

- Chiu SN, Wang JK, Wu MH, Chang CW, Chen CA, Lin MT, Wu ET, Hua YC, Lue HC (2008) Cardiac conduction disturbance detected in a pediatric population. *J Pediatr* **152**: 85-89
- Chun YS, Shin S, Kim Y, Cho H, Park MK, Kim TW, Voronov SV, Di Paolo G, Suh BC, Chung S (2010) Cholesterol modulates ion channels via down-regulation of phosphatidylinositol 4,5-bisphosphate. *J Neurochem* **112**: 1286-1294
- Colquhoun D, Neher E, Reuter H, Stevens CF (1981) Inward current channels activated by intracellular Ca in cultured cardiac cells. *Nature* **294**: 752-754
- Couet J, Li S, Okamoto T, Ikezu T, Lisanti MP (1997) Identification of peptide and protein ligands for the caveolin-scaffolding domain. Implications for the interaction of caveolin with caveolae-associated proteins. *J Biol Chem* **272**: 6525-6533
- Crnich R, Amberg GC, Leo MD, Gonzales AL, Tamkun MM, Jaggar JH, Earley S (2010) Vasoconstriction resulting from dynamic membrane trafficking of TRPM4 in vascular smooth muscle cells. *Am J Physiol Cell Physiol* **299**: C682-694
- Dai XQ, Kolic J, Marchi P, Sipione S, Macdonald PE (2009) SUMOylation regulates Kv2.1 and modulates pancreatic beta-cell excitability. *J Cell Sci* **122**: 775-779
- de Meeus A, Stephan E, Debrus S, Jean MK, Loiselet J, Weissenbach J, Demaille J, Bouvagnet P (1995) An isolated cardiac conduction disease maps to chromosome 19q. *Circ Res* **77**: 735-740
- Demion M, Bois P, Launay P, Guinamard R (2007) TRPM4, a Ca<sup>2+</sup>-activated nonselective cation channel in mouse sino-atrial node cells. *Cardiovasc Res* **73**: 531-538
- Earley S, Waldron BJ, Brayden JE (2004) Critical role for transient receptor potential channel TRPM4 in myogenic constriction of cerebral arteries. *Circ Res* **95**: 922-929
- Ector H, Rickards AF, Kappenberger L, Vardas P, Oto A, Santini M, Sutton R (2000) The registry of the European Working Group on Cardiac Pacing (EWGCP). A working group of the European Society of Cardiology. *Europace* **2**: 251-255
- Feliciangeli S, Bendahhou S, Sandoz G, Gounon P, Reichold M, Warth R, Lazdunski M, Barhanin J, Lesage F (2007) Does sumoylation control K2P1/TWIK1 background K<sup>+</sup> channels? *Cell* **130**: 563-569
- Fliegert R, Glassmeier G, Schmid F, Cornils K, Genisyuerk S, Harneit A, Schwarz JR, Guse AH (2007) Modulation of Ca<sup>2+</sup> entry and plasma membrane potential by human TRPM4b. *FEBS J* **274**: 704-713
- Fu Y, Hoang A, Escher G, Parton RG, Krozowski Z, Sviridov D (2004) Expression of caveolin-1 enhances cholesterol efflux in hepatic cells. *J Biol Chem* **279**: 14140-14146
- Fuhs SR, Insel PA (2011) Caveolin-3 undergoes SUMOylation by the SUMO E3 ligase PIASy: sumoylation

- affects G-protein-coupled receptor desensitization. *J Biol Chem* **286**: 14830-14841
- Geiss-Friedlander R, Melchior F (2007) Concepts in sumoylation: a decade on. *Nat Rev Mol Cell Biol* **8**: 947-956
- Gonzales AL, Amberg GC, Earley S (2010) Ca<sup>2+</sup> release from the sarcoplasmic reticulum is required for sustained TRPM4 activity in cerebral artery smooth muscle cells. *Am J Physiol Cell Physiol* **299**: C279-288
- Gonzales AL, Earley S (2012) Endogenous cytosolic Ca(2+) buffering is necessary for TRPM4 activity in cerebral artery smooth muscle cells. *Cell Calcium* **51**: 82-93
- Grant AO (2009) Cardiac ion channels. *Circ Arrhythm Electrophysiol* **2**: 185-194
- Grynkiewicz G, Poenie M, Tsien RY (1985) A new generation of Ca<sup>2+</sup> indicators with greatly improved fluorescence properties. *J Biol Chem* **260**: 3440-3450
- Guinamard R, Chatelier A, Demion M, Potreau D, Patri S, Rahmati M, Bois P (2004) Functional characterization of a Ca(2+)-activated non-selective cation channel in human atrial cardiomyocytes. *J Physiol* **558**: 75-83
- Guo B, Yang SH, Witty J, Sharrocks AD (2007) Signalling pathways and the regulation of SUMO modification. *Biochem Soc Trans* **35**: 1414-1418
- Guo D, Han J, Adam BL, Colburn NH, Wang MH, Dong Z, Eizirik DL, She JX, Wang CY (2005) Proteomic analysis of SUMO4 substrates in HEK293 cells under serum starvation-induced stress. *Biochem Biophys Res Commun* **337**: 1308-1318
- Hamill OP, Marty A, Neher E, Sakmann B, Sigworth FJ (1981) Improved patch-clamp techniques for high-resolution current recording from cells and cell-free membrane patches. *Pflugers Arch* **391**: 85-100
- Hannich JT, Lewis A, Kroetz MB, Li SJ, Heide H, Emili A, Hochstrasser M (2005) Defining the SUMO-modified proteome by multiple approaches in *Saccharomyces cerevisiae*. *J Biol Chem* **280**: 4102-4110
- Hecker CM, Rabiller M, Haglund K, Bayer P, Dikic I (2006) Specification of SUMO1- and SUMO2-interacting motifs. *J Biol Chem* **281**: 16117-16127
- Iwamoto T, Watanabe Y, Kita S, Blaustein MP (2007) Na<sup>+</sup>/Ca<sup>2+</sup> exchange inhibitors: a new class of calcium regulators. *Cardiovasc Hematol Disord Drug Targets* **7**: 188-198
- Kao JP (1994) Practical aspects of measuring [Ca<sup>2+</sup>] with fluorescent indicators. *Methods Cell Biol* **40**: 155-181
- Kim JH, Baek SH (2009) Emerging roles of desumoylating enzymes. *Biochim Biophys Acta* **1792**: 155-162
- Kockskamper J, Gisselmann G, Glitsch HG (1997) Comparison of ouabain-sensitive and -insensitive Na/K

- pumps in HEK293 cells. *Biochim Biophys Acta* **1325**: 197-208
- Kruse M, Schulze-Bahr E, Corfield V, Beckmann A, Stallmeyer B, Kurtbay G, Ohmert I, Brink P, Pongs O (2009) Impaired endocytosis of the ion channel TRPM4 is associated with human progressive familial heart block type I. *J Clin Invest* **119**: 2737-2744
- Launay P, Fleig A, Perraud AL, Scharenberg AM, Penner R, Kinet JP (2002) TRPM4 is a Ca<sup>2+</sup>-activated nonselective cation channel mediating cell membrane depolarization. *Cell* **109**: 397-407
- Liman ER (2007) The Ca<sup>2+</sup>-Activated TRP Channels: TRPM4 and TRPM5.
- Lingrel JB (2010) The physiological significance of the cardiotonic steroid/ouabain-binding site of the Na,K-ATPase. *Annu Rev Physiol* **72**: 395-412
- Liu H, El Zein L, Kruse M, Guinamard R, Beckmann A, Bozio A, Kurtbay G, Megarbane A, Ohmert I, Blaysat G, Villain E, Pongs O, Bouvagnet P (2010) Gain-of-function mutations in TRPM4 cause autosomal dominant isolated cardiac conduction disease. *Circ Cardiovasc Genet* **3**: 374-385
- Liu J, Kesiry R, Periyasamy SM, Malhotra D, Xie Z, Shapiro JI (2004) Ouabain induces endocytosis of plasmalemmal Na/K-ATPase in LLC-PK1 cells by a clathrin-dependent mechanism. *Kidney Int* **66**: 227-241
- Liu L, Mohammadi K, Aynafshar B, Wang H, Li D, Liu J, Ivanov AV, Xie Z, Askari A (2003) Role of caveolae in signal-transducing function of cardiac Na<sup>+</sup>/K<sup>+</sup>-ATPase. *Am J Physiol Cell Physiol* **284**: C1550-1560
- Mahajan R, Delphin C, Guan T, Gerace L, Melchior F (1997) A small ubiquitin-related polypeptide involved in targeting RanGAP1 to nuclear pore complex protein RanBP2. *Cell* **88**: 97-107
- Marigo V, Courville K, Hsu WH, Feng JM, Cheng H (2009) TRPM4 impacts on Ca<sup>2+</sup> signals during agonist-induced insulin secretion in pancreatic beta-cells. *Mol Cell Endocrinol* **299**: 194-203
- Mathar I, Vennekens R, Meissner M, Kees F, Van der Mieren G, Camacho Londono JE, Uhl S, Voets T, Hummel B, van den Bergh A, Herijgers P, Nilius B, Flockerzi V, Schweda F, Freichel M (2010) Increased catecholamine secretion contributes to hypertension in TRPM4-deficient mice. *J Clin Invest* **120**: 3267-3279
- McEwen DP, Li Q, Jackson S, Jenkins PM, Martens JR (2008) Caveolin regulates kv1.5 trafficking to cholesterol-rich membrane microdomains. *Mol Pharmacol* **73**: 678-685
- Miller WL, Hodge DO, Hammill SC (2008) Association of uncomplicated electrocardiographic conduction blocks with subsequent cardiac morbidity in a community-based population (Olmsted County, Minnesota). *Am J Cardiol* **101**: 102-106
- Mironov SL (2008) Metabotropic glutamate receptors activate dendritic calcium waves and TRPM channels which drive rhythmic respiratory patterns in mice. *J Physiol* **586**: 2277-2291
- Morenilla-Palao C, Pertusa M, Meseguer V, Cabedo H, Viana F (2009) Lipid raft segregation modulates

- TRPM8 channel activity. *J Biol Chem* **284**: 9215-9224
- Mundy DI, Li WP, Luby-Phelps K, Anderson RG (2012) Caveolin targeting to late endosome/lysosomal membranes is induced by perturbations of lysosomal pH and cholesterol content. *Mol Biol Cell* **23**: 864-880
- Neher E, Sakmann B (1992) The patch clamp technique. *Sci Am* **266**: 44-51
- Nelson PL, Zolochowska O, Figueiredo ML, Soliman A, Hsu WH, Feng JM, Zhang H, Cheng H (2011) Regulation of Ca<sup>2+</sup>-entry in pancreatic alpha-cell line by transient receptor potential melastatin 4 plays a vital role in glucagon release. *Mol Cell Endocrinol* **335**: 126-134
- Nilius B, Mahieu F, Prenen J, Janssens A, Owsianik G, Vennekens R, Voets T (2006) The Ca<sup>2+</sup>-activated cation channel TRPM4 is regulated by phosphatidylinositol 4,5-bisphosphate. *EMBO J* **25**: 467-478
- Nilius B, Prenen J, Droogmans G, Voets T, Vennekens R, Freichel M, Wissenbach U, Flockerzi V (2003) Voltage dependence of the Ca<sup>2+</sup>-activated cation channel TRPM4. *J Biol Chem* **278**: 30813-30820
- Nilius B, Prenen J, Janssens A, Owsianik G, Wang C, Zhu MX, Voets T (2005a) The selectivity filter of the cation channel TRPM4. *J Biol Chem* **280**: 22899-22906
- Nilius B, Prenen J, Janssens A, Voets T, Droogmans G (2004) Decavanadate modulates gating of TRPM4 cation channels. *J Physiol* **560**: 753-765
- Nilius B, Prenen J, Tang J, Wang C, Owsianik G, Janssens A, Voets T, Zhu MX (2005b) Regulation of the Ca<sup>2+</sup> sensitivity of the nonselective cation channel TRPM4. *J Biol Chem* **280**: 6423-6433
- Pearce D (2003) SGK1 regulation of epithelial sodium transport. *Cell Physiol Biochem* **13**: 13-20
- Pichler A, Knipscheer P, Oberhofer E, van Dijk WJ, Korner R, Olsen JV, Jentsch S, Melchior F, Sixma TK (2005) SUMO modification of the ubiquitin-conjugating enzyme E2-25K. *Nat Struct Mol Biol* **12**: 264-269
- Pike LJ, Casey L (1996) Localization and turnover of phosphatidylinositol 4,5-bisphosphate in caveolin-enriched membrane domains. *J Biol Chem* **271**: 26453-26456
- Rajan S, Plant LD, Rabin ML, Butler MH, Goldstein SA (2005) Sumoylation silences the plasma membrane leak K<sup>+</sup> channel K2P1. *Cell* **121**: 37-47
- Rodal SK, Skretting G, Garred O, Vilhardt F, van Deurs B, Sandvig K (1999) Extraction of cholesterol with methyl-beta-cyclodextrin perturbs formation of clathrin-coated endocytic vesicles. *Mol Biol Cell* **10**: 961-974
- Rook MB, Evers MM, Vos MA, Bierhuizen MF (2012) Biology of cardiac sodium channel Nav1.5 expression. *Cardiovasc Res* **93**: 12-23
- Sala-Rabanal M, Wang S, Nichols CG (2012) On Potential Interactions between Non-selective Cation Channel TRPM4 and Sulfonylurea Receptor SUR1. *J Biol Chem* **287**: 8746-8756

- Schott JJ, Alshinawi C, Kyndt F, Probst V, Hoorntje TM, Hulsbeek M, Wilde AA, Escande D, Mannens MM, Le Marec H (1999) Cardiac conduction defects associate with mutations in SCN5A. *Nat Genet* **23**: 20-21
- Schuetz F, Kumar S, Poronnik P, Adams DJ (2008) Regulation of the voltage-gated K(+) channels KCNQ2/3 and KCNQ3/5 by serum- and glucocorticoid-regulated kinase-1. *Am J Physiol Cell Physiol* **295**: C73-80
- Seeböhm G, Strutz-Seeböhm N, Baltaev R, Korniyuchuk G, Knirsch M, Engel J, Lang F (2005) Regulation of KCNQ4 potassium channel prepulse dependence and current amplitude by SGK1 in *Xenopus* oocytes. *Cell Physiol Biochem* **16**: 255-262
- Shimizu T, Owsianik G, Freichel M, Flockerzi V, Nilius B, Vennekens R (2009) TRPM4 regulates migration of mast cells in mice. *Cell Calcium* **45**: 226-232
- Simionescu N (1983) Cellular aspects of transcapillary exchange. *Physiol Rev* **63**: 1536-1579
- Smart EJ, Ying Y, Donzell WC, Anderson RG (1996) A role for caveolin in transport of cholesterol from endoplasmic reticulum to plasma membrane. *J Biol Chem* **271**: 29427-29435
- Sogaard R, Ljungstrom T, Pedersen KA, Olesen SP, Jensen BS (2001) KCNQ4 channels expressed in mammalian cells: functional characteristics and pharmacology. *Am J Physiol Cell Physiol* **280**: C859-866
- Song J, Durrin LK, Wilkinson TA, Krontiris TG, Chen Y (2004) Identification of a SUMO-binding motif that recognizes SUMO-modified proteins. *Proc Natl Acad Sci U S A* **101**: 14373-14378
- Song KS, Li S, Okamoto T, Quilliam LA, Sargiacomo M, Lisanti MP (1996a) Co-purification and direct interaction of Ras with caveolin, an integral membrane protein of caveolae microdomains. Detergent-free purification of caveolae microdomains. *J Biol Chem* **271**: 9690-9697
- Song KS, Scherer PE, Tang Z, Okamoto T, Li S, Chafel M, Chu C, Kohtz DS, Lisanti MP (1996b) Expression of caveolin-3 in skeletal, cardiac, and smooth muscle cells. Caveolin-3 is a component of the sarcolemma and co-fractionates with dystrophin and dystrophin-associated glycoproteins. *J Biol Chem* **271**: 15160-15165
- Stallmeyer B, Zumhagen S, Denjoy I, Duthoit G, Hebert JL, Ferrer X, Maugenre S, Schmitz W, Kirchhefer U, Schulze-Bahr E, Guicheney P (2012) Mutational spectrum in the Ca(2+)-activated cation channel gene TRPM4 in patients with cardiac conductance disturbances. *Hum Mutat* **33**: 109-117
- Szoke E, Borzsei R, Toth DM, Lengel O, Helyes Z, Sandor Z, Szolcsanyi J (2010) Effect of lipid raft disruption on TRPV1 receptor activation of trigeminal sensory neurons and transfected cell line. *Eur J Pharmacol* **628**: 67-74
- Tatham MH, Rodriguez MS, Xirodimas DP, Hay RT (2009) Detection of protein SUMOylation in vivo. *Nat Protoc* **4**: 1363-1371
- Thiele C, Hannah MJ, Fahrenholz F, Huttner WB (2000) Cholesterol binds to synaptophysin and is required

- for biogenesis of synaptic vesicles. *Nat Cell Biol* **2**: 42-49
- Ullrich ND, Voets T, Prenen J, Vennekens R, Talavera K, Droogmans G, Nilius B (2005) Comparison of functional properties of the Ca<sup>2+</sup>-activated cation channels TRPM4 and TRPM5 from mice. *Cell Calcium* **37**: 267-278
- Ulrich HD (2005) SUMO modification: wrestling with protein conformation. *Curr Biol* **15**: R257-259
- Vennekens R, Olausson J, Meissner M, Bloch W, Mathar I, Philipp SE, Schmitz F, Weissgerber P, Nilius B, Flockerzi V, Freichel M (2007) Increased IgE-dependent mast cell activation and anaphylactic responses in mice lacking the calcium-activated nonselective cation channel TRPM4. *Nat Immunol* **8**: 312-320
- Volonte D, McTiernan CF, Drab M, Kasper M, Galbiati F (2008) Caveolin-1 and caveolin-3 form heterooligomeric complexes in atrial cardiac myocytes that are required for doxorubicin-induced apoptosis. *Am J Physiol Heart Circ Physiol* **294**: H392-401
- Wang H, Haas M, Liang M, Cai T, Tian J, Li S, Xie Z (2004) Ouabain assembles signaling cascades through the caveolar Na<sup>+</sup>/K<sup>+</sup>-ATPase. *J Biol Chem* **279**: 17250-17259
- Wang Z, Fermini B, Nattel S (1993) Sustained depolarization-induced outward current in human atrial myocytes. Evidence for a novel delayed rectifier K<sup>+</sup> current similar to Kv1.5 cloned channel currents. *Circ Res* **73**: 1061-1076
- Weber KS, Hildner K, Murphy KM, Allen PM (2010) Trpm4 differentially regulates Th1 and Th2 function by altering calcium signaling and NFAT localization. *J Immunol* **185**: 2836-2846
- Webster MK, Goya L, Ge Y, Maiyar AC, Firestone GL (1993) Characterization of sgk, a novel member of the serine/threonine protein kinase gene family which is transcriptionally induced by glucocorticoids and serum. *Mol Cell Biol* **13**: 2031-2040
- Wible BA, Wang L, Kuryshev YA, Basu A, Haldar S, Brown AM (2002) Increased K<sup>+</sup> efflux and apoptosis induced by the potassium channel modulatory protein KChAP/PIAS3beta in prostate cancer cells. *J Biol Chem* **277**: 17852-17862
- Wible BA, Yang Q, Kuryshev YA, Accili EA, Brown AM (1998) Cloning and expression of a novel K<sup>+</sup> channel regulatory protein, KChAP. *J Biol Chem* **273**: 11745-11751
- Wilkinson KA, Henley JM (2010) Mechanisms, regulation and consequences of protein SUMOylation. *Biochem J* **428**: 133-145
- Wilkinson KA, Nakamura Y, Henley JM (2010) Targets and consequences of protein SUMOylation in neurons. *Brain Res Rev* **64**: 195-212
- Wilson VG, Rosas-Acosta G (2005) Wrestling with SUMO in a new arena. *Sci STKE* **2005**: pe32

Xu XZ, Moebius F, Gill DL, Montell C (2001) Regulation of melastatin, a TRP-related protein, through interaction with a cytoplasmic isoform. *Proc Natl Acad Sci U S A* **98**: 10692-10697

Xu Z, Chau SF, Lam KH, Chan HY, Ng TB, Au SW (2006) Crystal structure of the SENP1 mutant C603S-SUMO complex reveals the hydrolytic mechanism of SUMO-specific protease. *Biochem J* **398**: 345-352

Zareba W, Cygankiewicz I (2008) Long QT syndrome and short QT syndrome. *Prog Cardiovasc Dis* **51**: 264-278

# IX APPENDIX

## IX.1 Abbreviations

A	Alanine
Ab	Antibody
AM	Acetoxymethy
Amp	Ampicillin
ATP	Adenosine triphosphate
AV	Atrioventricular
bp	Base pair
BSA	Bovine serum albumin
C	Cysteine
Cav-1	Caveolin-1
Cav-3	Caveolin-3
cDNA	Complementary deoxyribonucleic acid
°C	Degree celcius
CSD	Caveolin-scaffolding domain
DMEM/F12	Dulbecco's Modified Eagle Medium: Nutrient Mixture F-12
DMSO	Dimethyl sulfoxide
DNA	Deoxyribonucleic acid
DNAse	Deoxyribonuclease
DCS	Donor calf serum
ECL	Enhanced Chemiluminescence
E.Coli	Escherichia coli
EDTA	Ethylenediamine tetraacetic acid
EGTA	Ethylene glycol tetraacetic acid
F	Phenylalanine
FRT	Flp recombination target
g	g-force
G	Glycine
GAPDH	Glyceraldehyde-3-phosphate dehydrogenase
HEPES	2-(4-(hydroxyethyl)-piperazine)-ethane sulfonic acid
HRP	Horseradish peroxidase
I	Isoleucine
ICCD	Isolated cardiac conduction disease
Ig	Immunoglobulin
IPTG	Isopropyl-D-thiogalactopyranoside
i.p	intraperitoneal injection
I-V	Current-Voltage relationship
K	Lysine
kb	Kilo base pairs
KChAP	K <sup>+</sup> channel chaperone protein
kDa	Kilo Dalton
μ	Micro (10 <sup>-6</sup> )

---

m	Mili ( $10^{-3}$ )
M $\beta$ CD	Methyl- $\beta$ -cyclodextrin
MES	2-(N-Morpholino) ethanesulfonic acid 4-Morpholineethane
n	Nano ( $10^{-9}$ )
N	Asparagine
NCX	Na, Ca-exchanger
NEM	N-Ethylmaleimide
OD	Optical density
PAGE	Polyacrylamide gel electrophoresis
PBS	Phosphate buffered saline
PCR	Polymerase chain reaction
PFHBI	Progressive familial heart block type I
PIP <sub>2</sub>	Phosphatidylinositol 4,5-bisphosphate
PKC	Protein Kinase C
Q	Glutamine
R	Arginine
RBBB	Right bundle-branch block
RMP	Resting membrane potential
RNA	Ribonucleic acid
rpm	Rotations per minute
S	Serine
SENp	Sentrin-specific protease
SDS	Sodium dodecyl sulfate
SDS-PAGE	Sodium dodecyl sulphate poly acrylamide gel electrophoresis
SGK	Serum-glucocorticoid-regulated protein kinase
TBS	Tris buffer saline
TM	Transmembrane domain
TRPM4	Transient receptor potential Melastatin 4
V	Volts
v/v	Volume per volume
w/v	Weight per volume
W	Tryptophan
Y	Tyrosine

## IX.2 Hazardous substances list

Hazardous Material	Hazard Class	R-S ätze (risk)	S-S ätze (safety)
CaCl <sub>2</sub>	Xi	36	22-24
Chloroform	Xn	22-38-40-48/20/22	36/37
DMSO	Xi	36/37/38	23-26-36
DTT	Xn	22-36/37/38	26/36
EDTA	Xi	36-52/53	26-61
EGTA			22-24/25
Ethanol	F	11	7-16
Ethidium bromide	T+	22-26-36/37/38-68	26-28-36/37-45
HCl (36.5-38.0%)		34-37	26-36/37/39-45
HCl (1M)	Xi	36/37/38	26
HEPES	Xi	36/37/38	26-36
KB-R7943		50	61
KCl			22-24/25
K <sub>2</sub> HPO <sub>4</sub>			22-24/25
KOH	C	22-35	22-36/37/39-45
β-Mercaptoethanol	T,N	20/22-24-34-51/53	26-36/37/39-45-61
Methanol	F,T	11-23/24/25-39/23/24/25	7-16-36/37-45
NaOH	C	35	26-37/39-45
Ouabain octahydrate		23/25	45
Penicillin G	Xn	42/43	22-36/37-45
Paraformaldehyde	Xn	20/22-36/37/38-40-43	22-26-36/37
SDS	F,Xn	11-21/22-36/37/38	26-36/37
Streptomycin	Xn	22	
Tris	Xi	36/38	
Triton X-100	Xn,N	22-41-51/53	26-36/39-61
Trypsin	Xn	36/37/38-42	22-24-26-36/37

## X ACKNOWLEDGEMENTS

I would first and foremost like to acknowledge my supervisor Prof. Dr. Olaf Pongs for providing facilities for this research, and for support and guidance during three and half years. I really admire his devotion and enjoyment in science and sense of humor in life.

I would also like to thank Prof. Dr. Peter Heisig for his generous time and assistance throughout the entire process of my PhD. Prof. Dr. Jens Rettig supported laboratory, facilities and useful discussion during last half year of my project, many thanks to him. Also, I appreciate support and discussion from Prof. Dr. Jürgen R. Schwarz and Prof. Dr. Ulrich Boehm.

I am especially grateful to Dr. Gregor Sachse for his fruitful discussions and his generosity with his time and advice. I received great encouragement from his never-ending enthusiasm, energy and optimism.

I am thankful for the assistance and friendships of my lab mates, Niklas Schütter, Frederik Flenner, Malte Stockebrand, Joanana Hermainski, and Dr. Ulrike Hahn. I am also grateful to Dr. Martin Kruse for introducing me to this interesting project. Mrs. Nina Kursawe offered excellent technical support in molecular biology and cardiomyocytes preparation, Dr. Michael Klaiber from Universität Würzburg helped me on Calcium measurement, which accelerated the completion of this thesis to a great extent. I am very grateful to them.

Finally, a lot of thanks to my parents and twin-brother Cong, they always support me with unwavering love and encouragement, which inspire me to accomplish my PhD thesis. In particular, my husband Kai, thank you for your unconditional love, patience and support in all aspects of life

---

## Curriculum Vitae

### Personal Information

Given name: Yu  
Family name: Wu  
Data of birth: 01.08.1981  
Gender: Female  
Nationality: P.R.China

### Education and Professional Experience

**04/2009-Present** Doctoral study  
Center for Molecular Neurobiology Hamburg (ZMNH), UKE,  
Hamburg University  
Department of Physiology, School of Medicine, University of  
Saarland

**08/2006-03/2009** Assistant Research Scientist  
National Institute for Control of Pharmaceutical and Biological  
Products (NICPBP), Beijing, China

**09/2003-07/2006** Master in Medical science  
National Institute for Control of Pharmaceutical and Biological  
Products (NICPBP), Beijing, China

**09/1999-06/2003** Bachelor in Biotechnology  
School of Biopharmacy, China Pharmaceutical University,  
Nanjing, China